



INDC International Nuclear Data Committee

Neutron Data Evaluation of ^{241}Am

V.M. Maslov, V.G. Pronyaev, N.A. Tetereva, K.I. Zolotarev, T. Granier, F.-J. Hamsch

- 1) Joint Institute of Power and Nuclear Research – SOSNY
220109, Minsk, Belarus
- 2) Institute of Physics and Power Engineering, 249020, Obninsk, Russia
- 3) CEA/DAM, Ile de France, Arpajon, France
- 4) EC-JRC Institute for Reference Materials and Measurements, B-2440, Geel, Belgium

January 2025

IAEA Nuclear Data Section

Vienna International Centre, P.O. Box 100, 1400 Vienna, Austria

INDC documents may be downloaded in electronic form from

<http://nds.iaea.org/publications>.

Requests for hardcopy or e-mail transmittal should be directed to

NDS.Contact-Point@iaea.org

or to:

Nuclear Data Section
International Atomic Energy Agency
Vienna International Centre
PO Box 100
1400 Vienna
Austria

Neutron Data Evaluation of ^{241}Am

V.M. Maslov¹, V.G. Pronyaev², N.A. Tetereva¹,
K.I. Zolotarev², T. Granier³, F.-J. Hamsch⁴

- ¹) Joint Institute of Power and Nuclear Research – SOSNY
220109, Minsk, Belarus
- ²) Institute of Physics and Power Engineering, 249020, Obninsk, Russia
- ³) CEA/DAM, Ile de France, Arpajon, France
- ⁴) EC-JRC Institute for Reference Materials and Measurements, B-2440, Geel,
Belgium

Abstract

The diverse measured data base of $n+^{241}\text{Am}$ was evaluated using a statistical theory and GMA generalized least squares codes. Consistent description of total, capture and fission measured data provides an important constraint for the inelastic scattering cross section. Important constraints for the measured capture cross section in the 0.15-300 keV energy range come from the average radiative and neutron S_0 and S_1 strength functions. Ground and metastable states yields ratio for $^{241}\text{Am}(n,\gamma)^{242g}\text{Am}$ and $^{241}\text{Am}(n,\gamma)^{242m+g}\text{Am}$ reactions is evaluated. Predicted change of the inelastic cross section shape at $E_n \sim 1.5$ MeV is attributed to the sharp increase of the level density of the residual odd-even nuclide ^{241}Am due to the onset of three-quasi-particle excitations.

The influence of exclusive (n, xnf) pre-fission neutrons on prompt fission neutron spectra (PFNS) and (n, xn) spectra is modelled. Contributions of emissive/non-emissive fission and exclusive spectra of (n, xnf) reactions are defined by a consistent description of $^{241}\text{Am}(n, F)$ and $^{241}\text{Am}(n, 2n)$ reaction cross sections.

This work performed under the project Agreement B-1604 with the International Science and Technology Center (Moscow). The financing party is EU. Partial support of International Atomic Energy Agency under Research Contract 14809 is acknowledged by JIPNR¹. Affiliations of the authors as in July of 2011. Data file is available at <https://www-nds.iaea.org/minskact/data/original/za095241>

Contents

1. Introduction.....	4
2. Resonance Parameters	5
3. Evaluation of neutron capture and fission cross sections for ^{241}Am in the generalized least-squares method.....	5
3.1. ^{241}Am (n,f) cross section evaluation	6
3.2. ^{241}Am (n, γ) cross section evaluation.....	13
4. Unresolved resonance parameters (150 eV – 93.9917 keV)	17
4.1. Neutron resonance spacing.....	17
4.2. Neutron width	17
4.3. Radiative capture width.....	18
4.4. Neutron inelastic width.....	18
4.5. Fission width.....	18
4.6. Total cross section in the region 0.15 keV-93.9917 keV	19
4.7. Elastic scattering cross section	19
4.8. Capture cross section	19
4.9. Inelastic scattering cross section.....	23
4.10. Fission cross section	23
5. Optical potential.....	23
6. Total and scattering cross section	25
7. Statistical model.....	25
7.1. Level Density.....	27
7.2. Fission cross section	31
7.2.1. Fission Channel.....	31
7.2.2. Fission transmission coefficient, level density and transition state spectrum.....	34
7.3. Fission data analysis	35
7.4. Inelastic scattering	35
7.4.1. Neutron Channel	35
7.4.2. Ground State Rotational Band.....	35
7.4.3. Total inelastic cross section.....	35
7.5. Capture cross sections.....	40
7.6. Branching ratio of short-lived ^{242g}Am (1^-) and long-lived ^{242m}Am (5^-) states of ^{242}Am	42
7.7. Analysis of experimental data for the isomeric capture cross section ratio for ^{241}Am	45
8. Fission cross section above emissive fission threshold	48
9. (n,2n) and (n,3n) cross section.....	49
10. Average prompt fission neutron yield $\langle v_p \rangle$ for $^{241}\text{Am}(n,f)$ reaction	53
11. Delayed neutron yield.....	57
12. Energy distributions of secondary neutrons.....	59

12.1 (n, $x\gamma$) and (n, xnf) neutron emission spectra.....	59
12.2 Prompt Fission Neutron Spectra	61
12.3 (n,xn) Reaction Neutron Spectra.....	65
13. Conclusion.....	68
References.....	69

1. Introduction

Americium-241 ($t_{1/2}=433$ yr) evolves in U/Pu-containing nuclear fuels after β^- -decay of ^{241}Pu ($t_{1/2}=14.4$ yr) and is one of major constituent of the spent nuclear fuel. The transmutation of the ^{241}Am in thermal power reactors is affected by the neutron capture cross sections of the reaction chains $^{241}\text{Am}(n, \gamma) ^{242\text{m}}\text{Am}$ and $^{241}\text{Am}(n, \gamma) ^{242\text{g}}\text{Am}(\beta^-)^{242}\text{Cm}$ or $^{241}\text{Am}(n, \gamma) ^{242\text{g}}\text{Am}(\beta^+)^{242}\text{Pu}$ and subsequent fission reactions. The neutron capture reaction $^{241}\text{Am}(n, \gamma)$ populates either the 16-h ground state of $^{242\text{g}}\text{Am}$ or the $^{242\text{m}}\text{Am}$ isomer with $T_{1/2}=141$ yr. The former state $^{242\text{g}}\text{Am}$ subsequently β^- -decays to ^{242}Cm . The yield of the $^{242\text{g}}\text{Am}$ short-lived ground state in reaction chain $^{241}\text{Am}(n, \gamma) ^{242\text{g}}\text{Am}(\beta^-)^{242}\text{Cm}$ increases the α -activity and neutron activity of the spent fuel due to the spontaneous fission of ^{242}Cm . The yield of the $^{242\text{m}}\text{Am}$ long-lived isomer state in the capture reaction $^{241}\text{Am}(n, \gamma) ^{242\text{m}}\text{Am}$ influences the neutron activity of the spent fuel due to spontaneous fission of $^{242\text{m}}\text{Am}$.

Repository or transmutation of ^{241}Am as one of the major constituent of the spent fuel needs rather precise knowledge of the ^{241}Am neutron-induced fission, capture, inelastic scattering, (n, 2n) cross sections and branching ratio for the yields of short-lived $^{242\text{g}}\text{Am}$ and long-lived $^{242\text{m}}\text{Am}$ states in $^{241}\text{Am}(n, \gamma)$ reaction. Prompt fission neutron spectrum (PFNS) and prompt fission neutron multiplicity are another important items, though measurements of the former for the $^{241}\text{Am}(n, F)$ reaction are unavailable. These characteristics of n+ ^{241}Am interaction would affect the criticality (critical mass) of the stored ^{241}Am , investigated by Kessler [1], which might be important for the optimization of the long-term storage of metallic/oxidized ^{241}Am . In [2] the calculated criticality of steel reflected metallic ^{241}Am sphere was much affected by the nuclear data used. The prompt fission neutron spectrum of $^{241}\text{Am}(n, F)$ reaction and $^{241}\text{Am}(n, n')$ reaction cross section might be potentially very strong factors influencing the (n,F) fission rate in a ^{241}Am . The prompt fission neutron spectra $^{241}\text{Am}(n, F)$ potentially might be rather influential factor, moreover so that its realistic uncertainties might be much higher than those imposed by the observed differences of various evaluations of PFNS [3].

The improvements of the nuclear reaction modeling and nuclear parameter systematic, developed based on neutron data description of neutron data for major actinides ^{232}Th , ^{233}U , ^{235}U , ^{238}U , ^{239}Pu and Z-odd target ^{237}Np provide a sound basis for critical assessment of the (n, F), (n, γ), (n, n), (n, n') cross sections and secondary neutron spectra for the n+ ^{241}Am interaction. The main reasons of improvement might be consistent description of fission, total, and capture data in 0.15 keV – 5 MeV energy range, the former coming from GMA analysis [4] of measured data. For neutron capture reaction on ^{241}Am target nuclide in the unresolved resonance and fast neutron energy ranges the methods, proven in case of $^{232}\text{Th}(n, \gamma)$ [5] or $^{238}\text{U}(n, \gamma)$ [6] and ^{237}Np [7, 8] data analysis would be used. Disentangling of the model deficiencies and model parameter uncertainties with GMA-fits or measured cross section database is of major importance. Especially when the data are scattering and there are systematic shifts between different data sets, it turns out to be a major problem in case of Z-odd actinides like ^{241}Am . Important constraints for the calculated capture cross section come from the average radiation width and neutron strength functions S_0 and S_1 . For the $^{241}\text{Am}+n$ interaction we have used almost the same optical potential, which allowed consistent description of total, fission and partial inelastic scattering data in 1~3 MeV incident neutron energy range for ^{237}Np target nuclide [8]. It provides an important constraint for the absorption cross section, which is quite important for the robust estimate of the capture cross section in keV- energy range.

At higher incident neutron energies consistent description of $^{241}\text{Am}(n, 2n)$ and $^{241}\text{Am}(n, F)$ cross sections was considered an important constraint in view of large scatter and systematic shifts of fission data around ~ 15 MeV. $^{241}\text{Am}(n, F)$ observed fission cross section is represented as superposition of the (n, f) and $(n, \chi f)$ reactions, with simultaneous calculation of exclusive neutron spectra of $(n, \chi n)$ and $(n, \chi n f)$ reactions. This approach provides robust estimates of prompt fission neutron spectra and their average energies for major actinides like ^{232}Th or ^{238}U and Z-odd target ^{237}Np [8]. The average energies of prompt fission neutron spectra (PFNS) and PFNS for $^{237}\text{Np}(n, F)$ reaction [6] are consistent with available experimental data base. That is a strong impetus to provide a new evaluation of PFNS for $^{241}\text{Am}(n, F)$.

2. Resonance Parameters

Resolved and unresolved resonance parameters from our previous evaluation [7], i.e., resolved resonance parameters for multilevel Breit-Wigner formalism (up to 150 eV) adopted. Then, simultaneous analysis of integral measurements, capture cross sections etc., used to upgrade possibly the negative resonance parameters.

Table 2.1 Thermal total, elastic, capture and fission cross sections and resonance integrals

Reaction	σ^{th} , barn	RI	σ^{th} , barn	RI	σ^{th} , barn	RI
	Present		JENDL-4.0		ENDF/B-VII.0	
Total	599.449		699.22		647.619	
Elastic	11.531		11.82		11.302	
Fission	3.13574	14.64	3.122	13.3	3.1384	15.793
Capture	584.783	1349.05	684.28	1590	633.179	1384.77

3. Evaluation of neutron capture and fission cross sections for ^{241}Am with the generalized least-squares method

There are a number of systematic discrepancies between ^{241}Am measured neutron data sets and different evaluations as well as between different evaluated data. However, the measured database on fission and capture cross sections is quite diverse to initiate a combined evaluation effort with a statistical theory and generalized least squares code GMA [4].

The approach developed by W. Poenitz, the GMA code and database of experimental results have been used in the latest evaluation of the neutron cross section standards [9]. The most measurements of the neutron capture and fission cross sections for ^{241}Am target nuclide have been done relative to these standard reactions. These standards can be used in new evaluation of $^{241}\text{Am}(n, \gamma)$ and $^{241}\text{Am}(n, F)$ reaction cross sections in two ways. In the first one, the results of standards evaluation (cross sections and covariance matrices of respective uncertainties) can be used as a prior in a Bayesian approach. Uninformative prior estimates should be assigned to the $^{241}\text{Am}(n, \gamma)$ and $^{241}\text{Am}(n, f)$ cross sections. Using Bayesian procedure a

posterior evaluation for combined standards and ^{241}Am cross sections can be obtained in the least squares fit by adding relevant experimental data sets. In the second option, the generalized least-squares fit can be accomplished for the combined set of standard, $^{241}\text{Am}(n, \gamma)$ and $^{241}\text{Am}(n, F)$ cross sections. The final evaluation will contain the standards, which may be slightly modified, and evaluated $^{241}\text{Am}(n, \gamma)$ and $^{241}\text{Am}(n, F)$ cross sections with covariance matrix of their uncertainties, including the blocks with all cross-reaction correlations. The results obtained in both approaches practically coincide.

The combined fit with standard cross sections was used in the evaluation of capture cross section for the ^{241}Am . Because the $^{241}\text{Am}(n, \gamma)$ experimental data include only those of shape cross section measurements and absolute ratio of $^{241}\text{Am}(n, \gamma)$ to $^{197}\text{Au}(n, \gamma)$ cross sections, only standard $^{197}\text{Au}(n, \gamma)$ reaction cross section was used in the combined fit. That is a reasonable approximation, since changes in the values of the standard capture reaction of $^{197}\text{Au}(n, \gamma)$ due to the influence of the $^{241}\text{Am}(n, \gamma)$ data, are within 0.01 – 0.1 %.

3.1 $^{241}\text{Am}(n, F)$ cross section evaluation

About 50 experimental data sets were considered as possible candidates for the analysis and least squares fit of $^{241}\text{Am}(n, F)$ reaction cross section. Finally, 30 data sets were selected for the evaluation. Their list is in Table 3.1 [10-27]. The rejected/omitted data sets were either too discrepant with the others or valuable information was missing for estimation of their quality and uncertainty. Only 30 data sets were added to the complete GMA database used in the evaluation of the standards. To reduce the size of evaluated data vector below ~1200 and correspondingly the size of the covariance matrix of the evaluated data to be less than 1200×1200 , $^{238}\text{U}(n, \gamma)$ reaction, weakly correlated (coupled) with $^{241}\text{Am}(n, F)$ reaction data, was excluded from the combined fit. The $^{241}\text{Am}(n, F)$ reaction cross section was evaluated at the thermal energy (as point-wise value at 0.0253 neutron energy), as group-wise cross section in the energy range from 100 eV to 20 keV and as values at several points between 20 keV and 20 MeV. Four iterations accomplished to reduce technically the Peelle's Pertinent Puzzle (PPP, when absolute uncertainties of experimental data adopted as their relative uncertainties, multiplied by the posterior evaluated values) and to determine and introduce additional uncertainties for the outlying data. The original $^{241}\text{Am}(n, F)$ experimental data were rather discrepant and iterations without prior analysis and proper treatment of outlying data lead to the divergent fit. With the analysis of the outlying data (see comments in the Table 3.1) and addition of the uncertainty component to this data, the good convergence was obtained. Chi-square per degree of freedom of about 1.2 – 1.3 for $^{241}\text{Am}(n, F)$ data and that of 0.76 for fit of the data accounted in the GMA database was obtained.

The results of the evaluation (original and smoothed) are shown in Figs. 3.1-3.7 in comparison with other evaluations. As we see at figure 3.1, the consistency with recent ENDF/B-VII.0 is generally good with exclusion of the region of 6 – 8 MeV, where GMA evaluation does not show such behaviour of (n, nf) cross section in the maximum above the threshold. The evaluated fission cross section at thermal point (0.0253 eV) equals 3.1258 ± 0.0154 b as consistent with the ENDF/B-VII.0 value (3.1384 b).

The largest difference between evaluations is observed in the energy range between 0.1 and 100 keV, where GMA evaluation is about 25 % higher than ENDF/B-VII.0. The reason is that the cross section is rather small (few tens of mb) in this energy range. Then the experimental

Table 3.1. The datasets for $^{241}\text{Am}(n,f)$ reaction cross section included in the GMA combined fit with all reactions used in the evaluation of the standards, with $^{238}\text{U}(n,\gamma)$ reaction excluded.

Data set number	First author	EXFOR entry, (date)	Data	Type of measurement	Energy range covered, MeV	Comments
5001	J.W. Behrens	10652002 (1981)	$^{241}\text{Am}(n,f)/^{235}\text{U}(n,f)$	shape of ratio	0.2189 – 32.16	Shape data because normalization was for the energy range 1.75-4 MeV. Can be converted into absolute ratio if self-consistent iteration procedure will be applied. Below 600 keV additional component of the uncertainty was introduced, because shape of ratio is outlying relative to the other data
5002	A. Prindle	10913007 (1979)	$^{241}\text{Am}(n,f)/^{238}\text{U}(n,f)$	Absolute ratio	14.8	Uncertainty was increased because of outlying value
5004	J.W.T. Dabbs	12809002 (1983)	$\text{Am}(n,f)$	Shape of the cross section	0.019 eV–88.6 keV	Cross sections below 20 keV were converted into the group structure. The cross sections were normalized using 245 b*eV integral of $^{235}\text{U}(n,F)$ in the energy range 7.8 – 11 eV. Present value (ENDF/B-VII.0 standard) is only slightly higher (246.4 b*eV). The cross section at 0.0253 eV obtained with that normalization is 3.009 b and is generally consistent with thermal cross section evaluated of 3.1257 b. Since above 100 eV, Dabbs data are lower by ~25 % of the other data, they have been used as a shape data with increased uncertainties at energies lower than 500 eV to account the change of the shape.
5005	J.W.T. Dabbs	12809004 (1983)	$^{241}\text{Am}(n,f)/^{235}\text{U}(n,f)$	Absolute ratio	0.1029 – 18.74	Data below 235 keV are treated as outlier, additional component of the uncertainties was introduced
5006	B.B. Cunningham	13574002 (1951)	$^{241}\text{Am}(n,f)$	Absolute	Thermal maxwellian spectrum	Corrected at Westcott g-factor
5007	H.H. Knitter	20764005 (1979)	$^{241}\text{Am}(n,f)/^{235}\text{U}(n,f)$	Absolute ratio	0.006 – 0.275	Some uncertainties (samples) correlated with same uncertainties of data sets 5008 and 5009
5008	H.H. Knitter	20764004 (1979)	$^{241}\text{Am}(n,f)/^{235}\text{U}(n,f)$	Absolute ratio	0.153 – 5.34	Some uncertainties (samples) correlated with same uncertainties of data sets 5007 and 5009
5009	H.H. Knitter	20764006 (1979)	$^{241}\text{Am}(n,f)/^{235}\text{U}(n,f)$	Absolute ratio	0.00025–2.6	Some uncertainties (samples) correlated with same uncertainties of data sets 5007 and 5008
5010	K. Wisshak	20774011	$^{241}\text{Am}(n,f)/$	Absolute	0.01 – 0.09	Nu-prompt as a monitor at thermal

		(1980)	$^{235}\text{U}(n,f)$	ratio		point, corrected in standard file (2006) for ^{235}U and ENDF/B-VII.0 for ^{241}Am . All LERC and part of MERC uncertainties correlated with the same in Data Set (DS)5011 and DS5012.
5011	K. Wisshak	20774012 (1980)	$^{241}\text{Am}(n,f)/$ $^{235}\text{U}(n,f)$	Absolute ratio	0.02 – 0.08	Nu-prompt as a monitor at thermal point, corrected at standard file (2006) for ^{235}U and ENDF/B-VII.0 for ^{241}Am . All LERC and part of MERC uncertainties correlated with those of DS5010 and DS5012.
5012	K. Wisshak	20774013 (1980)	$^{241}\text{Am}(n,f)/$ $^{235}\text{U}(n,f)$	Absolute ratio	0.06 – 0.25	Nu-prompt as a monitor at thermal point, corrected at standard file (2006) for ^{235}U and ENDF/B-VII.0 for ^{241}Am . All LERC and part of MERC uncertainties correlated with those of DS5010 and DS5011.
5013	W. Hage	20775004 (1980)	$^{241}\text{Am}(n,f)/$ $^{235}\text{U}(n,f)$	Absolute ratio	0.12 – 1.03	Nu-prompt as a monitor at thermal point. All LERC and part of MERC uncertainties correlated with those of DS5014.
5014	W. Hage	20775004 (1980)	$^{241}\text{Am}(n,f)/$ $^{235}\text{U}(n,f)$	Absolute ratio	0.0222 – 0.1102	Nu-prompt as a monitor at thermal point. All LERC and part of MERC uncertainties correlated with those of DS5013.
5016	M. Cance	21159002 (1977)	$^{241}\text{Am}(n,f)$	Absolute	0.93 – 2.66	Total uncertainty of 15% was splitted into 3 equal parts (LERC, MERC and SERC componenets)
5017	M. Cance	21621002 (1981)	$^{241}\text{Am}(n,f)$	Absolute	14.6	Time-correlated associated particles method
5018	K. Kobayashi	22344002 (1981)	$^{241}\text{Am}(n,f)$	Absolute	Maxwellian $kT=0.0253$ eV	Reduced to thermal point (0.0253 eV) value by correcting at the Westcott g-factor, reduced to the new $^{235}\text{U}(n_{th},f)$ standard
5019	S. Yamamoto	22479002 (1997)	$^{241}\text{Am}(n,f)$	Absolute	0.1 eV – 10.61 keV	Low-resolution lead slowing-down spectrometer. Data below 1 keV reduced to the group-structure form.
5021	D.L.Shpak	40010002 (1969)	$^{241}\text{Am}(n,f)$	Absolute	0.008 – 3.3	Large uncertainty below 0.6 MeV. Because of outlier from 0.12 to 0.26 MeV and 0.54 to 0.60 MeV the MERC type additional uncertainty was added
5022	K.D. Zhuravlev	40436003 (1975)	$^{241}\text{Am}(n,f)$	Absolute	Maxwellian $kT=0.0253$ eV	Reduced to point (0.0253 eV) value by correcting at the Westcott g-factor, reduced to the new $^{235}\text{U}(n_{th},f)$ standard
5023	A.N. Protopopov	40443002 (1959)	$^{241}\text{Am}(n,f)$	Absolute	14.6	
5024	V.M. Kuprijanov	40507005 (1978)	$^{241}\text{Am}(n,f)/$ $^{239}\text{Pu}(n,f)$	Absolute ratio	0.13 – 7.0	High accuracy data, uncertainties of LERC and partial MERC are correlated with the same uncertainties of DS5025. Basis of evaluation in the energy range of 0.1 — 7 MeV

5025	V.M. Kuprijanov	40507003 (1978)	$^{241}\text{Am}(n,f)/$ $^{239}\text{Pu}(n,f)$	Absolute ratio	2 – 3	High accuracy data, uncertainties of LERC and partial MERC are correlated with the same uncertainties of DS5024. For the normalization, the data in 1.5 — 6 MeV range are used.
5026	B.M. Aleksandrov	40546002 (1979)	$^{241}\text{Am}(n,f)$	Absolute	2.5	
5027	M.I. Kazarinova	40636009 (1960)	$^{241}\text{Am}(n,f)/$ $^{238}\text{U}(n,f)$	Absolute	14.6	Very high uncertainty, outlying data
5028	M.I. Kazarinova	40636009 (1960)	$^{241}\text{Am}(n,f)/$ $^{238}\text{U}(n,f)$	Absolute	2.5	Very high uncertainty, outlying data
5029	B.M. Aleksandrov	40673002 (1979)	$^{241}\text{Am}(n,f)$	Absolute	2.9	$^{235}\text{U}(n,f)$ and $^{238}\text{U}(n,f)$ monitor values are absent
5030	P.E. Vorotnikov	40948002 (1986)	$^{241}\text{Am}(n,f)$	Absolute	0.29 – 1.31	LERC uncertainty is correlated with the uncertainty in DS5032, DS5033, DS5034
5032	P.E. Vorotnikov	40948002 (1986)	$^{241}\text{Am}(n,f)$	Absolute	0.16 – 0.31	LERC uncertainty is correlated with the uncertainty in DS5030, DS5033, DS5034
5033	P.E. Vorotnikov	40948002 (1986)	$^{241}\text{Am}(n,f)$	Absolute	0.08 – 0.35	LERC uncertainty is correlated with the uncertainty in DS5030, DS5032, DS5034
5035	V.Ya. Golovnya	41361002 (1999)	$^{241}\text{Am}(n,f)$	Absolute	14.7	Time-correlated associated particles method

data have rather low statistics and relatively large background in this energy range. The difference between present and ENDF/B-VII.0 evaluation is probably because ENDF/B-VII.0 evaluation is based mostly on the data by Dabbs [12], which generally lay below all other data. Dabbs [12] data, were normalized using $^{235}\text{U}(n, f)$ average cross section in the energy range of 7.8 - 11 eV. This normalization gives thermal cross section value for Dabbs [12] data about ~4 % lower than present evaluation. Due to just mentioned problems with low statistics and background, data [12] treated in the energy range 100 eV – 100 keV as shape data. In the GMA' fit they normalized as $\times 1.25$. The fitted values compared with different evaluations on Figs. 3.1–3.7.

Comparison of all experimental data used in the fit of $^{241}\text{Am}(n,f)$ cross section with evaluated data from 100 eV to 20 MeV is provided on figures. The results of the absolute measurements are shown by closed symbols, open symbols presents the data, which were converted from the absolute ratio data to the absolute cross sections, using standards obtained in given fit. Data by Dabbs [12] used as shape data were normalized within the GMA approach during the fit. Experimental data are shown as reduced to the same energy nodes. Uncertainties shown include also additional component of the uncertainty, introduced for the outlying data. Data points with difference larger than ~65% from posterior evaluation were excluded from the fit.

Detailed comparison of the evaluations and experimental data in the energy range from 100 eV to 500 keV shown in Fig. 3.4. Because the data by Dabbs [12] processed as a shape data and normalized in the GMA fit as $\times 1.25$, practically all experimental data in the energy range below ~100 keV are laying above the ENDF/B-VII.0 evaluation. Uncertainty of the evaluation is about ~0.5% at thermal point, at the level of ~5 % between 100 eV and 20 keV, 3~4 % for 20

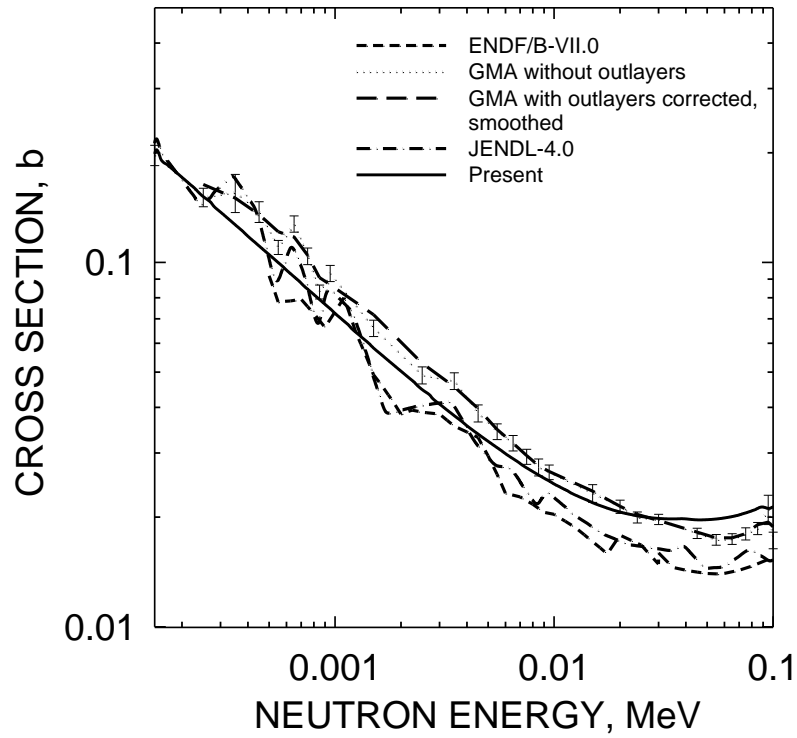


Fig. 3.1 Comparison of GMA's evaluated fission cross section of ^{241}Am with previous evaluation

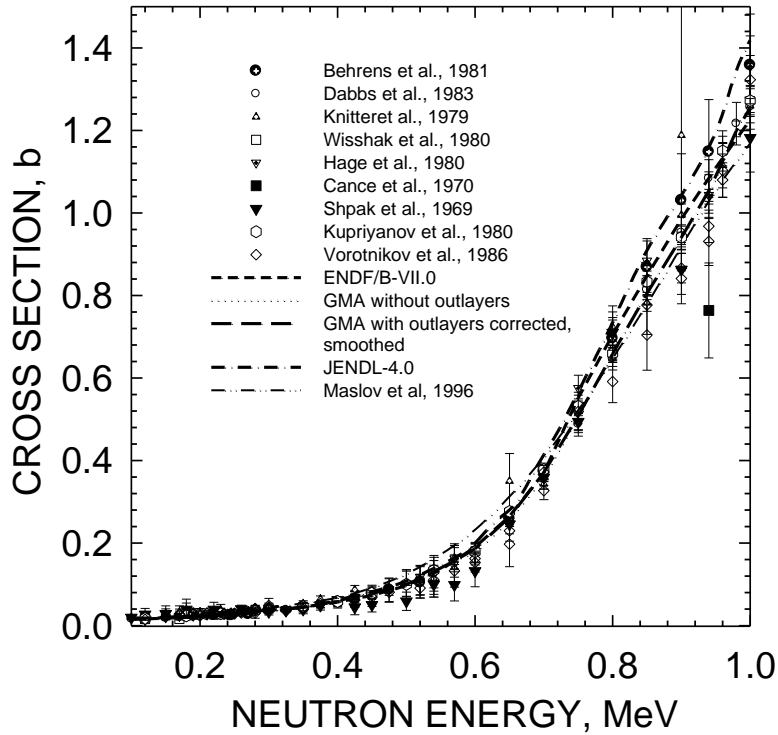


Fig. 3.2 Comparison of GMA's evaluated fission cross section of ^{241}Am with previous evaluations and measured data.

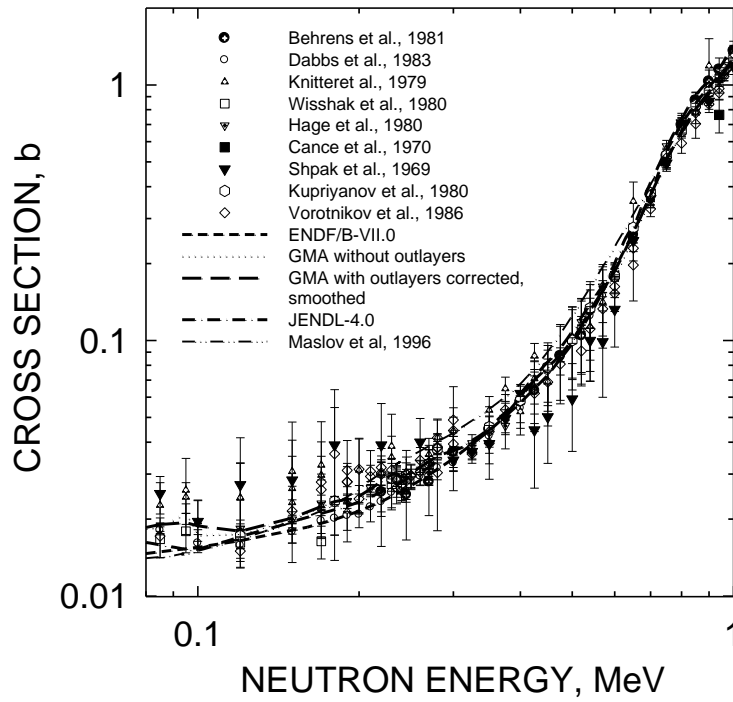


Fig. 3.3 Comparison of GMA' evaluated fission cross section of ^{241}Am with previous evaluations and measured data.

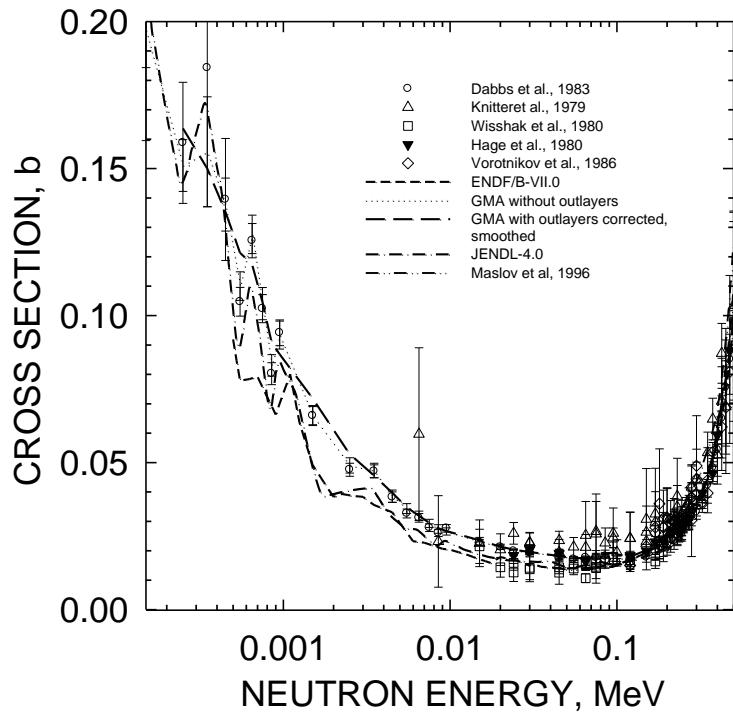


Fig. 3.4 Comparison of GMA' evaluated fission cross section of ^{241}Am with previous evaluations.

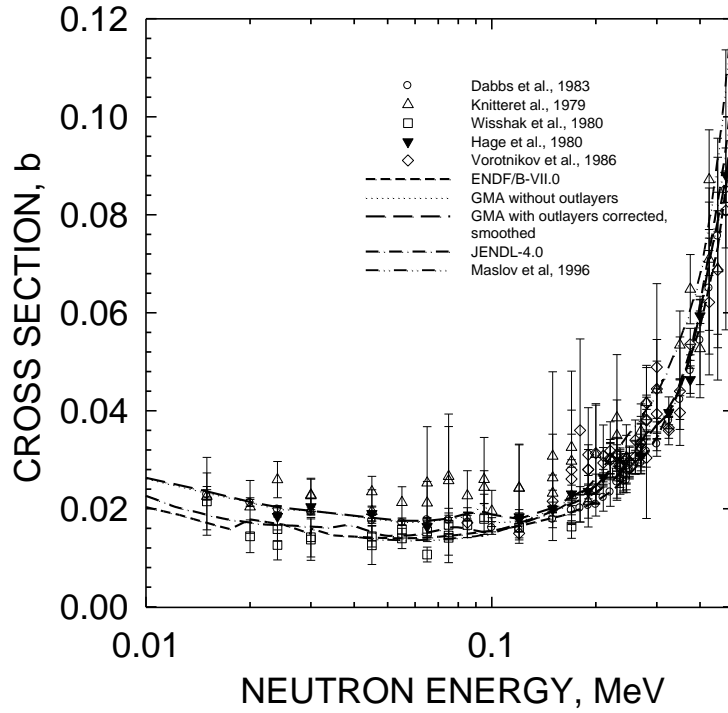


Fig. 3.5 Comparison of GMA' evaluated fission cross section of ^{241}Am with previous evaluations and measured data.

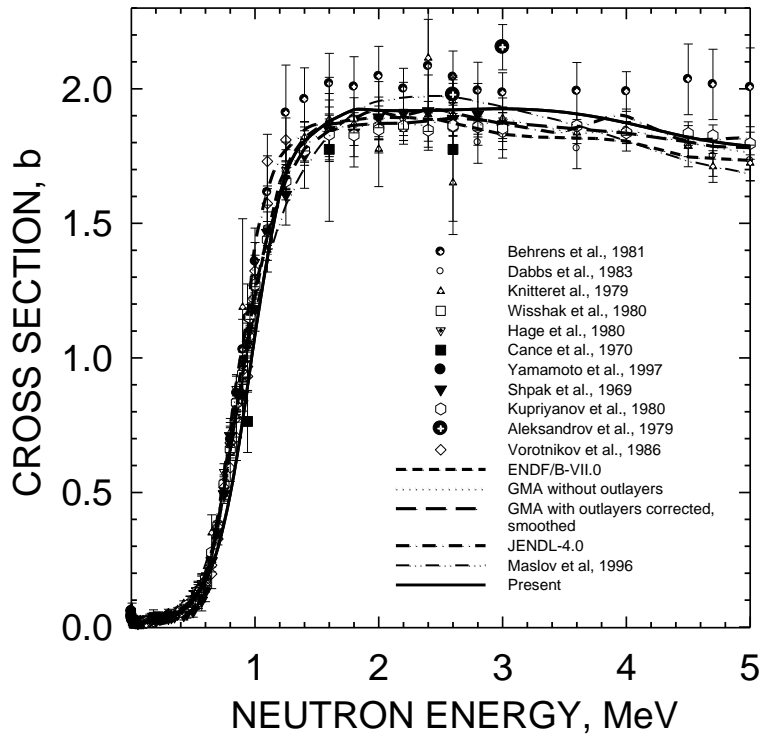


Fig. 3.6 Comparison of GMA' evaluated fission cross section of ^{241}Am with measured data.

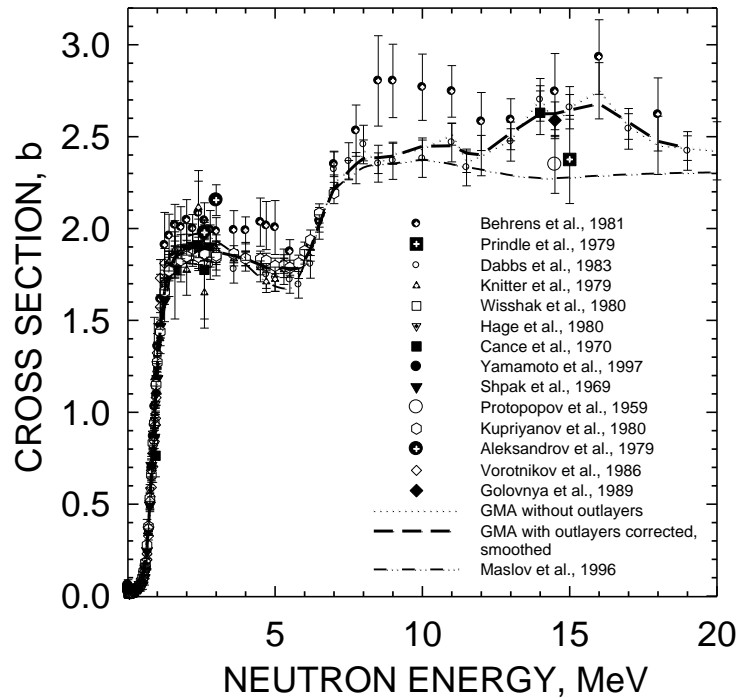


Fig. 3.7 Comparison of GMA' evaluated fission cross section of ^{241}Am with previous evaluations and measured data.

keV – 500 keV, decreasing to 1.2 – 1.5 % between ~500 keV and ~5 MeV and increasing again up to 2 – 3 % between ~5 and ~20 MeV. Strength of cross-energy correlations of uncertainties of evaluated data reflects the structure of the experimental data used in the fit, but there are energy ranges where the level of correlation is rather high (e.g. between 2 and 5 MeV at the “plateau” of the ^{241}Am (n, f) reaction).

Detailed comparison of the evaluations and experimental data in the energy range from 100 eV to 500 keV is shown in Fig. 3.4. Because the data by Dabbs [12] processed as a shape type data and normalized in the GMA fit with a coefficient 1.25, practically all experimental data in the energy range below 100 keV are laying above the ENDF/B-VII.0 evaluation. Uncertainty of the evaluation is about 0.5% at thermal point, at the level of 5 % between 100 eV and 20 keV, 3 – 4 % for 20 keV – 500 keV, decreasing to 1.2 – 1.5 % between ~500 keV and ~5 MeV and increasing again up to 2~3 % between ~5 and ~20 MeV. Level of cross-energy correlations of uncertainties of evaluated data reflects the structure present in the experimental data, used in the fit, but in some energy ranges the level of correlation is rather high (e.g. between ~2 and ~5 MeV at the “plateau” range of the ^{241}Am (n, f) reaction).

As we see from figures 3.6 and 3.7, there is rather large spread of experimental data in the MeV energy region. New measurements are needed in the energy range 100 eV – 100 keV and in the 14 -20 MeV energy range.

3.2 $^{241}\text{Am}(n, \gamma)$ cross section evaluation

The experimental [28-36] data used in the evaluation given in Table 3.2. The data set

By Weston and Todd [28] encompass the energy range from thermal to keV-energy and is, in fact, an absorption cross section. As the data set by Gayther and Thomas [29], which is absorption cross section as well, the data [28] corrected for the small admixture of the fission cross section to obtain the capture cross section.

Present evaluated data compared at Fig. 3.8 with relevant experimental data. Each data set of the shape was assigned the specific normalization parameter. At Fig. 3.8 all data are shown as original. The chi-square value per degree of freedom obtained in the fit is at the level of ~ 1 . That means the data are internally consistent. There is no data set in the database assigned an outlier status. Data by Gayther and Thomas [29] show some inconsistency in the shape with the posterior evaluation, but it is within the limits of uncertainties of the shape, which are about $\sim 12\%$ for these data. As we see from Fig. 3.8, there is difference in the shape with the ENDF/B-VII.0 evaluation and results of the present statistical model calculations.

The evaluated thermal value 664.6 ± 16.0 barn is in disagreement with the value of 587 ± 16 barn recommended by S.F. Mughabghab [30] and adopted for the present data file. That could emerge due to evaluation of thermal value cross section from integral measurements in the presence of the strong resonance at ~ 0.307 eV or systematic underestimation of the cross section in some measurements. Time-of-flight measurements done by Jandel et al. [31] for thermal and resolved resonance energy range give the value at 0.0253 eV of 665 ± 33 barn. For the independent linear fit of the data by Jandel et al. [31], transformed from cross section to cross section times the square root of incident neutron energy in the range of 0.02 – 0.03 eV, the thermal capture cross section value derived is 665.5 barn.

Table 3.2. Data sets for $^{241}\text{Am}(n,\gamma)$ included in the GMA combined fit with $^{197}\text{Au}(n,\gamma)$ reaction standard.

Data set num.	First author	EXFOR entry, (date)	Data	Type of measurem.	Energy range covered, MeV	Comments
4001	K. Wisshak	20774002 (1980)	$^{241}\text{Am}(n,\gamma)/$ $^{197}\text{Au}(n,\gamma)$	absolute	0.0139 – 0.0838	66.4 m flight path; new correction factor for detector efficiency
4002	K. Wisshak	20774004 (1980)	$^{241}\text{Am}(n,\gamma)/$ $^{197}\text{Au}(n,\gamma)$	absolute	0.0143 – 0.0881	64 m flight path; new correction factor for detector efficiency
4003	K. Wisshak	20774006 (1980)	$^{241}\text{Am}(n,\gamma)/$ $^{197}\text{Au}(n,\gamma)$	absolute	0.0104 – 0.0807	50 m flight path; new correction factor for detector efficiency
4004	K. Wisshak	20774008 (1980)	$^{241}\text{Am}(n,\gamma)/$ $^{197}\text{Au}(n,\gamma)$	absolute	0.0581 – 0.23	65.3 m flight path; new correction factor for detector efficiency
4005	K. Wisshak	20774010 (1980)	$^{241}\text{Am}(n,\gamma)/$ $^{197}\text{Au}(n,\gamma)$	absolute	0.0164 – 0.0897	64 m flight path; thin sample; new correction factor for detector efficiency
4006	G. VanPraet	21978 (1985)	$^{241}\text{Am}(n,\gamma)$	shape	0.00015 – 0.15	High-resolution data averaged for the energy groups
4007	L.W. Weston	10767 (1976)	$^{241}\text{Am}(n,\text{abs})$	shape	Therm – 0.35	High-resolution absorption cross section averaged for the energy groups
4008	D.B. Gayther	20785	$^{241}\text{Am}(n,\text{abs})$	shape	0.000125 – 0.45	High-resolution absorption

		(1977)				cross section averaged for the energy groups by authors
4009	M. Jandel	14209 (2008)	$^{241}\text{Am}(n,\gamma)$	absolute	thermal	Point-wise value (665 ± 33 b) derived by authors from time-of-flight measurements
4010	G. Fioni	22691 (2008)	$^{241}\text{Am}(n,\gamma)$	absolute	thermal	Maxwellian spectrum averaged value (696 ± 48 b) for ^{242g}Am and ^{242m}Am states
4011	K. Wisshak	21690 (1982)	$^{241}\text{Am}(n,\gamma)$	absolute	thermal	(620.9 ± 39.7 b)
4012	S. Nakamura	22998 (2007)	$^{241}\text{Am}(n,\gamma)$	absolute	thermal	Cross section at 0.0253 eV (628 ± 22 b for ^{242g}Am ground state)
4013	N.L. Maidana	31518 (2001)	$^{241}\text{Am}(n,\gamma)$	absolute	thermal	Cross section at 0.0253 eV (602 ± 9 b for ^{242g}Am residual nucleus)

New measurements done in frameworks of Mini-INCA project [36] gave even higher capture cross section value (705 ± 23 b) at 0.0253 eV. This value was derived from 609 ± 20 b effective cross section obtained in a pure Maxwellian neutron flux for the yield of the ground state ^{242g}Am , 0.8947 ± 0.0038 isomeric branching ratio determined by the authors, and g-factor value which can be obtained from the evaluated data. If for branching ratio (0.908) values given in [36] and g-factor (1.051) are used, the 0.0253 eV cross section derived from 609 b effective cross section will be the same (705 barn). The data from Mini-INCA project were not used in the

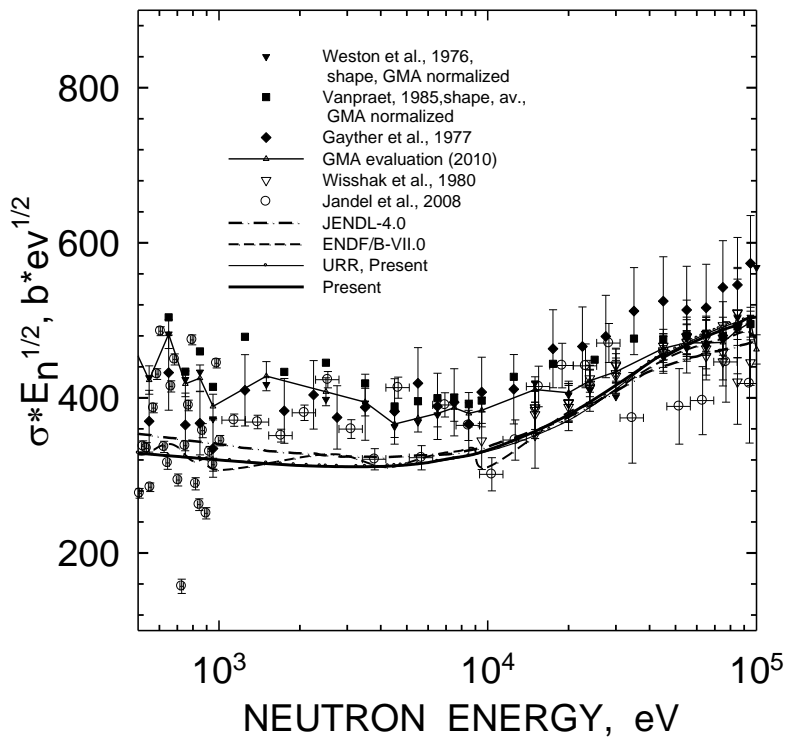


Fig. 3.8 Comparison of GMA' evaluated capture cross section of ^{241}Am with previous evaluations and measured data.

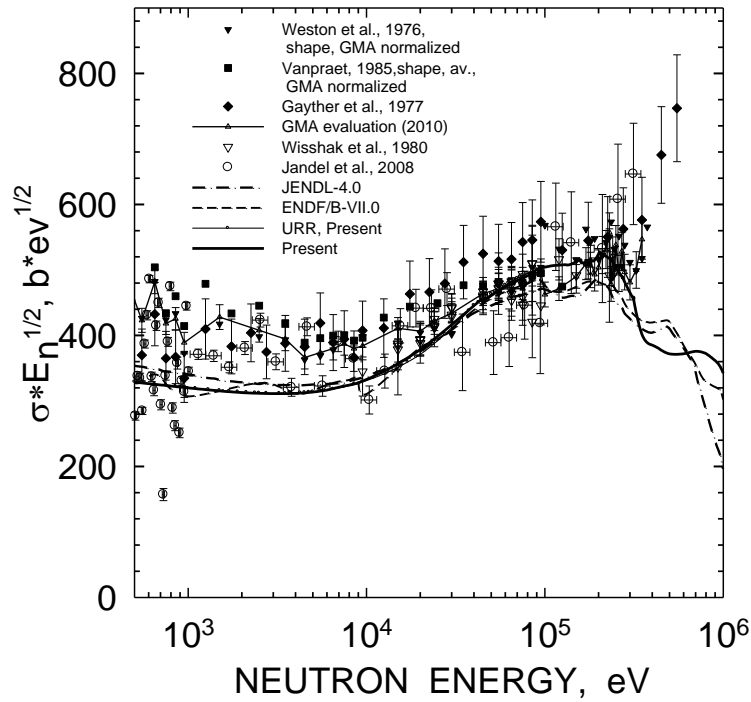


Fig. 3.9 Comparison of GMA' evaluated capture cross section of ^{241}Am with previous evaluations and measured data.

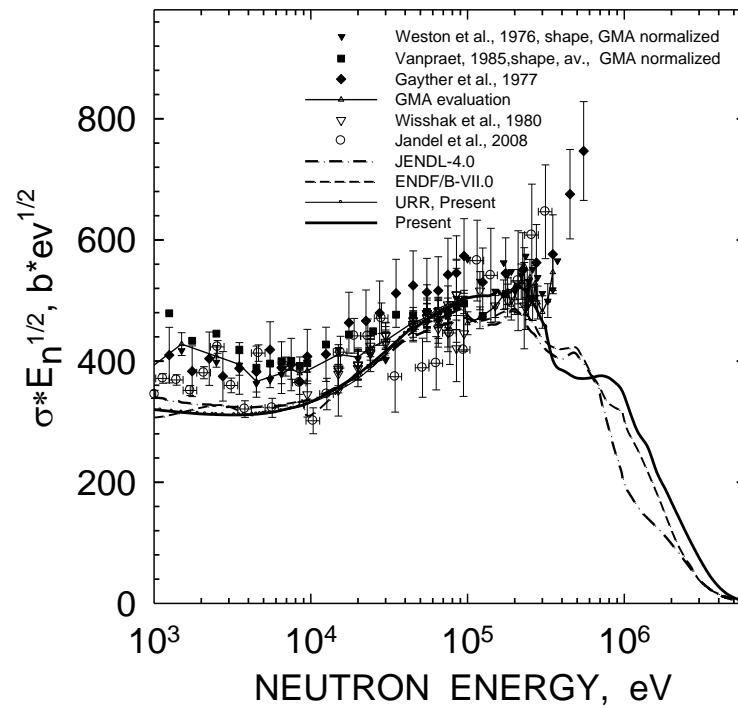


Fig. 3.10 Comparison of GMA' evaluated capture cross section of ^{241}Am with previous evaluations and measured data.

present evaluation, but they endorse the higher value of the thermal capture cross section evaluated in this work in comparison with the value given in BNL [30].

4. Unresolved resonance parameters (0.150 - 93.9917 keV)

Here we will briefly review the status of unresolved neutron resonance parameters of ^{241}Am and provide a cross section parameterization of total, capture, elastic and inelastic scattering cross sections. The average resonance parameters were determined, as described in [8], to reproduce average cross sections in the energy range of 0.15 keV-93.998 keV. Provided are energy dependent average resonance parameters.

We assume that the the upper energy is ~ 94 keV, twice higher than in previous evaluations [37], the lower is 150 eV. We suppose s-, p- and d-wave neutron-nucleus interactions to be effective (see Tables 4.1).

Table 4.1 Average neutron resonance parameters for ^{241}Am

	D_{obs} , eV	Γ_{γ} , meV	$S_0 \times 10^{-4}$	$S_1 \times 10^{-4}$	R, fm
JENDL-4.0 [37]	0.55	45	0.99	2.66	9.49
RIPL	0.58 ± 0.04	46 ± 2	0.97 ± 0.07		
Present	0.551	48.4	1.006	2.335	9.516

4.1 Neutron resonance spacing

Basically neutron resonance spacing D_{obs} was calculated with the phenomenological model [38] by Ignatyuk, which takes into account the shell, pairing and collective effects. It was modified to reproduce few-quasiparticle effects in level density [5]. The main parameter of the model, asymptotic value of level density parameter a , was normalized to the observed neutron resonance spacing $D_{\text{obs}} = 0.551$ eV.

4.2 Neutron width

Average neutron width is calculated as follows

$$\langle \Gamma_n^{lJ} \rangle = S_l \langle D \rangle_J E_n^{1/2} P_l \nu_n^{lJ}, \quad (4.1)$$

where E_n is the incident neutron energy, P_l is the transmission factor for the l -th partial wave, which was calculated within black nucleus model, ν_n^{lJ} is the number of degrees of freedom of the Porter-Thomas distribution. The p-wave neutron strength function $S_1 = 2.335 \times 10^{-4}$ at 150 eV was calculated with the optical model, using the deformed optical potential, described below. Figure 4.1 compares the average reduced neutron widths for the particular (l, J) - state, which is excited in the unresolved resonance energy range. The $\langle \Gamma_n^{0lJ} \rangle$ values for the s-wave neutrons in ENDF/B-VII.0 [39] data file are much less energy-dependent than those of present evaluation.

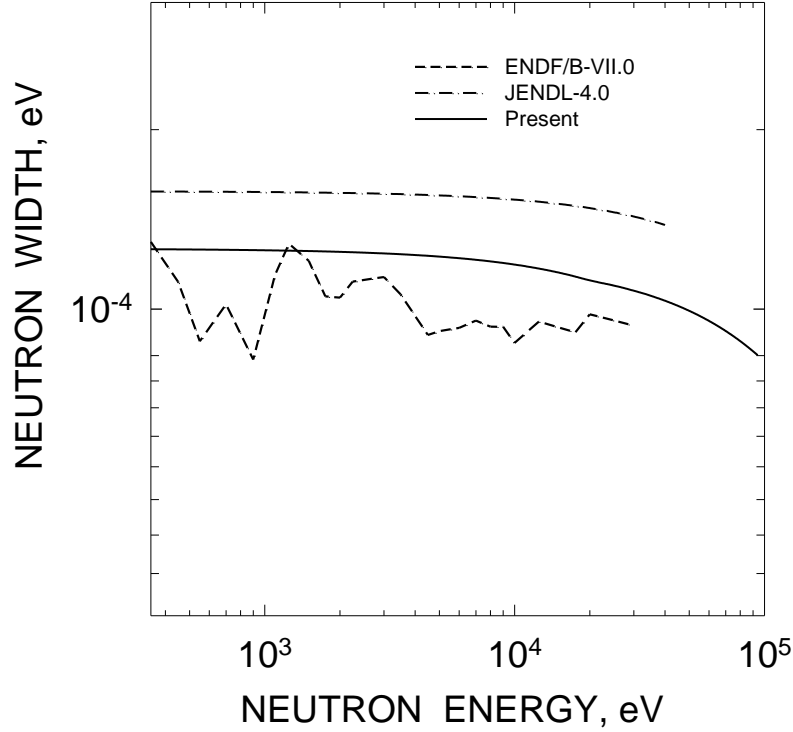


Fig. 4.1 Reduced neutron width of ^{241}Am , $l=0$, $J=2$.

4.3 Radiative capture width

Energy and angular momentum dependence of radiative capture widths are calculated within a two-cascade γ -emission model with allowance for the $(n, \gamma n')$ [40] and $(n, \gamma f)$ [41] reactions competition with the $(n, \gamma\gamma)$ reaction. The $(n, \gamma\gamma)$ reaction is supposed to be a radiation capture reaction. The radiation capture width was normalized to the value of $\Gamma_\gamma = 48.4$ meV, adopted here to describe the neutron capture cross section data. Detailed treatment is described below.

4.4 Neutron inelastic width

Average neutron inelastic width calculated as follows

$$\langle \Gamma_{n'}^{lJ} \rangle_s = S_l \langle D \rangle_J (E_n - E')^{1/2} P_l(E_n - E') \nu_{n'}^{lJ}, \quad (4.2)$$

where $\nu_{n'}^{lJ}$ is number of degrees of freedom of Porter-Thomas distribution. Excited levels of ^{241}Am are taken from Nuclear Data Sheets [42].

4.5 Fission width

Fission widths calculated within a double-humped fission barrier model by Strutinsky [43]. Energy and angular momentum dependence of fission width defined by the transition state

spectra at inner and outer barrier humps as in [7]. We constructed transition spectra by supposing the triaxiality of inner saddle and mass asymmetry at outer saddle.

4.6 Total cross section in the region 0.15 keV-93.9917 keV

Total cross section data by Phillips and Howe [44] in the energy range 0.45-24.8 MeV were reproduced with the rigid rotator optical model calculations. Coupled channel parameters, fitting the measured data are those defined for the $^{237}\text{Np}+n$ interaction [8]. In the energy ranges 0.15 -20 keV and 20-93.998 keV the optical model calculations of the total cross section were reproduced assuming a decreasing trends of S_o , S_I and S_2 strength function values as the latter and potential radius, which was adopted from the optical model calculations, define total cross section up to $E_n= 93.998$ keV.

To reproduce the ^{241}Am total cross section, calculated with the optical model, we assume S_o value linearly decreasing starting from 0.15 keV to 0.82335×10^{-4} , while S_I decreases linearly to 2.0660×10^{-4} at 93.998 keV (see Fig. 4.2). The d-wave neutron strength function was assumed to be equal to $S_2= 1.0773 \times 10^{-4}$.

4.7 Elastic scattering cross section

The elastic scattering cross section is composed of shape elastic (see Fig. 4.3) and compound elastic contributions. Compound elastic scattering cross section estimate is rather insensitive to the ^{241}Am fission cross section estimate. Present and JENDL-4.0 [37] estimates from 0.15 keV and up to 93.998 keV, shown on Fig. 4.3 differ a lot below 200 keV; lower solid curve shows the shape elastic contribution.

4.8 Capture cross section

The description of capture cross section data by Weston et al. [28], Vanpraet et al. [32], Wisshak et al. [15] and Jandel et al. [31] in the energy range of 0.15 keV–100 keV is quite possible, but it is very sensitive to the shape of the neutron absorption cross section. It was shown in [7] that around $E_n \sim 1$ MeV the total cross section of Z-odd target nuclide is virtually insensitive to the lowering/increasing of the neutron absorption cross section. Lowering of the absorption cross section, simulated by the decrease of the imaginary surface potential term W_D , was cross-checked by the consistency of fission and inelastic scattering cross sections.

Measured data for the $^{241}\text{Am}(n, \gamma)$ reaction cross section [15, 28, 31, 32] shown on Figs. 4.4, 4.5, 4.6 are scattering a lot, or there are a systematic shifts between different data sets. At lower energy range the GMA fits are inconsistent with statistical model calculations, defined by estimate of radiation strength function and neutron absorption cross section. Figure 4.6 shows the calculated curve, corresponding to the consistent description of the total, fission and inelastic scattering cross section with $\langle I\gamma \rangle = 48.4$ meV and $\langle D_{obs} \rangle = 0.551$ eV. Recent measured data by Jandel et al. [30] are scattering a lot, predicting distinctly different cross section shape than the other measured data, especially in the vicinity of the $E_n \sim 100$ eV and $E_n \sim 100$ keV. The capture

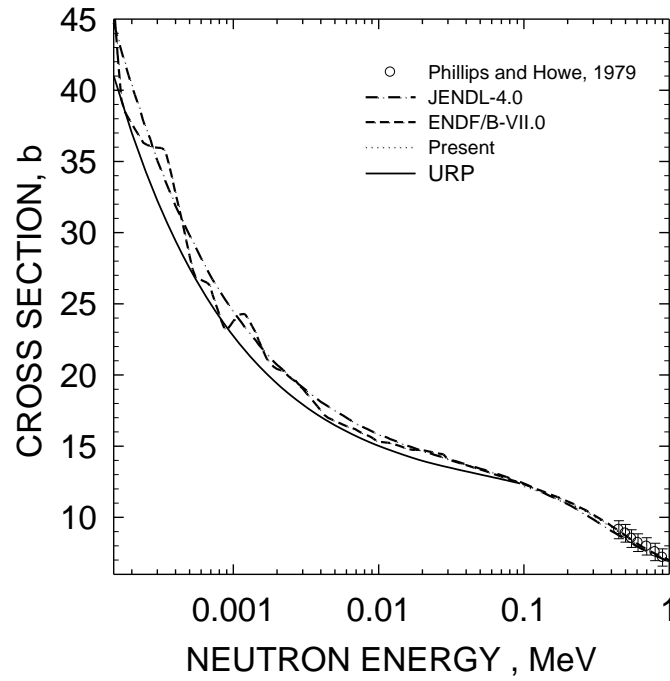


Fig. 4.2 Total cross section of ^{241}Am .

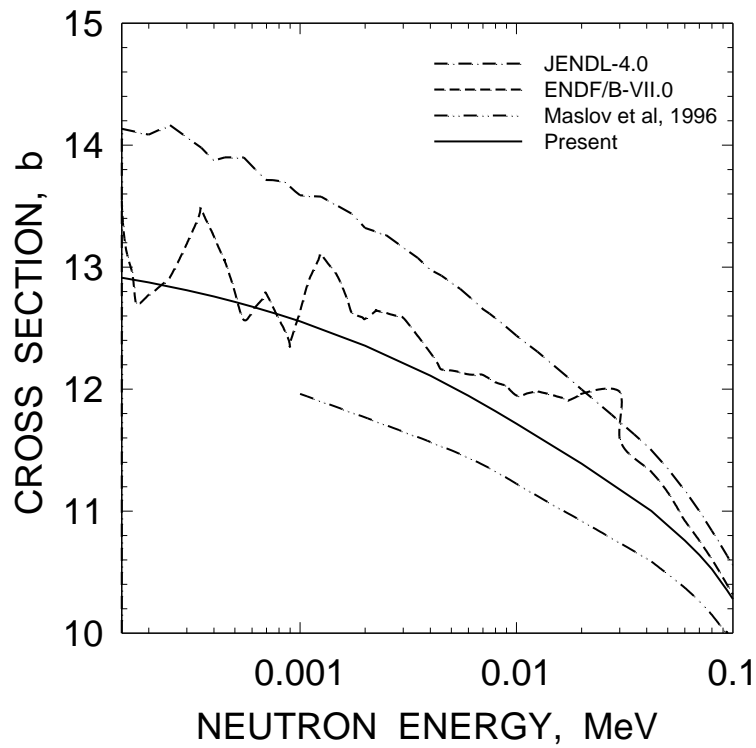
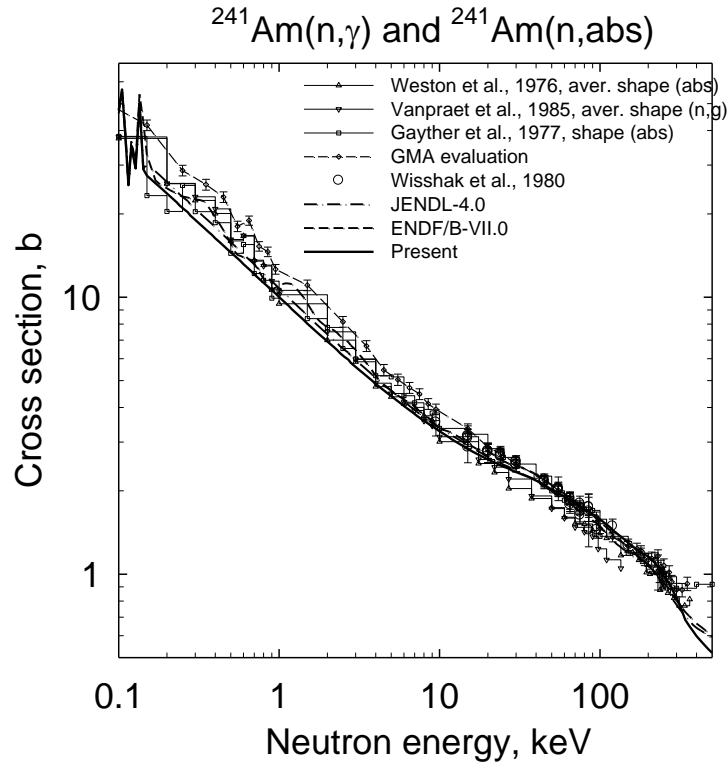
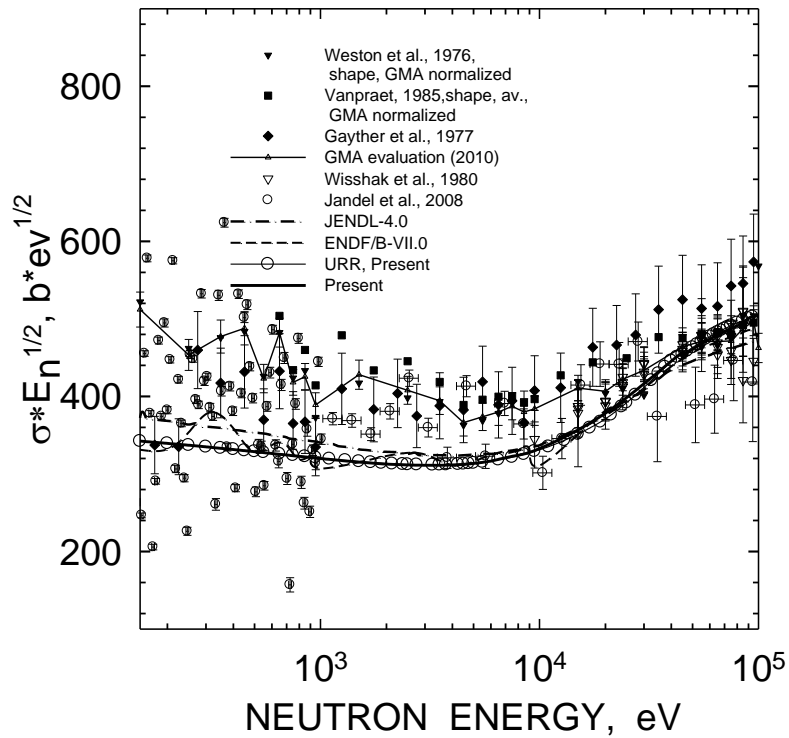


Fig. 4.3 Elastic cross section of ^{241}Am .

Fig. 4.4 Capture cross section of ^{241}Am .Fig. 4.5 Capture cross section of ^{241}Am .

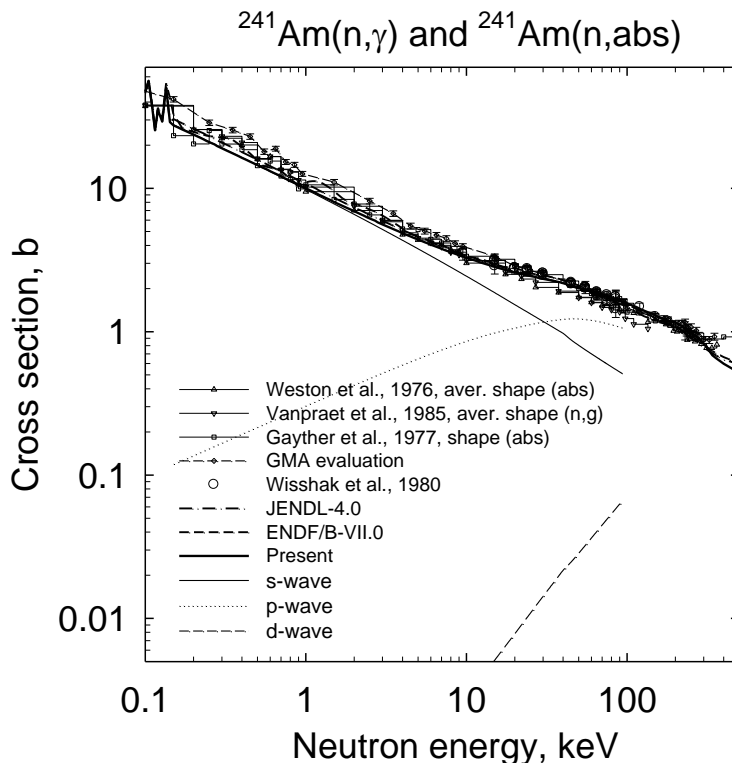


Fig. 4.6 Capture cross section of ^{241}Am .

cross section level in 0.10-100 keV energy range could be reproduced with rather high value of $\langle\Gamma_\gamma\rangle = 48.4$ meV. That value of $\langle\Gamma_\gamma\rangle$ gives still too low capture cross section value for incident neutron energies of 0.15-100 keV energy range, than GMA fit predicts.

To follow a much higher lying data trend of the GMA-fit one would need rather large values of s -wave neutron strength function S_0 , almost $\sim 50\%$ higher than the established value (see Table 4.1). Obviously, the S_0 value could be increased by increasing the β_2 , quadrupole deformation parameter value, but after that the calculated capture cross section will again misfit the data around 200 keV.

The important peculiarity of the calculated $^{238}\text{U}(n, \gamma)$ and $^{232}\text{Th}(n, \gamma)$ [5, 6] capture cross sections, Wigner' cusp above first excited level threshold, is pronounced in case of calculated $^{241}\text{Am}(n, \gamma)$ reaction cross section rather differently, because of larger number of levels in odd residual ^{241}Am nuclide. The pattern of s -, p - and d -wave entrance channel contributions to the capture cross section in the energy range of 0.15 – 93.998 keV is different from that of ^{232}Th [5] or ^{238}U [6] target nuclides (see Fig. 4.6). That might be traced back to higher fissility of ^{242}Am compound nuclide as well. In case of $^{238}\text{U}(n, \gamma)$ reaction main contribution comes from p -wave neutrons above ~ 10 keV. The p -wave contribution to the $^{241}\text{Am}(n, \gamma)$ reaction cross section is higher than that of s -wave above ~ 30 keV, while that of d -wave neutrons is the lowest.

Calculated capture cross section roughly describes the following data trend: Wisshak et al. [15], Weston et al. [28], Jandel et al. [31] and VanPraet et al. [32], using average radiation width $\Gamma_\gamma=0.0484$ eV and observed neutron resonance spacing $D_{obs}=0.551$ eV (see Figs. 4.4, 4.5, 4.6).

Ground and metastable states [45] yields ratio for $^{241}\text{Am}(n,\gamma)^{242g}\text{Am}$ and $^{241}\text{Am}(n,\gamma)^{242m+g}\text{Am}$ reactions is evaluated using the approach of [46], implemented in [47]. The

yields ratio was measured in [48-56].

4.9 Inelastic scattering cross section

Calculated inelastic scattering cross section is very close to previous evaluation of ENDF/B-VII.0 [39], but much different from that of JENDL-4.0 [37] (see Fig. 4.7). Conventional ENDF/B processing codes (i.e. RECENT [61], NJOY [62]) exemplify Hauser-Feshbach-Moldauer formalism. Figure 4.7 shows partial contributions to the inelastic scattering coming from different (l, J)-channels. Major contribution, unlike in case of $^{238}\text{U}+n$ interaction [6], comes from s -wave channels (decay of 2^- and 3^- states), the intermediate contribution comes from p -wave channel (decay of $0^+, 1^+, 2^+, 3^+, 4^+$ compound nucleus states) and the lowest comes from d -wave neutrons (decay of $0^-, 1^-, 2^-, 3^-, 4^-, 5^-$ compound nucleus states). At $E_n \geq 60$ keV, the contribution from p -wave channel (decay of $0^+, 1^+, 2^+, 3^+, 4^+$ compound nucleus states) becomes the largest, as shown on Fig. 4.7. However, that might be considered imposed by the fitting procedures employed. Because Hauser-Feshbach-Moldauer formalism is adopted in conventional ENDF/B processing codes (i.e. RECENT [57], NJOY [58]), the direct excitation of the 0.0418 MeV, $J^\pi=7/2^-$ level is not accounted for explicitly. To compensate for that relevant strength function S_2 for inelastic scattering exit channel was increased at 93.998 keV up to 2.866×10^{-4} . That helped to attain, using conventional processing codes, the fit of relevant capture cross section, calculated with the Hauser-Feshbach-Moldauer formalism.

4.10 Fission cross section

Evaluated fission cross section describes the trend, predicted by the data of Knitter et al. [14], Yamamoto et al. [19], Vorotnikov et al. [26]. We estimated fission cross section in the unresolved resonance energy region using for transition state spectra of ^{242}Am fissioning nuclide, fission barrier parameters were obtained fitting fission cross section data in the first plateau region (see Fig. 4.8). The fission cross section, calculated with the Hauser-Feshbach-Moldauer formalism, reproduces the GMA evaluation within assigned errors in the incident neutron energy range of 0.15 keV~93.998 keV.

5. Optical potential

Calculated total, elastic scattering and absorption cross sections were obtained with the coupled-channel potential parameters, obtained for the ^{237}Np , as described in [7]. The experience of describing the capture cross section of ^{232}Th [5] was the motivation to decrease the real volume potential term V_R by 0.5 MeV. Rotational levels of ground state band $5/2^-$ - $7/2^-$ - $9/2^-$ - $11/2^-$ are assumed coupled (see Table 5.1).

Deformation parameters were tuned to fit S_o and S_l strength function values. Optical model potential parameters are defined as follows:

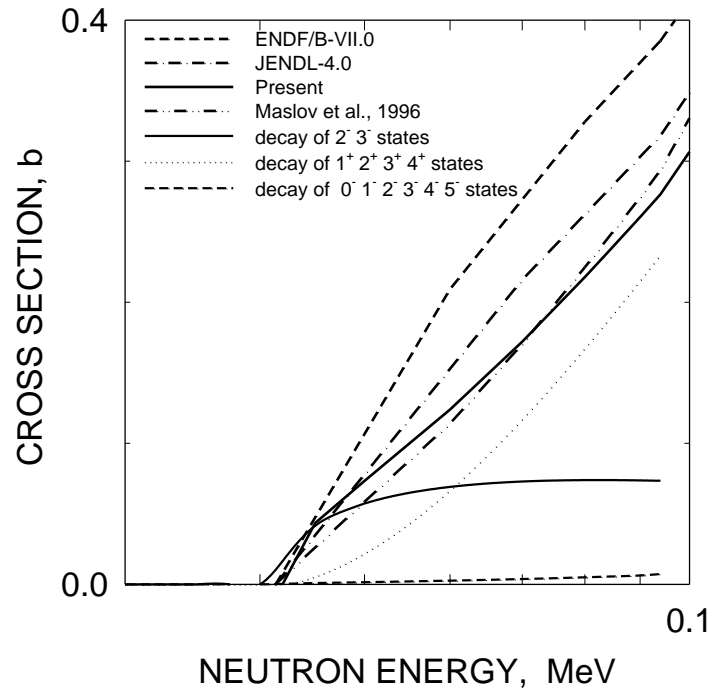


Fig. 4.7 Inelastic cross section of ^{241}Am .

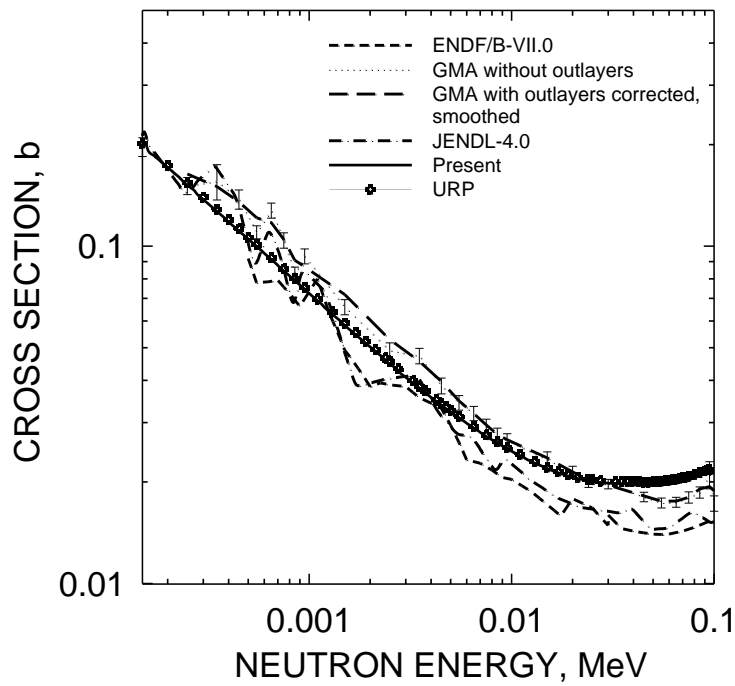


Fig. 4.8 Fission cross section of ^{241}Am .

$$\begin{array}{ll}
V_R=(45.7-0.334E) \text{ MeV}; & r_R=1.2600 \text{ fm}; \quad a_R=.6300 \text{ fm}; \\
W_D=(3.690+0.400E) \text{ MeV}, \quad E_n < 10 \text{ MeV} & r_D=1.24 \text{ fm}; \\
W_D= 7.690 \text{ MeV}, \quad E_n \geq 10 \text{ MeV} & a_D=.5200 \text{ fm}; \\
V_{SO}= 6.2 \text{ MeV}; & r_{SO}=1.12 \text{ fm}; \\
a_{SO}=.47 \text{ fm}; & \beta_2= 0.180 \quad \beta_4=0.06.
\end{array}$$

Table 5.1 ^{241}Am level schema [42].

No.	E	J^π
1	0.0	5/2 ⁻
2	0.0418	7/2 ⁻
3	0.0936	9/2 ⁻
4	0.158	11/2 ⁻
5	0.2059	5/2 ⁺
6	0.234	13/2 ⁻
7	0.235	7/2 ⁺
8	0.239	3/2 ⁻
9	0.272	9/2 ⁺
10	0.273	5/2 ⁻
11	0.312	15/2 ⁻

Partitioning of the total cross section into absorption (reaction) and scattering cross sections allows get reasonable description of available fission and capture cross sections.

6. Total and elastic scattering cross section

Phillips and Howe [44] measured $^{241}\text{Am}+n$ total cross section in the energy range of 0.4-25 MeV. In case of ENDF/B-VII.0 [3] the elastic scattering was simply adjusted to balance total and partial cross sections (see Fig. 6.1).

7. Statistical model

We calculated neutron cross sections within Hauser-Feshbach theory, coupled channel optical model and double-humped fission barrier model.

Hauser-Feshbach-Moldauer [59] and Tepel-Hoffman-Weidenmuller [60] statistical theory is employed for partial cross section calculations below emissive fission threshold. Fissioning and residual nuclei level densities as well as fission barrier parameters are key ingredients, involved in actinide neutron-induced cross section calculations.

In case of fast neutron ($E_n \leq 6$ MeV) interaction with ^{241}Am target nucleus, the main reaction channel is the fission reaction and fission cross section data description serves as a major constraint, except those of GMA-fits, for the neutron inelastic scattering and radiative neutron capture cross section estimates. Below there is an outline of the statistical model employed. For energies below incident neutron energy equal to the cut-off energy of discrete level spectrum, the neutron cross sections arecalculated with Hauser-Feshbach approach with

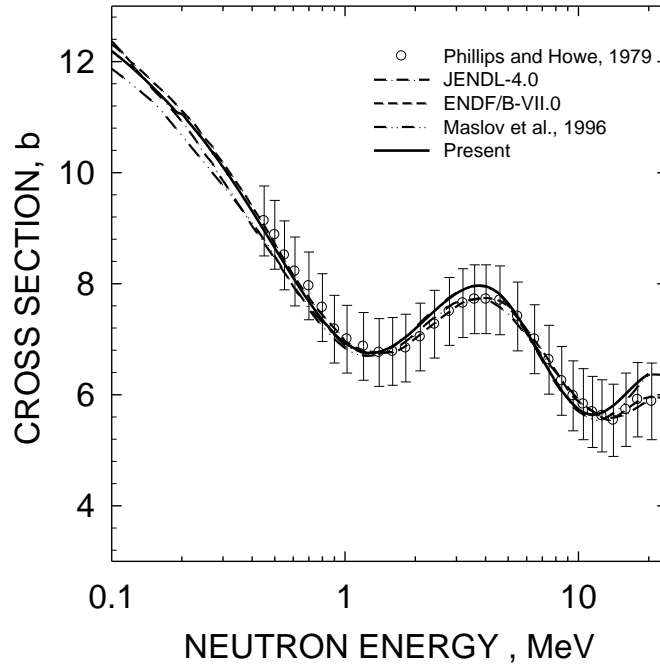


Fig. 6.1 Total cross section of ^{241}Am .

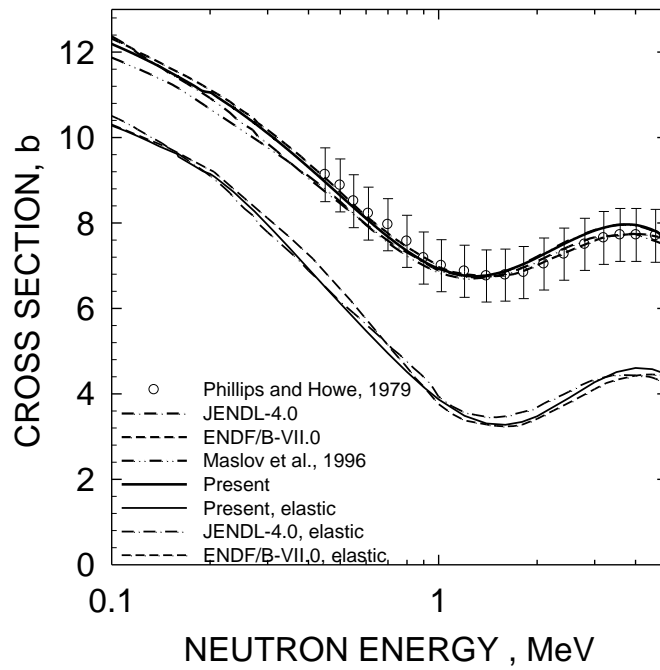


Fig. 6.2 Total and elastic cross section of ^{241}Am .

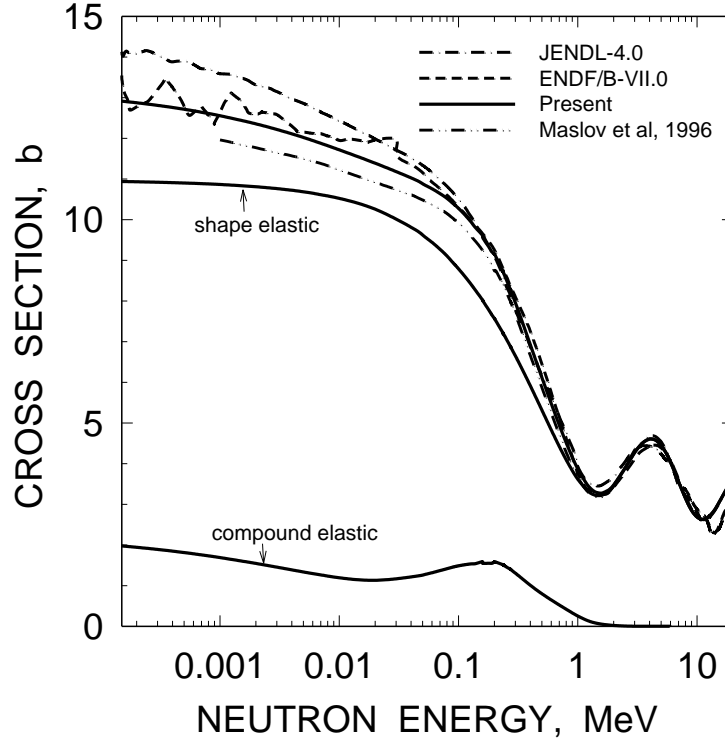


Fig. 6.3 Total and elastic cross section of ^{241}Am .

correction for width fluctuation by Moldauer [59]. For width fluctuation correction calculation only Porter-Thomas fluctuations are taken into account. Effective number of degrees of freedom for fission channel is defined at the higher fission barrier saddle as $\nu_f^{J\pi} = T_f^{J\pi} / T_{\text{fmax}}^{JK\pi}$ where $T_{\text{fmax}}^{JK\pi}$ is the maximum value of the fission transmission coefficient. At higher incident neutron energy the Tepel et al. [60] approach is employed. It describes cross section behavior in case of large number of open entrance/exit channels correctly.

7.1 Level Density

Level density is the main ingredient of statistical model calculations. Level density of fissioning, residual and compound nuclei define transmission coefficients of fission, neutron scattering and radiative decay channels, respectively. The level density was calculated, basically, with a phenomenological model by Ignatyuk et al.. It takes into account shell, pairing and collective effects in a consistent way

$$\rho(U, J^\pi) = K_{\text{rot}}(U, J) K_{\text{vib}}(U) \rho_{\text{qp}}(U, J^\pi), \quad (7.1)$$

where quasi-particle level density is defined as

$$\rho_{\text{qp}}(U, J^\pi) = \frac{(2J+1)\omega_{\text{qp}}(U)}{4\sqrt{2\pi}\sigma_\perp^2\sigma} \exp\left[-\frac{J(J+1)}{2\sigma_\perp^2}\right], \quad (7.2)$$

$\rho_{qp}(U, J^\pi)$ is the state density, $K_{rot}(U, J)$ and $K_{vib}(U)$ are factors of rotational and vibrational enhancement of the level density. The closed-form expressions for thermodynamic temperature and other relevant equations which one needs to calculate $\rho(U, J^\pi)$ provided by Ignatyuk model, see also [5].

To calculate the residual nucleus level density at the low excitation energy, i.e. just above the last discrete level excitation energy where $N^{exp}(U) \approx N^{theor}(U)$, we employ a Gilbert-Cameron-type approach. The procedure is as follows. First, level density parameters are defined, using neutron resonance spacing $\langle D_{obs} \rangle$ estimate for ^{241}Am target nuclide. Constant temperature level density parameters T_o , E_o , U_c (see below for details) are defined by fitting cumulative number of low-lying levels of ^{241}Am (see Fig. 7.1). Figure 7.2 shows the estimate of cumulative number of low-lying levels of ^{242}Am , obtained using systematic of constant temperature level density parameters T_o , E_o , U_c . On this figure levels of odd-odd ^{242}Am nuclide are compared with constant temperature model estimate. The constant temperature approximation of the level density

$$\rho(U) = \frac{dN(U)}{dU} = \frac{1}{T} \exp\left(\frac{U - U_o}{T}\right) \quad (7.3)$$

is extrapolated up to the matching point U_c to the $\rho(U)$ value, calculated with a phenomenological model by Ignatyuk with the condition

$$U_c = U_o - T \ln(T\rho(U_c)). \quad (7.4)$$

In this approach $U_o \approx -m\Delta_o$, where Δ_o is the pairing correlation function, $\Delta_o = 12/\sqrt{A}$, A is the mass number of the nucleus, $m = 2$ for odd-odd, 1 for odd-even nuclei, i.e. U_o has the meaning of the odd-even energy shift. The value of nuclear temperature parameter T obtained by the matching conditions of Eq. (7.4) at the excitation energy U_c .

In present approach the modeling of total level density

$$\rho(U) = K_{rot}(U, J) K_{vib}(U) \frac{\omega_{qp}(U)}{\sqrt{2\pi\sigma}} = \frac{1}{T} \exp\left(\frac{U - U_o}{T}\right) \quad (7.5)$$

in Gilbert-Cameron-type approach looks like a simple renormalization of quasi-particle state density $\omega_{qp}(U)$ at excitation energies $U < U_c$. The cumulative number of observed levels for odd-even ^{241}Am and odd-odd nuclide ^{242}Am [42] are compared with constant temperature approximations for ^{241}Am and ^{242}Am on Figs. 7.1 and 7.2, respectively. Missing of levels above ~ 0.5 MeV is evident in case ^{242}Am .

Few-quasi-particle effects, which are due to pairing correlations, are essential for state density calculation at low intrinsic excitation energies only for equilibrium ^{241}Am deformations. Few-quasi-particle effects in fissioning nuclide ^{242}Am are unimportant because of its odd-odd nature. The partial n-quasi-particle state densities for odd ^{241}Am , which sum-up to intrinsic state density of quasi-particle excitations, modelled using the Bose-gas model prescriptions [61, 62]. The intrinsic state density of quasi-particle excitations $\omega_{qp}(U)$ could be represented as a sum of n-quasi-particle state densities $\omega_{nqp}(U)$:

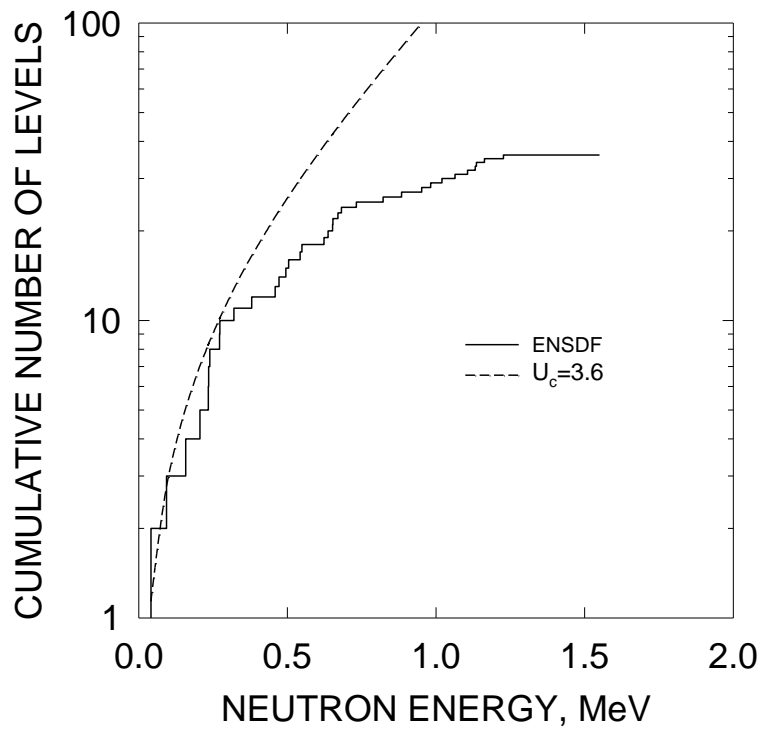


Fig. 7.1 Cumulative sum of levels of ^{241}Am .

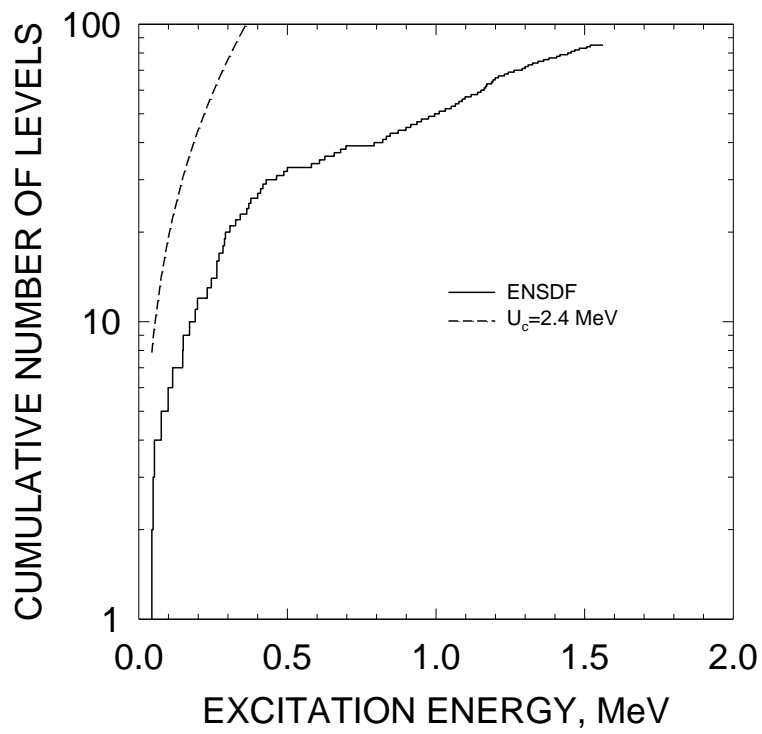
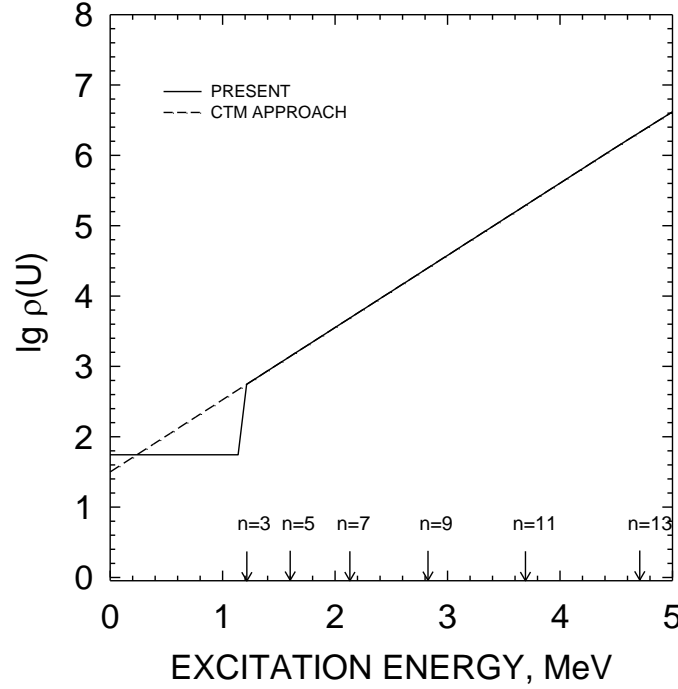


Fig. 7.2 Cumulative sum of levels of ^{242}Am .Fig. 7.3 Level density of ^{241}Am .

$$\omega_{qp}(U) = \sum_n \omega_{nqp}(U) = \sum_n \frac{g^n (U - U_n)^{n-1}}{((n/2)!)^2 (n-1)!}, \quad (7.6)$$

where $g = 6a_{cr}/\pi^2$ is a single-particle state density at the Fermi surface, n is the number of quasi-particles. The important model parameters are threshold values U_n for excitation of n -quasi-particle configurations employed, as applied for fission, inelastic scattering or capture reaction calculations, is provided in [61, 62]. In case of an odd-odd nucleus ^{242}Am Gilbert-Cameron-type approximation of $\rho(U)$ is employed. Nuclear level density $\rho(U)$ of odd nuclide ^{241}Am at equilibrium deformation, as compared with the Gilbert-Cameron-type approximation of $\rho(U)$ is shown on Fig. 7.3. The arrows on the horizontal axis of Fig. 7.3 indicate the excitation thresholds of odd n -quasi-particle configurations.

Main parameters of the level density model for equilibrium, inner and outer saddle deformations are as follows: shell correction δW , pairing correlation functions Δ and Δ_f , at equilibrium deformations $\Delta_o = 12/\sqrt{A}$, quadrupole deformation ε and momentum of inertia at zero temperature F_o/h^2 are given in Table 7.1. For ground state deformations the shell corrections might be calculated as $\delta W = M^{\text{exp}} - M^{\text{MS}}$, where M^{MS} denotes liquid drop mass (LDM), calculated with Myers-Swiatecki parameters [63], and M^{exp} is the experimental nuclear mass. Shell correction values at inner and outer saddle deformations $\delta W_f^{\text{A(B)}}$ are adopted following the comprehensive review by Bjornholm and Lynn [64].

Table 7.1. Level density parameters of fissioning nucleus and residual nucleus

Parameter	Inner saddle	Outer saddle	Neutron channel
δW , MeV	2.5*	0.6	LDM
Δ , MeV	$\Delta_o + \delta^{**}$	$\Delta_o + \delta^{**}$	Δ_o
ε	0.6	0.8	0.24
F_o/h^2 , MeV	100	200	73

*) for axially asymmetric deformations, 1.5 MeV for axially symmetric deformations;

**) $\delta = \Delta_f - \Delta_o$ value is defined by fitting fission cross section in the plateau region.

7.2 Fission cross section

Fission data, processed with GMA-code, are used as a major constraint for capture, elastic and inelastic scattering, (n,2n) and (n,3n) cross sections as well as secondary neutron spectrum estimation. Description of measured fission cross section might justify a validity of level density description and fission barrier parameterization.

7.2.1 Fission Channel

Fission barrier of Am is double-humped [43], in the first "plateau" region and at higher energies we can use double-humped barrier model and relevant barrier parameters. Even at lower energies we could describe the general shape of the fission cross section starting from 0.150 keV.

Neutron-induced fission in a double humped fission barrier model could be viewed as a two-step process, i.e. a successive crossing over the inner hump A and over the outer hump B. Hence, the transmission coefficient of the fission channel $T_f^{J\pi}(U)$ can be represented as

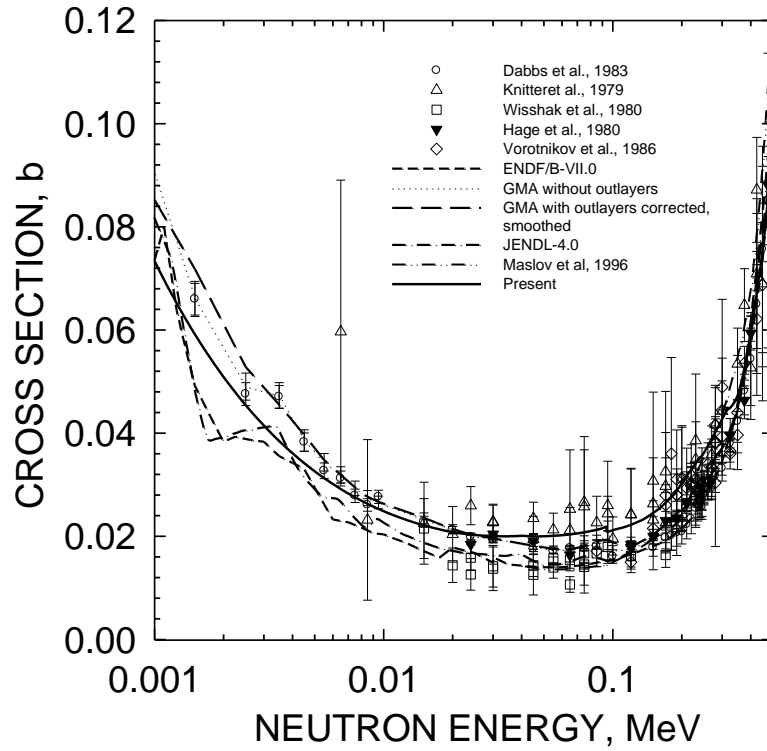
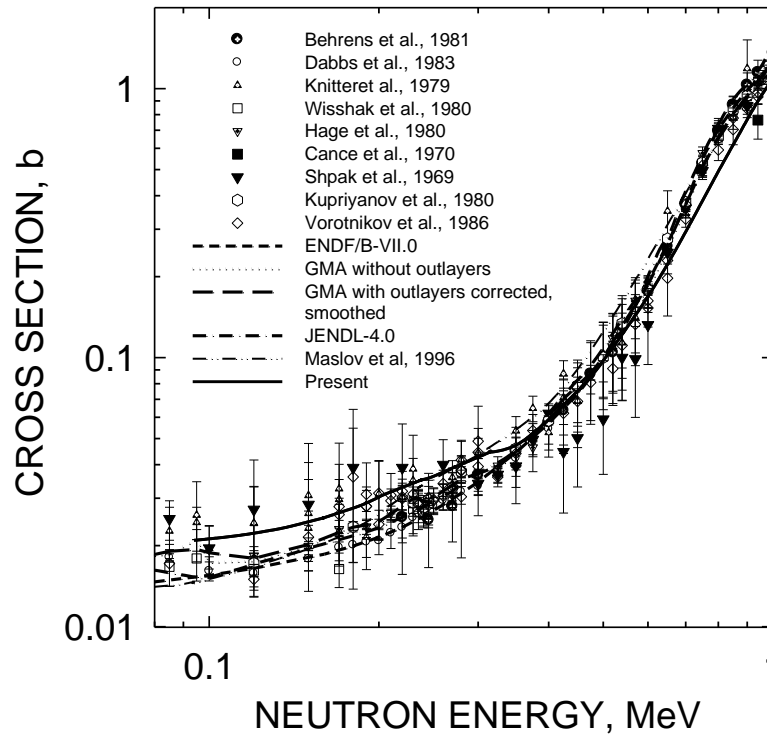
$$T_f^{J\pi}(U) = \frac{T_{fA}^{J\pi}(U)T_{fB}^{J\pi}(U)}{T_{fA}^{J\pi}(U) + T_{fB}^{J\pi}(U)}. \quad (7.7)$$

$T_{fi}^{J\pi}(U)$ is the transmission coefficient, its value is defined by the level density $\rho_{fi}(\varepsilon, J, \pi)$ of the fissioning nucleus at the inner and outer humps ($i = A, B$, respectively):

$$T_{fi}^{J\pi}(U) = \sum_{K=-J}^J T_{fi}^{JK\pi}(U) + \int_0^U \frac{\rho_{fi}(\varepsilon, J, \pi) d\varepsilon}{1 + \exp(2\pi(E_{fi} + \varepsilon - U)/h\omega_i)}, \quad (7.8)$$

where the first term denotes the contribution of low-lying collective states and the second term defines the contribution, coming from the continuum levels at the saddle deformations, ε is the intrinsic excitation energy of fissioning nucleus. The first term contribution due to discrete transition states depends upon saddle symmetry. The total level density $\rho_{fi}(\varepsilon, J, \pi)$ of the fissioning nucleus is determined by the order of symmetry of nuclear saddle deformation.

Inner and outer fission barrier heights and curvatures as well as level densities at both saddles are the model parameters. They are defined by fitting fission cross section data at incident neutron energies below emissive fission threshold. Fission barrier height values and saddle order of symmetry are strongly inter-dependent. The order of symmetry of nuclear shape

Fig.7.4 Fission cross section of ^{241}Am .Fig. 7.5 Fission cross section of ^{241}Am .

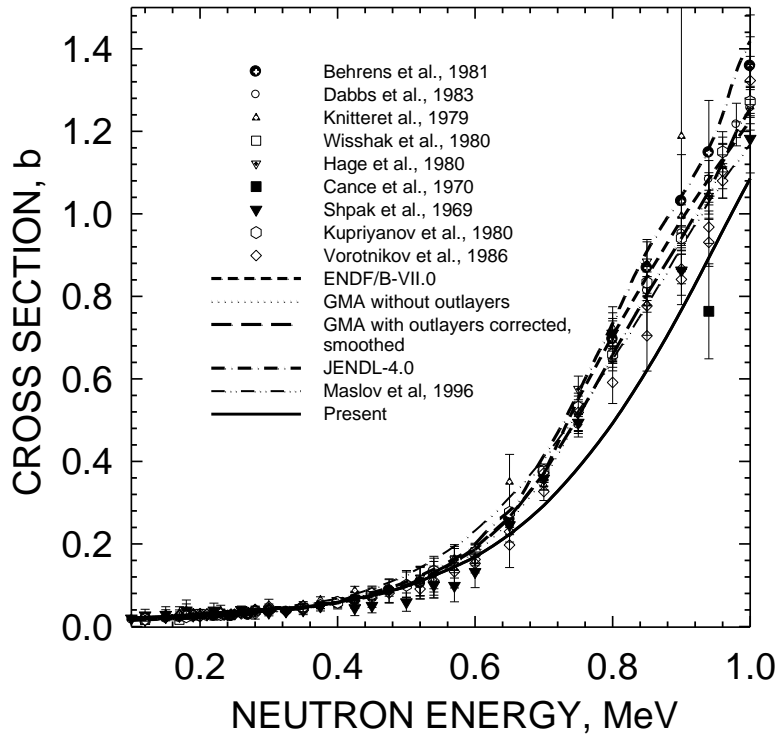


Fig. 7.6 Fission cross section of ^{241}Am .

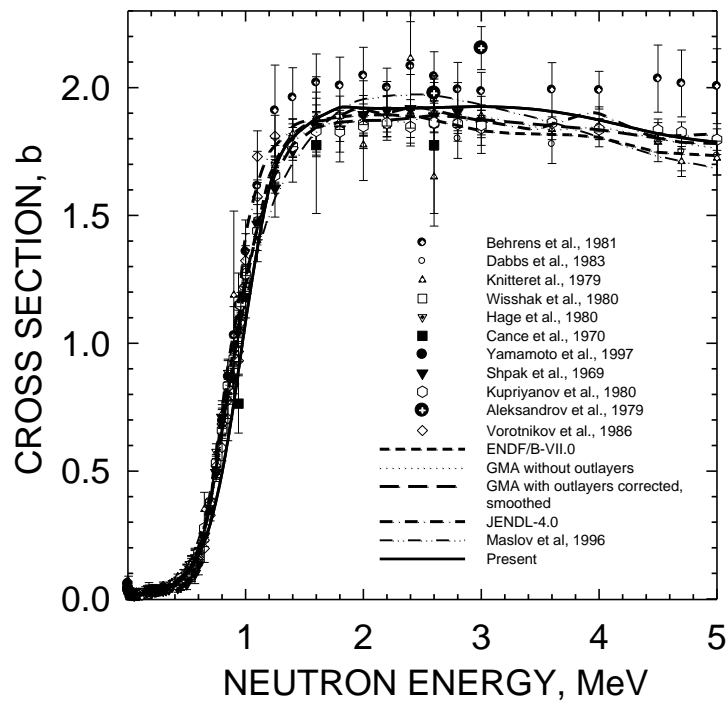


Fig. 7.7 Fission cross section of ^{241}Am .

at saddles was defined by Howard and Moller [69] within shell correction method (SCM) calculation. We adopt the saddle point asymmetries from SCM calculations. According to shell correction method (SCM) calculations of Howard and Moller [65] the inner barriers were assumed axially asymmetric. Outer barriers for the neptunium nuclei are assumed mass-asymmetric.

7.2.2 Fission transmission coefficient, level density and transition state spectrum

Adopted level density description allows describe shape of measured fission cross section data of ^{241}Am (see Figs. 7.4-7.7). One- and tree-quasi-particle states in odd residual nuclide ^{241}Am could be excited. The transition state spectra of odd-odd ^{242}Am nuclide for the band-heads of Table 7.2 were constructed using values of F_o/h^2 at the inner and outer saddles shown in Table 7.1.

We construct the discrete transition spectra up to ~ 175 keV, using collective states of Table 7.2. The discrete transition spectra, as well as continuous level contribution to the fission transmission coefficient are dependent upon the order of symmetry for fissioning nucleus at inner and outer saddles. With transition state spectra defined as described, the fission barrier parameters are obtained.

Table 7.2 Transition spectra band-heads, Z-odd, N-even nuclei

Inner saddle A		Outer saddle B	
K^π	$E_{K\pi}$, MeV	K^π	$E_{K\pi}$, MeV
2^+	0	2^+	0
3^+	0.05	3^+	0.05
3^-	0.05	3^-	0.05
2^-	0.05	2^-	0.05

7.3 Fission data analysis

Fission cross section is calculated with the statistical model from 0.15 keV up to the emissive fission threshold. Measured fission data [10-27] analysis was accomplished within GMA approach [4], as described above. Calculated cross section is consistent with data by Dabbs [12], Knitter et al. [14], Yamamoto et al. [19], Kupriyanov et al. [23], Vorotnikov et al. [26], Protopopov et al. [22], Prindle et al. [11].

Statistical model calculations in the energy of 0.15 keV~6 MeV are maintained, calculated cross sections do not deviate from the GMA evaluation within the GMA-estimated uncertainties, except part of the threshold range.

We fit the weakly decreasing trend of the fission cross section data above $E_n \approx 3$ MeV increasing the correlation function value at outer saddle, which controls the ^{241}Am (n, f) cross section shape. For incident neutron energies up to $E_n \approx 3$ MeV the threshold shape is roughly reproduced by varying the density of one-quasi-particle states of the residual nuclide ^{241}Am , as described in [7, 62] (see Figs. 7.4-7.7). Smooth statistical model calculations are adopted as evaluated fission cross section in the energy range of 0.15 keV~5.5 MeV.

7.4 Inelastic scattering

Fission data fit largely defines the compound inelastic neutron scattering contribution to the total inelastic scattering cross section. The relative contribution of direct discrete level excitation cross sections is much higher than in case of say ^{238}U target nuclide due to much higher fission competition to the compound neutron scattering. That explains the sensitivity of the ^{241}Am compound inelastic scattering cross section to the fission competition and modeling of the residual nuclide level density.

7.4.1 Neutron Channel

The lumped transmission coefficient of the neutron scattering channel is given by the equation

$$T_n^{J\pi}(U) = \sum_{l'j'q'} T_{l'j'}^{J\pi}(E - E_{q'}) + \sum_{l'j'l'} \int_0^{U - U_c} T_{l'j'}^{J\pi}(E') \rho(U - E', I'^{\pi}) dE', \quad (7.9)$$

where $\rho(U - E', I'^{\pi})$ is the level density of the residual nucleus. Levels of residual nuclide ^{241}Am are provided in Table 5.1. The neutron transmission coefficients for the entrance channel $T_{l'j'}^{J\pi}(E')$ are calculated within a rigid rotator coupled channel approach. The compound and direct inelastic scattering components are added incoherently. The exit channel neutron transmission coefficients $T_{l'j'}^{J\pi}(E')$ were calculated using the re-normalized deformed optical potential of entrance channel without coupling, which describes a neutron absorption cross section.

7.4.2 Ground State Rotational Band

Predicted discrete level excitation cross section shape, calculated within a rigid rotator model, depends upon optical potential used. We assume strong missing of levels above excitations of 0.313 MeV (see Fig. 7.1), so only 10 excited levels up to this excitation energy were included when calculating inelastic scattering cross sections. Predicted discrete level excitation cross section shape, calculated within a rigid rotator model, strongly depends upon optical potential used. Calculated compound contribution is controlled mainly by fission competition (see Figs. 7.8-7.15). Figures 7.8, 7.9 and 7.10 show that direct scattering essentially defines the excitation cross section of $J^{\pi}=7/2^-$, $J^{\pi}=9/2^-$ and $J^{\pi}=11/2^-$ levels of the ground state band levels at $E_n \geq 1$ MeV. Discrepancies with previous evaluations are due to both compound and direct contributions differences. The compound component tends to be zero above incident neutron energy of ~ 3 MeV.

7.4.3 Total inelastic cross section

Direct inelastic contributions were added incoherently to Hauser-Feshbach calculated values of compound nucleus inelastic scattering cross sections. It seems that $E_n \sim 1$ MeV is a

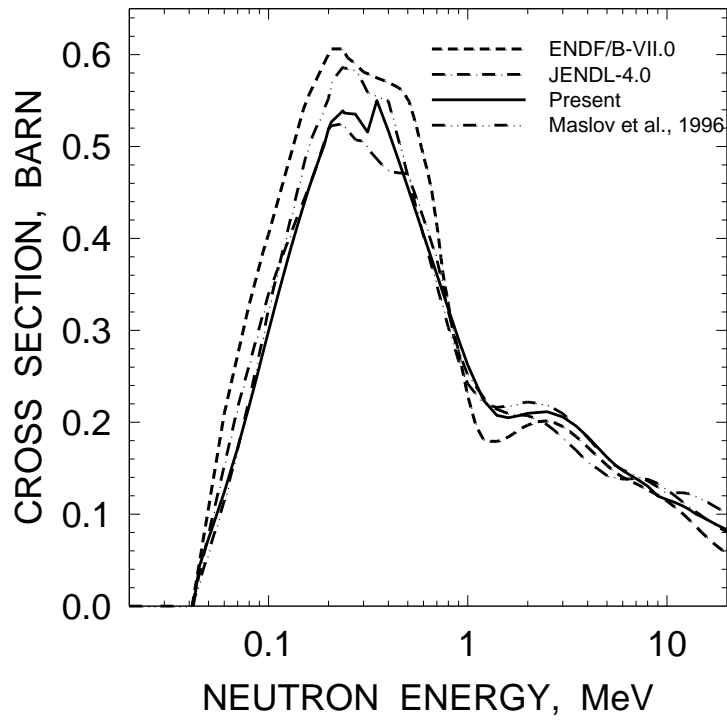


Fig. 7.8 Inelastic cross section of 1st level of ²⁴¹Am.

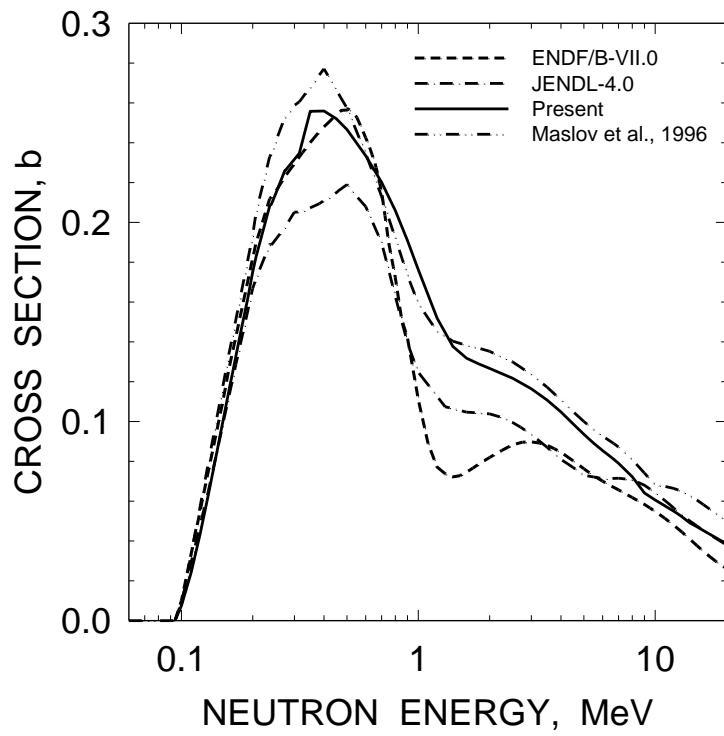


Fig. 7.9 Inelastic cross section of 2nd level of ²⁴¹Am.

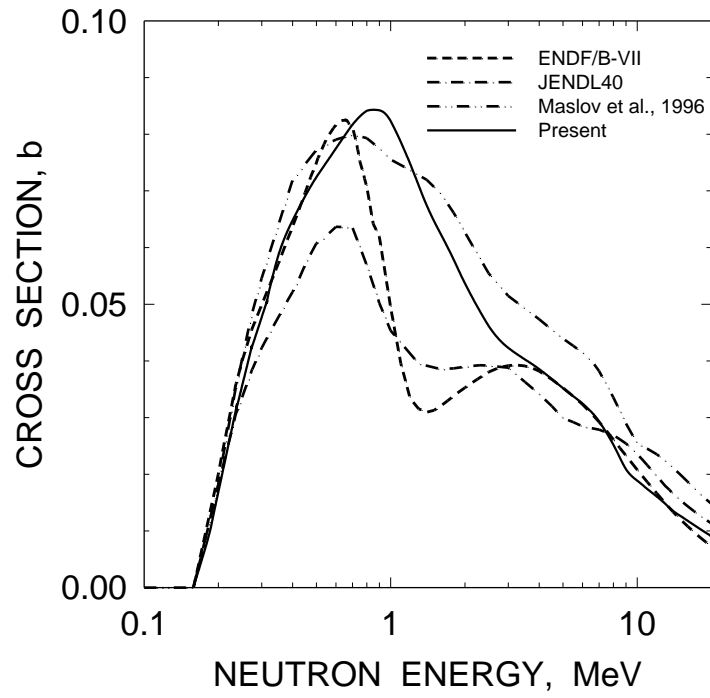


Fig. 7.10 Inelastic cross section of 3rd level of ²⁴¹Am.

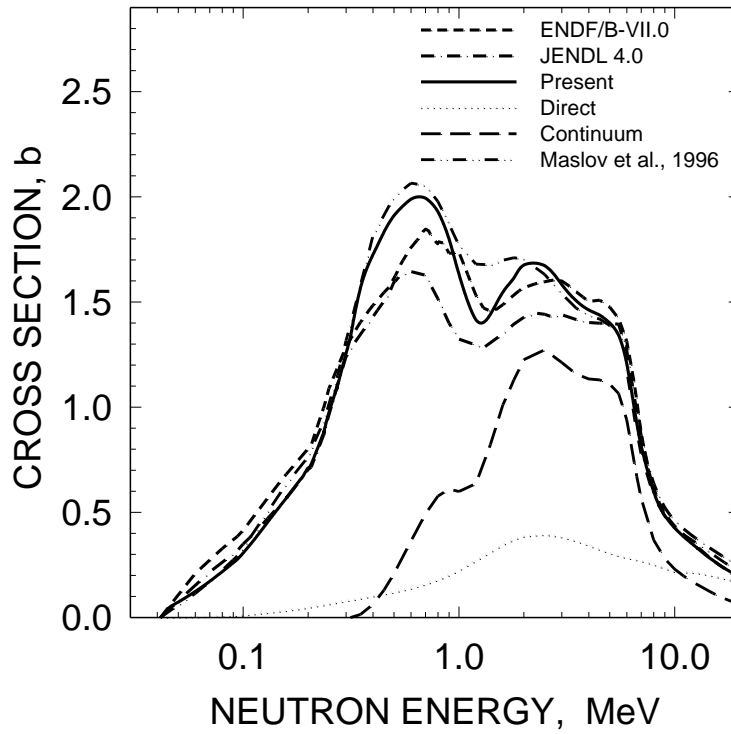


Fig. 7.11 Inelastic cross section of ²⁴¹Am.

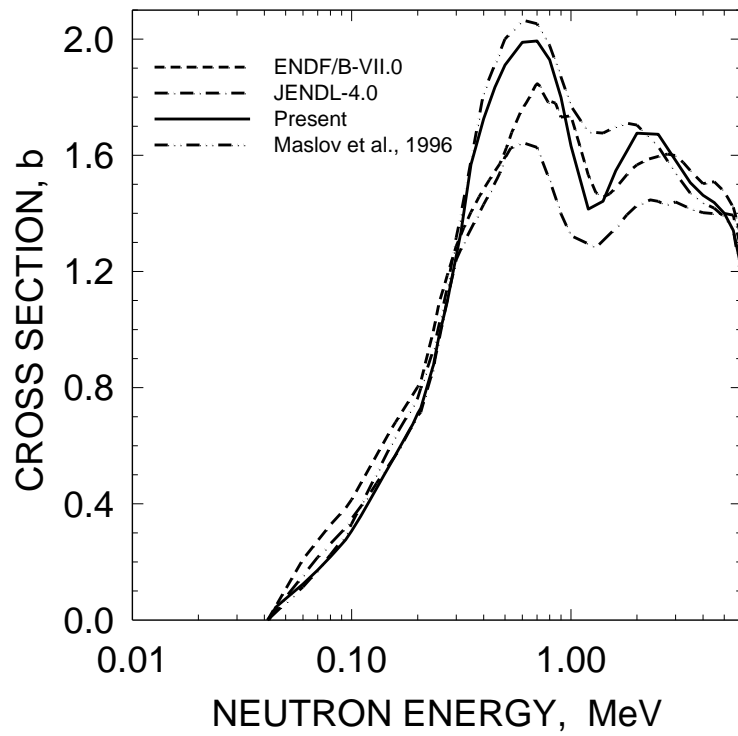


Fig. 7.12 Inelastic cross section of ^{241}Am .

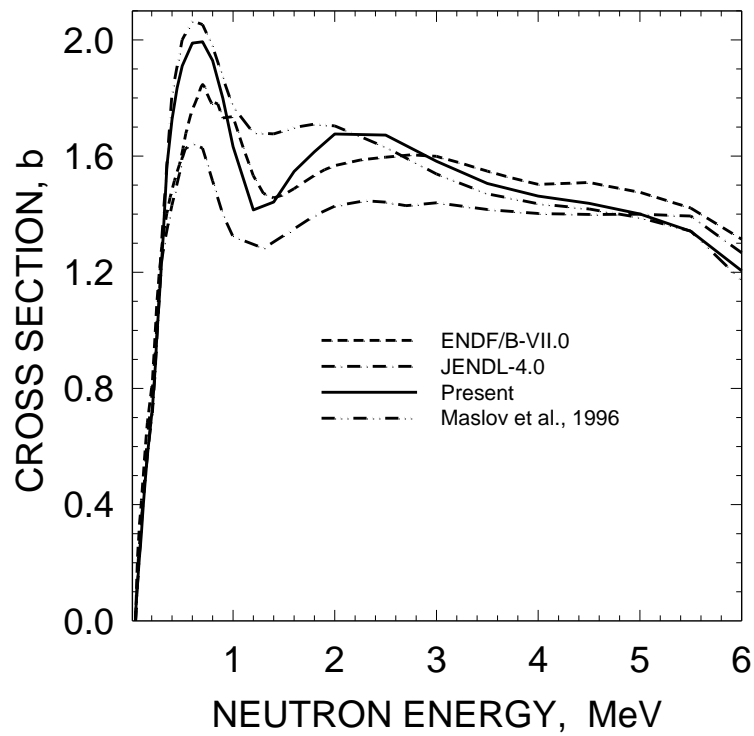


Fig. 7.13 Inelastic cross section of ^{241}Am .

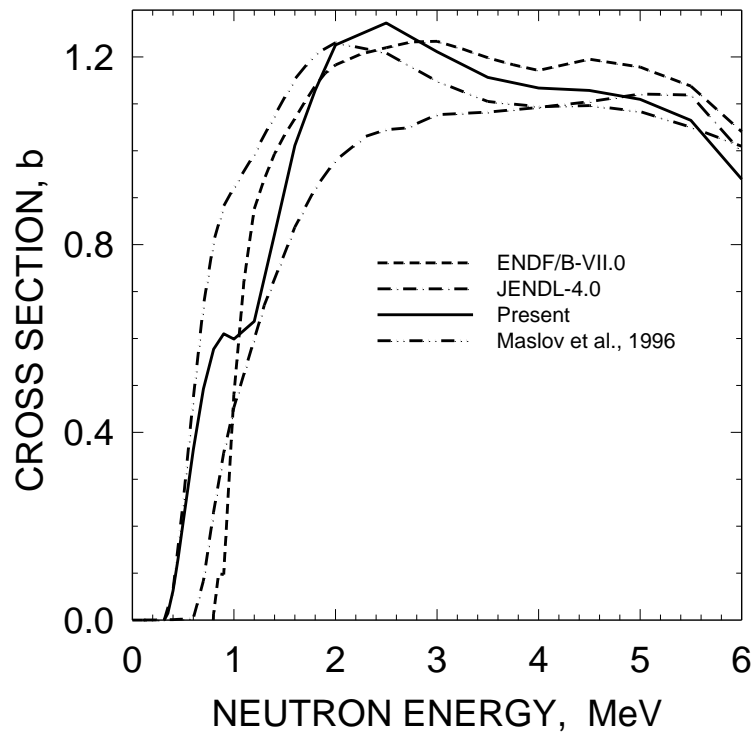


Fig. 7.14 Inelastic cross section of ^{241}Am (continuum contribution).

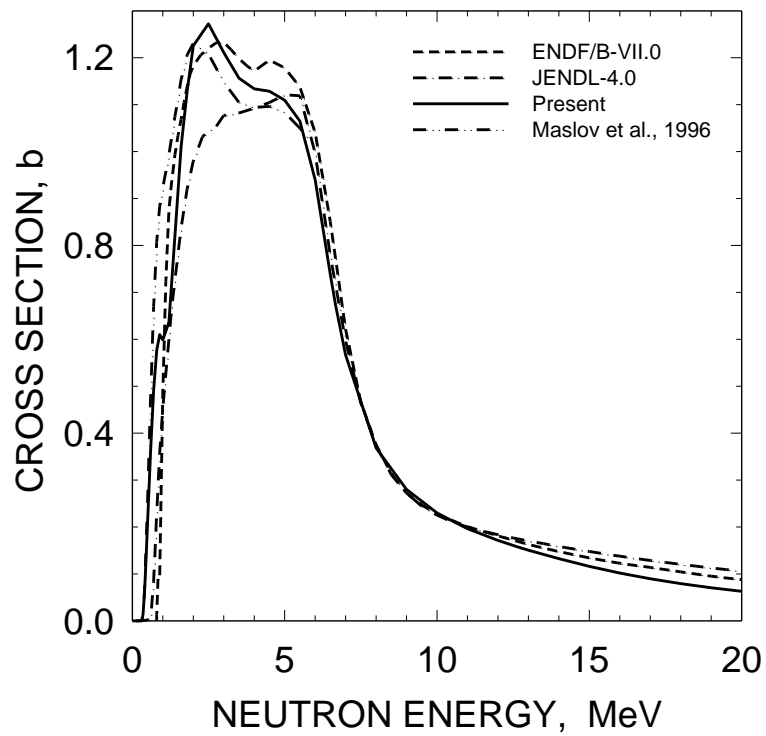


Fig. 7.15 Inelastic cross section of ^{241}Am (continuum contribution)

“stabilization point” of inelastic scattering cross section for present, our previous and ENDF/B-VII.0 [39] evaluations (see Figs. 7.10-7.15). Present calculation is based on the fits of the total and fission cross sections. The evaluated inelastic cross sections of ENDF/B-VII.0 [39] and JENDL-4.0 [37] evaluations are in severe disagreement with our evaluation in the energy range 0.30 MeV – 2 MeV) (see Fig. 7.12 and 7.13).

Upward trend of the inelastic data at $E_n \geq 1.5$ MeV might be explained by the sharp increase of the level density of the residual nuclide ^{241}Am due to the onset of three-quasi-particle excitations [8]. That conclusion is qualitatively supported by the measured data by Kornilov et al [66] for ^{237}Np target nuclide [(see Figs. 7.11-7.12). The total inelastic scattering cross section of JENDL-4.0 [37] is much lower, than present evaluation. The continuum levels contribution to the total inelastic scattering cross section is shown on Figs. 7.14, 7.15.

7.5 Capture cross sections

We have demonstrated by the analysis of measured capture cross sections of $^{238}\text{U}(n, \gamma)$, $^{232}\text{Th}(n, \gamma)$ and $^{237}\text{Np}(n, \gamma)$ [5, 6, 7] that neutron capture data could be described within a Hauser-Feshbach-Moldauer [59] statistical model, reproducing delicate variations of the measured cross sections with the increase of the incident neutron energies. Specifically, in a few-keV energy region calculated capture cross section is defined by the radiative strength function value $S_\gamma = \Gamma_\gamma/D$. At incident neutron energies above $E_n \approx 100$ keV calculated capture cross section shape is defined by the energy dependence of the radiative strength function S_γ . Energy dependence of S_γ is controlled mainly by the energy dependence of the level density of the compound nuclide ^{242}Am . Alongside with neutron emission [40] at the second γ -cascade rather low fission threshold for the ^{242}Am nuclide defines appreciable competition of fission [41], i.e. after first γ -quanta emission.

Then "true" capture reaction cross section $(n, \gamma\gamma)$ is defined using transmission coefficient $T_{\gamma\gamma}^{J\pi}(E)$, which is defined in a two-cascade approximation as

$$T_{\gamma\gamma}^{J\pi}(E) = \frac{2\pi C_{\gamma 1}}{3(\pi\hbar c)^2} \int_0^{E_n + B_n} \varepsilon_\gamma^2 \sigma_\gamma(\varepsilon_\gamma) \sum_{I=|J-1|}^{I=J+1} \rho(U - \varepsilon_\gamma, I, \pi) \frac{T_\gamma^{I\pi}(U)}{T_f^{I\pi}(U) + T_{n'}^{I\pi}(U) + T_\gamma^{I\pi}(U)} d\varepsilon_\gamma. \quad (7.10)$$

The last term of the integrand describes the competition of fission, neutron emission and γ -emission at excitation energy $(U - \varepsilon_\gamma)$ after emission of the first γ -quanta, $C_{\gamma 1}$ is the normalizing coefficient. The transmission coefficients $T_f^{I\pi}(U)$, $T_{n'}^{I\pi}(U)$, $T_\gamma^{I\pi}(U)$ are defined at excitation energy $(U - \varepsilon_\gamma)$. The neutron emission after emission of first γ -quanta strongly depends on the ^{241}Am residual nuclide level density. Namely, at excitations around the pair-breaking threshold U_3 in odd nuclide. The contribution of $(n, \gamma f)$ -reaction [41] to the fission cross section is defined by $T_{\gamma f}^{J\pi}(E)$ value. The energy dependence of $(n, \gamma f)$ reaction transmission coefficient $T_{\gamma f}^{J\pi}(E)$ was calculated with the expression

$$T_{\gamma f}^{J\pi}(E) = \frac{2\pi C_{\gamma 1}}{3(\pi\hbar c)^2} \int_0^{E_n + B_n} \varepsilon_\gamma^2 \sigma_\gamma(\varepsilon_\gamma) \sum_{I=|J-1|}^{I=J+1} \rho(U - \varepsilon_\gamma, I, \pi) \frac{T_f^{I\pi}(U)}{T_f^{I\pi}(U) + T_{n'}^{I\pi}(U) + T_\gamma^{I\pi}(U)} d\varepsilon_\gamma. \quad (7.11)$$

Competition of $(n, \gamma n')$ reaction is taken into account in a similar way. Above neutron energy 5.5 MeV capture cross section value is assumed to be 0.001 barn.

Trends of the measured data by Wisshak et al. [15], Weston et al. [28], Vanpraet et al. [32], and Jandel et al. [31] are inconsistent with each other. Measured data for the $^{241}\text{Am}(n, \gamma)$ reaction cross section [15, 28, 31, 32] shown on Figs. 3.8, 3.9, 3.10, are scattering a lot, or there are a systematic shifts between different data sets. The GMA-fit follows the data by Weston et al. [288] and Vanpraet et al. [32]. In the incident neutron energy range of 20-300 keV, the calculated capture cross section closely follows the GMA-fit. The lower trend, which follows from the data of Wisshak et al. [15] is divergent with the former one at $E_n < 20$ keV. However, the data by Wisshak et al. [15] in the range of 10~100 keV support the theoretical calculation, based on consistent description of total and fission measured data, as well as the estimate of radiation strength function ($\langle \Gamma_\gamma \rangle = 48.4$ meV and $\langle D_{obs} \rangle = 0.551$ eV) and absorption cross section.

Recent measured data by Jandel et al. [31] predict distinctly different cross section shape than the previous data [15, 28, 32] in tens of keV range, and scatter a lot at lower energies. Relatively high cross section data in 0.150 - 20 keV energy range could be reproduced with much increased value of $\langle \Gamma_\gamma \rangle = 65$ meV or increased by ~ 1 MeV value of $W_D = 4.69$ MeV. Combined influence of both factors brings the calculated cross section in consistency with the data by Weston et al. [28], Vanpraet et al. [32] in the 0.15 keV – 20 keV energy range. However, the resulting value of $S_o = 1.5 \times 10^{-4}$ appears to be much higher than the evaluated value. Obviously, the s -wave neutron strength function S_o value could be decreased by decreasing the β_2 , quadrupole deformation parameter value, but after that the calculated capture cross section will again misfit the data, shown on Figs. 3.8, 3.9, 3.10, 7.16. The high cross section level below

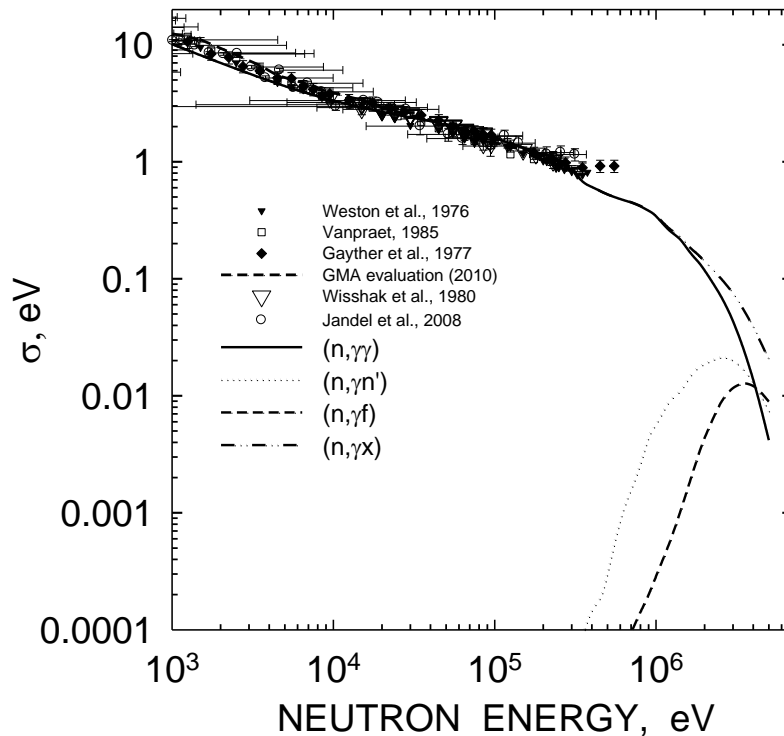


Fig. 7.16 Capture cross section of ^{241}Am

20 keV could be reproduced only by drastic increase of the absorption cross section value. In that case the value of S_0 would increase up to 1.5×10^{-4} . That possibility also should be rejected. The shape of the capture cross section, shown on Figs. 7.16, 7.17, 7.18 resembles the increased competition of fission and inelastic scattering channels to the radiation capture channel. Another factor is the entrance channel, exemplified by the neutron transmission coefficients. The evaluated cross section of ENDF/B-VII.0 [39] and JENDL-4.0 [37] are consistent with present calculation in the energy range of 0.15 – 200 keV. They also do not reproduce the measured data by Weston et al. [28] and Vanpraet et al. [32] in the energy range of 0.15-20 keV. At $E_n \sim 1.5$ MeV one observes strong increase of the inelastic scattering cross section $^{241}\text{Am}(n, n')$ (see Fig. 7.13).

Finally, Fig. 7.16 shows calculated capture cross section and competition of $^{241}\text{Am}(n, \gamma f)$ and $^{241}\text{Am}(n, \gamma n')$ reactions to the “true” capture reaction $^{241}\text{Am}(n, \gamma \gamma)$, they define the capture cross section shape at $E_n \geq 2$ MeV.

7.6 Branching ratio of short-lived ^{242g}Am (1^-) and long-lived ^{242m}Am (5^-) states of ^{242}Am

The neutron capture reaction $^{241}\text{Am}(n, \gamma)$ populates either the $T_{1/2} = 16\text{h}$ ground state ^{242g}Am with $J^\pi = 1^-$ or the ^{242m}Am isomer $J^\pi = 5^-$ with $T_{1/2} = 141\text{y}$. The ground state ^{242g}Am mostly β^- -decays to ^{242}Cm , or goes to ^{242}Pu via electron capture. The yield of the ^{242g}Am short-lived ground state in the reaction chain $^{241}\text{Am}(n, \gamma) ^{242g}\text{Am}(\beta^-) ^{242}\text{Cm}$ influences the α -activity and neutron activity of the spent fuel due to emerging nuclides ^{242}Cm and ^{238}Pu . The yield of the ^{242m}Am long-lived isomer state, which due to large and odd value of $J^\pi = 5^-$ may decay to ^{242g}Am via isomeric transition only, emerging in the capture reaction $^{241}\text{Am}(n, \gamma) ^{242m}\text{Am}$, influences the neutron activity of the spent fuel due to spontaneous fission of ^{242m}Am . It gives a path for the ^{244}Cm yield via $^{242m}\text{Am}(n, \gamma) ^{243}\text{Am}(n, \gamma) ^{244m}\text{Am}(\beta^-(\epsilon)) ^{244}\text{Cm} (^{244}\text{Pu})$ or $^{242m}\text{Am}(n, \gamma) ^{243}\text{Am}(n, \gamma) ^{244g}\text{Am}(\beta^-) ^{244}\text{Cm}$. If not the forbidden β^- -decay of ^{242m}Am state, the major path for the ^{244}Cm accumulation would have been closed. Ground ^{242g}Am and isomer ^{242m}Am states of the residual nuclide ^{242}Am are excited in the reaction $^{243}\text{Am}(n, 2n) ^{242g(m)}\text{Am}$ as well. The same approach as in case of capture reaction is applied to predict the branching ratio $R(E_n) = 1/(1 + r(E_n))$, $r(E_n) = \sigma_{n\gamma}^g(E_n)/\sigma_{n\gamma}^m(E_n)$ from thermal energy to 20 MeV could be defined by the ratio of the populations of two lowest states in ^{242}Am (see Sood et al. [45]). These populations are defined by the γ -decay of the excited states, described by the kinetic equation, developed by Strutinsky et al. [46]. The branching ratio $r(E_n)$ is defined by the ratio of the populations of the two lowest states, ^{242g}Am , with spin $J = 1$ and ^{242m}Am , with spin $J = 5$.

The γ -decay of the excited nucleus is described by the kinetic equation [46] as further developed by Dovbenko et al. [51]:

$$\frac{\partial \omega_k(U, J^\pi, t)}{\partial t} = \sum_{J^{\pi'}} \int_0^{U_g} \omega_{k-1}(U', J^{\pi'}, t) \frac{\Gamma_\gamma(U', J^{\pi'}, U, J^\pi)}{\Gamma(U', J^{\pi'})} dt - \omega_k(U, J^\pi, t) \frac{\Gamma_\gamma(U, J^\pi)}{\Gamma(U, J^\pi)}, \quad (7.12)$$

here $\omega_k(U, J^\pi, t)$ is the population of the state J^π at excitation U at time t , after emission of k γ -quanta; $\Gamma_\gamma(U', J^{\pi'}, U, J^\pi)$ is the partial width of γ -decay from the $(U', J^{\pi'})$ to the state (U, J^π) , while $\Gamma(U, J^\pi)$ is the total decay width of the state (U, J^π) . For any state (U, J^π) with the excitation energy $0 \leq U \leq U_g$, the initial population is

$$(7.13)$$

$$\omega_k(U, J^\pi, t=0) = \delta_{k0} \omega_0(U, J^\pi) \quad (7.13)$$

That equation means in the initial state we deal with the ensemble of states (U, J^π) . Integrating the Eq. (7.12) over t , one gets the population $W(U, J^\pi)$ of the state (U, J^π) after emission of k γ -quanta:

$$\begin{aligned} \omega_k(U, J^\pi, \infty) - \omega_k(U, J^\pi, 0) &= \sum_{J^{\pi'}} \int_U^{U_g} \frac{\Gamma_\gamma(U', J^{\pi'}, U, J^\pi)}{\Gamma(U', J^{\pi'})} \int_0^\infty \omega_{k-1}(U', J^{\pi'}, t) dt dU' - \\ &\frac{\Gamma_\gamma(U, J^\pi)}{\Gamma(U, J^\pi)} \int_0^\infty \omega_k(U, J^\pi, t) dt \end{aligned} \quad (7.14)$$

Denoting the population of the state (U, J^π) after emission of k γ -quanta

$$W_k(U, J^\pi) = \frac{\Gamma_\gamma(U, J^\pi)}{\Gamma(U, J^\pi)} \int_0^\infty \omega_k(U, J^\pi, t) dt, \quad (7.15)$$

and taking into account the condition that $\omega_k(U, J^\pi, \infty) = 0$ for any state, belonging to ensemble (U, J^π) , Eq. (7.14) could be rewritten as

$$W_k(U, J^\pi) = \sum_{J^{\pi'}} \int_U^{U_g} \frac{\Gamma_\gamma(U', J^{\pi'}, U, J^\pi)}{\Gamma(U', J^{\pi'})} W_{k-1}(U', J^{\pi'}) dU' + \omega_k(U, J^\pi, 0). \quad (7.16)$$

The population of any state (U, J^π) after emission of any number of γ -quanta is

$$W(U, J^\pi) = \sum_k W_k(U, J^\pi), \quad (7.17)$$

then from Eq. (7.16) one easily gets

$$W(U, J^\pi) = \sum_{J^{\pi'}} \int_U^{U_g} \frac{\Gamma_\gamma(U', J^{\pi'}, U, J^\pi)}{\Gamma(U', J^{\pi'})} W(U', J^{\pi'}) dU' + W_0(U, J^\pi). \quad (7.18)$$

The integral equation (7.18) in the code STAPRE [47] is solved as a system of linear equations, the integration range (U, U_g) is binned, in the assumption that there are no γ -transitions inside the bins.

The isomer branching ratio depends mostly on the low-lying levels scheme and relevant γ -transitions probabilities. Though some experimental data are available for ^{242}Am [45], we will use a simplified approach, since level scheme and gamma-decay intensities are still incomplete. Modeling of low-lying levels of ^{242}Am in [45] is accomplished based on the assumption that ground and first few excited states are of two-quasi-particle nature. For actinides with quadrupole deformations the superposition principle is usually adopted, the band-head energies of the doubly-odd nucleus are generated by adding to the each unpaired configuration (Ω_p, Ω_n) , as observed in the isotopic/isotonic $(A-1)$ nucleus, the rotational energy contribution and residual

n - p interaction energy contribution. The angular momenta of neutron and proton quasi-particles could be parallel or anti-parallel. In the independent quasi-particle model the two-quasi-particle states, $K^+ = |K_n + K_p|$ and $K^- = |K_n - K_p|$, are degenerate. Gallaher-Moshkowsky doublets [45] appear because of n - p residual interaction. Figure 7.17 shows employed band-head energies for the two-quasi-particle states expected in the odd-odd nuclide ^{242}Am up to 700 keV. The spectroscopic properties of two pairs of proton and neutron single particle states were derived from those experimentally observed in the isotopic ($Z=95$) and isotonic ($N=147$) odd-mass nuclei with mass ($A-1$). Figure 7.19 shows levels expected, which have similar ordering as experimentally observed levels [45]. For the band-heads, shown on Figure 7.19, the generated rotational band levels are

$$E_{JK\pi} = E_{JK} + 5.5[J(J+1) - K(K+1)]. \quad (7.19)$$

Obviously, the schema presented on Fig. 7.17 does not represent a complete set to allow the calculation of absolute yields of ^{242}Am (n,γ) $^{242\text{m}}\text{Am}$ and ^{242}Am (n,γ) $^{242\text{g}}\text{Am}$ reactions. Rotational bands were constructed up to 700 keV excitation, modeling levels with spin $J^\pi \leq 10$, in total up to ~ 70 levels. It was shown in [38], that simple estimate of the number of levels in odd-odd nuclei as

$$N(U) = e^{2\Delta_0/U} (e^{U/T} - 1), \quad (7.20)$$

predicts up to ~ 280 level at $U \sim 700$ keV, $T = 0.388$ MeV, $\Delta = 12/A^{1/2}$, MeV. We assume that the modeled angular momentum distribution would not be much different from more realistic

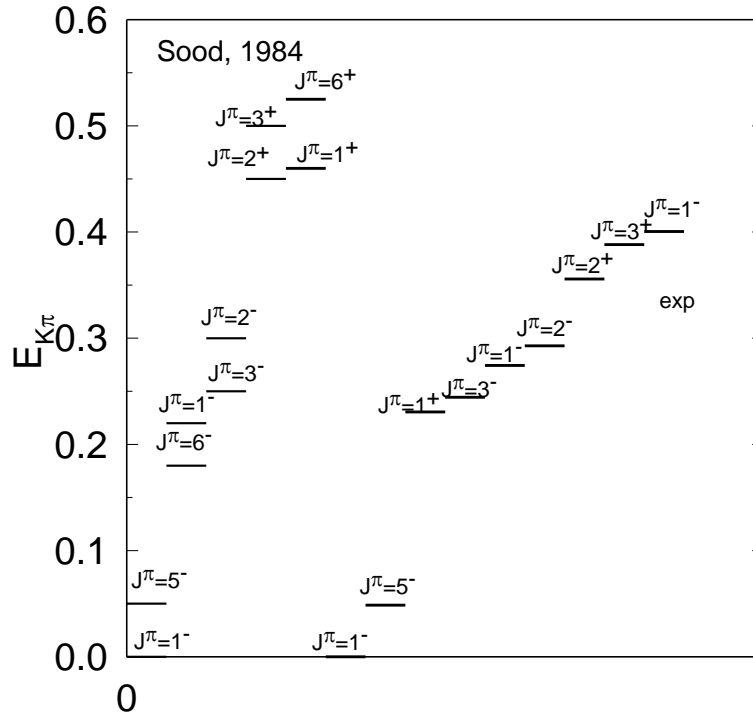


Fig. 7.17 Levels of ^{242}Am .

estimates. Since the complete data on the γ -transitions are missing, we assumed the simple decay scheme: only E1, E2 and M1 transitions are allowed in a continuum excitation energy range. Inter-band transitions forbidden, only γ -transitions within the rotational bands are possible. In such approach the populations of the lowest five level doublets could be calculated. Then we assumed that the transition to the isomer state $J^\pi = 5^-$ or low-spin, short-lived ground state $J^\pi = 1^-$ is defined by the “minimal multipolarity” rule. That means the states with spins $J < 3$ should populate the ground state, while those with $J \leq 3$ should feed the isomer state. Then the branching ratio could be obtained as the ratio of the populations, derived from Eq. (8.9):

$$r(E_n) = \frac{\sum_{J < (J_I + J_g)/2} W(U, J^\pi)}{\sum_{J \geq (J_I + J_g)/2} W(U, J^\pi)} \quad (7.21)$$

Figures 7.18, 7.19 show the yield of $^{241}\text{Am}(n,\gamma)^{242g}\text{Am}$ relative to $^{241}\text{Am}(n,\gamma)^{242m+g}\text{Am}$ reactions cross section., calculated for the modeled level schema, presented at Fig. 7.17. The modeled level scheme appears to be quite compatible with the measured data set on the ^{242g}Am ground state yield. The measured data allow without further normalizations accept calculated relative yield in the range 100 keV-20 MeV. It strongly depends on the incident neutron energy and differs from previous evaluations. From thermal energy, where the most measurements are grouping, to the 100 keV linear approximation is adopted.

7.7. Analysis of experimental data for the isomeric capture cross section ratio for ^{241}Am

The main goal was to analyze and correct experimental cross section data to the latest standards and to evaluate the isomeric cross section ratio for $^{241}\text{Am}(n,\gamma)^{242g}\text{Am}$ and $^{241}\text{Am}(n,\gamma)^{242m+g}\text{Am}$ reactions [35, 48–55].

The neutron radiative capture on ^{241}Am leads to formation of long-lived metastable ^{241m}Am ($T_{1/2} = 141 \pm 2$ year) and “short-lived” ground state ^{241g}Am ($T_{1/2} = 16.02 \pm 0.02$ hour), total and partial thermal capture cross sections and related resonance integrals are measured. Microscopic experimental cross section data for the $^{241}\text{Am}(n,\gamma)^{242m+g}\text{Am}$ reaction are presented in [35, 48-55]. Experimental information on the $^{241}\text{Am}(n,\gamma)^{242m+g}\text{Am}$ reaction excitation function covers the neutron energy range from 0.020 eV to 313.9 keV. Integral cross sections of the $^{241}\text{Am}(n,\gamma)$ reaction measured for the ^{235}U fission spectrum and for neutron spectra of fast reactors are presented in [48, 55, 56]. Corrected to new standards experimental data at neutron energy 0.0253 eV and averaged over thermal neutron spectra are given on Figs. 7.20 and 7.21.

Integral cross-section for the $^{241}\text{Am}(n,\gamma)^{242g}\text{Am}$ by Ivanova et al. [56], which were obtained by the irradiation of the ^{241}Am sample in the ^{235}U neutron fission spectrum, may be used for testing the $^{241}\text{Am}(n,\gamma)^{242g}\text{Am}$ reaction yield. Below, in Table 7.1, are given the results of testing evaluated yields for the $^{241}\text{Am}(n,\gamma)^{242g}\text{Am}$ reaction from present evaluation, ENDF/B-VII.0 and JENDL-4.0 libraries and relevant experimental data [56]. Data for the ^{235}U thermal fission neutron spectrum were taken from three different sources. It is evident from Table 7.1, that present evaluation of yield of ^{242g}Am state in a 50 keV- 2 MeV energy range is compatible with experimental data [60].

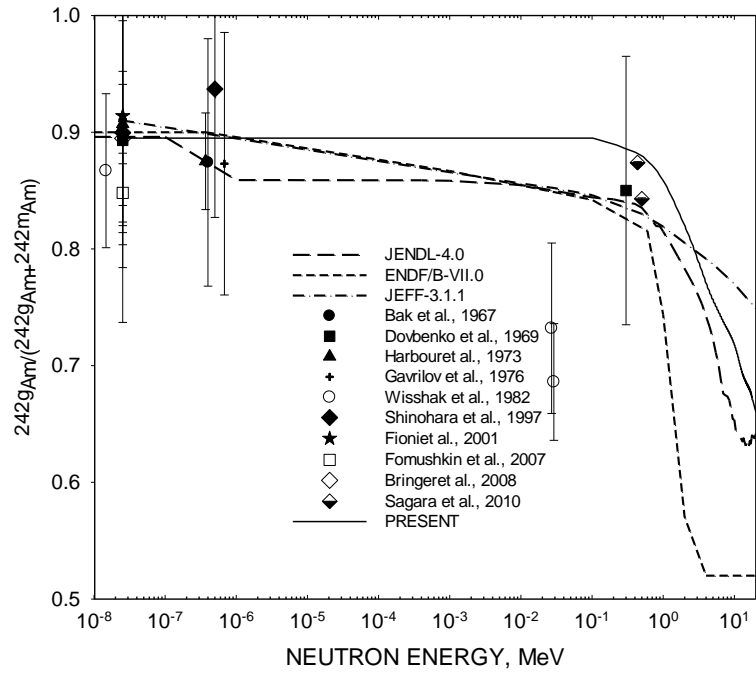


Fig. 7.18 Yield of $^{241}\text{Am}(n,\gamma)^{242g}\text{Am}$ relative to $^{241}\text{Am}(n,\gamma)^{242m}\text{Am}$ reactions cross section.

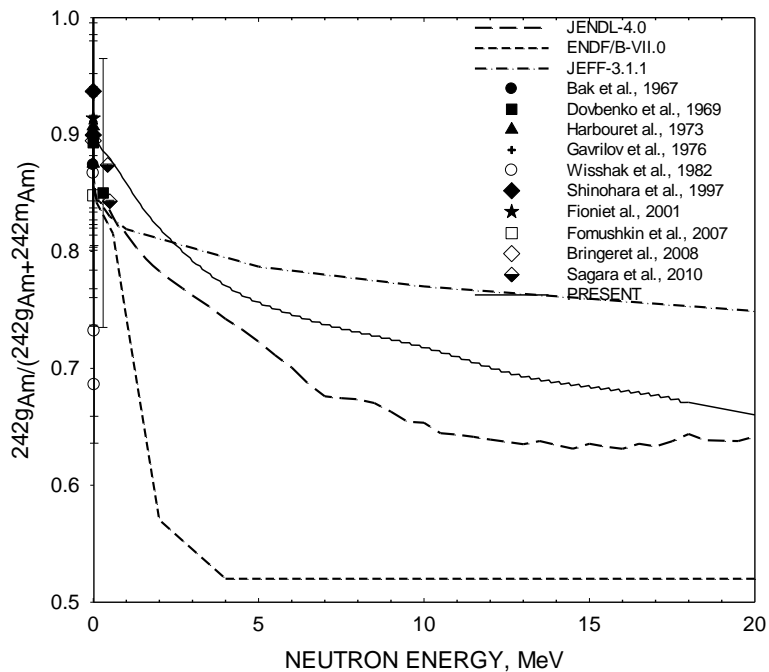


Fig. 7.19 Yield of $^{241}\text{Am}(n,\gamma)^{242g}\text{Am}$ relative to $^{241}\text{Am}(n,\gamma)^{242m}\text{Am}$ reactions cross section.

Table 7.1. Integral cross section for the reaction $^{241}\text{Am}(n,\gamma)^{242g}\text{Am}$ in the ^{235}U thermal fission neutron spectrum.

$^{235}\text{U}(n, F)$ thermal prompt fission neutron spectrum adopted from ENDF/B-VI evaluation

Source of data	$\langle\sigma^g\rangle$, mb	C/E	90%-Response range, MeV
present	240.17	1.00071	0.0575 - 2.10
ENDF/B-VII.0	205.99	0.85829	0.0500 - 1.80
JENDL-4.0	192.72	0.80300	0.0500 - 1.90
[56]	240 ± 30.0		

$^{235}\text{U}(n, F)$ thermal prompt fission neutron spectrum adopted from Maslov et al. [3]

Source of data	$\langle\sigma^g\rangle$, mb	C/E	90%-Response range, MeV
Present	248.20	1.03417	0.0550 - 2.10
ENDF/B-VII.0	213.71	0.89046	0.0475 - 1.80
JENDL-4.0	200.18	0.83408	0.0550 - 1.90
[56]	240 ± 30.0		

$^{235}\text{U}(n, F)$ thermal prompt fission neutron spectrum adopted from GMA evaluation Maslov et al. [3]

Source of data	$\langle\sigma^g\rangle$, mb	C/E	90%-Response range, MeV
Present	252.55	1.05229	0.0550 - 2.10
ENDF/B-VII.0	217.91	0.90796	0.0475 - 1.80
JENDL-4.0	204.32	0.85133	0.0550 - 1.90
[56]	240 ± 30.0		

8. Fission cross section above emissive fission threshold

$$\sigma_{\text{nf}}(E_n) = q(E_n) \frac{\pi \hat{\lambda}^2}{2(2I+1)} \sum_{J\pi} (2J+1) T_1(E_n) P_f^{J\pi}(E_n), \quad (8.1)$$

and x-th chance fission contributions as

$$\sigma_{\text{nF}}(E_n) = \sigma_{\text{nf}}(E_n) + \sum_{x=1}^X \sigma_{\text{n,xnf}}(E_n). \quad (8.2)$$

The contributions to the observed fission cross section $\sigma_{\text{n,xnf}}(E_n)$, coming from (n, xnf), $x=0, 1, 2, 3 \dots X$, fission of relevant equilibrated americium nuclei are weighted with a probability of x neutron emission before fission. These cross sections are calculated as

$$\sigma_{\text{n,xnf}}(E_n) = \sum_{J\pi} \int_0^{U_{\text{max}}} W_{x+1}^{J\pi}(U) P_{f(x+1)}^{J\pi}(U) dU, \quad (8.3)$$

where $W_x^{J\pi}$ is the population of (x+1)-th nucleus at excitation energy U after emission of x neutrons, excitation energy U_{max} is defined by the incident neutron energy E_n and the energy, removed from the composite system ^{242}Am by the $^{241}\text{Am}(n, \text{xnf})$ pre-fission neutrons.

Contribution of first-chance fission $\sigma_{\text{nf}}(E_n)$ is defined by the pre-equilibrium emission of the first neutron and the fission probability P_{f1} of the ^{242}Am nuclide

$$\sigma_{f1} = \sigma_c (1 - q(E)) P_{f1}. \quad (8.4)$$

Once the contribution of first neutron pre-equilibrium emission fraction $q(E)$ is fixed, the first-chance fission probability P_{f1} of the ^{242}Am is defined by the level densities of fissioning ^{242}Am and residual ^{241}Am nuclides. Actually, it depends on the ratio of shell correction values $\delta W_{fA(B)}$ and δW_n . Different theoretical calculations of the shell corrections as well as of the fission barriers vary by 1-2 MeV. The same is true for the experimental shell corrections, which are obtained with a smooth component of potential energy calculated according to the liquid-drop or droplet model. However the isotopic changes of $\delta W_{fA(B)}$ and δW_n [64] are such that P_{f1} viewed as a function of the difference $(\delta W_{fA(B)} - \delta W_n)$ is virtually independent on the choice of smooth component of potential energy. Therefore, we shall consider the adopted $\delta W_{fA(B)}$ estimates to be effective, provided that δW_n are obtained with the liquid drop model. In the first "plateau" region and at higher energies we can safely use double-humped barrier model and relevant barrier parameters (see Table 8.1).

The fission probabilities $P_{fx}^{J\pi}$ of ^{241}Am and ^{240}Am nuclides, fissioning in ^{241}Am (n, nf) and $^{241}\text{Am}(n, 2nf)$ reactions, respectively, could be estimated using data of surrogate fission reaction data. Surrogate data were obtained in $^{240}\text{Pu}(^3\text{He}, \text{df})$ reaction. The consistent description of a most complete set of measured data on the (n, F), (n, 2n), (n, 3n) and (n, 4n) reaction cross sections for the ^{238}U target nuclide up to 20 MeV [67] enables one to consider the estimates of first neutron

Table 8.1 Fission barrier parameters of Am nuclei

Nuclide	E_{fA}	δE_{fA}	sym.A	E_{fB}	δE_{fB}	sym.B	$h\omega_A$	$\delta h\omega_A$	$h\omega_B$	$\delta h\omega_B$	δ
^{239}Am	6.0	0.5	axial	5.4	0.3	mass- asym.	1.0	0.2	0.5	0.2	0.0
^{240}Am	5.8	0.5	axial	5.5	0.3	mass- asym.	0.6	0.2	0.4	0.2	0.0
^{241}Am	6.3	0.5	axial	5.15	0.3	mass- asym.	0.8	0.2	0.51 5	0.2	0.0
^{242}Am	6.51 5	0.1	Non- axial	5.95	0.05	mass- asym.	0.7	0.05	0.44	0.2	0.02

spectra emitted from the composite ^{242}Am nuclide fairly realistic. In case of $^{241}\text{Am}(n, F)$ cross section, for which there are systematic discrepancies in measured data [10-27], calculated cross section is consistent with data by Dabbs [12], Knitter et al. [14], Yamamoto et al. [19], Kupriyanov et al. [23], Vorotnikov et al. [26], Protopopov et al. [22] and Prindle et al. [11].

Figures 8.1-8.2 demonstrate the fission data fit from 100 keV up to 20 MeV. The contributions of emissive $^{241}\text{Am}(n, nf)$ and $^{241}\text{Am}(n, 2nf)$ fission to the total fission cross section, shown on Figs. 8.1 - 8.2 were further tuned within the statistical model [64], reproducing the $^{241}\text{Am}(n, 2n)$ and $^{241}\text{Am}(n, F)$ reaction cross sections consistently.

9. (n,2n) and (n,3n) cross sections

The reaction chain $^{241}\text{Am}(n, 2n)^{240}\text{Am}$ is used to measure the (n,2n) cross section by induced γ -activity. Data by Filatenkov et al. [68], by Loughheed et al. [69], by Perdikakis et al. [70], Vieira et al. [71], Tonchev et al. [72] and by Sage et al. [73] are used. Cross sections of (n,2n) and (n,3n) reactions are obtained from the statistical model calculations with account of pre-equilibrium neutron emission (modified STAPRE code [47] was used). Pre-equilibrium neutron emission contribution fixed according to the consistent description of (n, F) and (n, xn) reaction data for ^{238}U and ^{232}Th target nuclides [67].

Experimental data [68-73] were renormalized to the new standards in the decay data and cross sections for the monitor reactions. Excitation functions for the $^{27}\text{Al}(n, \alpha)^{24}\text{Na}$, $^{58}\text{Ni}(n, p)^{58}\text{Co}$, $^{58}\text{Ni}(n, 2n)^{57}\text{Ni}$, $^{93}\text{Nb}(n, 2n)^{92m}\text{Nb}$ and $^{197}\text{Au}(n, 2n)^{196}\text{Au}$ monitor reactions used here as a new standards were tested on recent evaluated integral experimental data by Mannhart [57, 58] for the ^{235}U thermal fission and ^{252}Cf spontaneously fission neutron spectra.

Around ~14 MeV neutron energy data by Loughheed et al. [69] agree in the limit of uncertainties with experimental data by Filatenkov et al. [68]. However, the $^{241}\text{Am}(n, 2n)^{240}\text{Am}$ reaction cross sections determined by Loughheed et al. by α counting of the ^{240}Am agree slightly better with data [68] and [69-73].

Experimental data given in [71] are preliminary. Final results of the $^{241}\text{Am}(n, 2n)^{240}\text{Am}$ reaction cross sections measurement in the energy range 7.59-14.46 MeV are presented in [72].

Cross sections measured by Perdikakis et al. [70] at 8.80 and 9.60 MeV agree within uncertainties with experimental data [72, 73], in the interval 10.6-11.4 MeV they are 1.7 times higher than predicted by theoretical modeling calculations and experimental data [68-73].

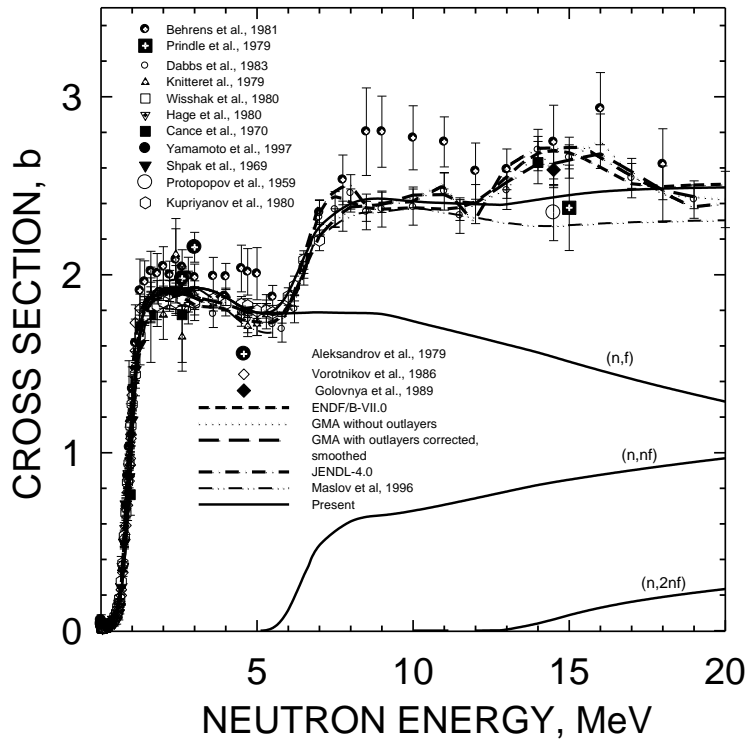


Fig. 8.1 Fission cross section of $^{241}\text{Am}(n, f)$.

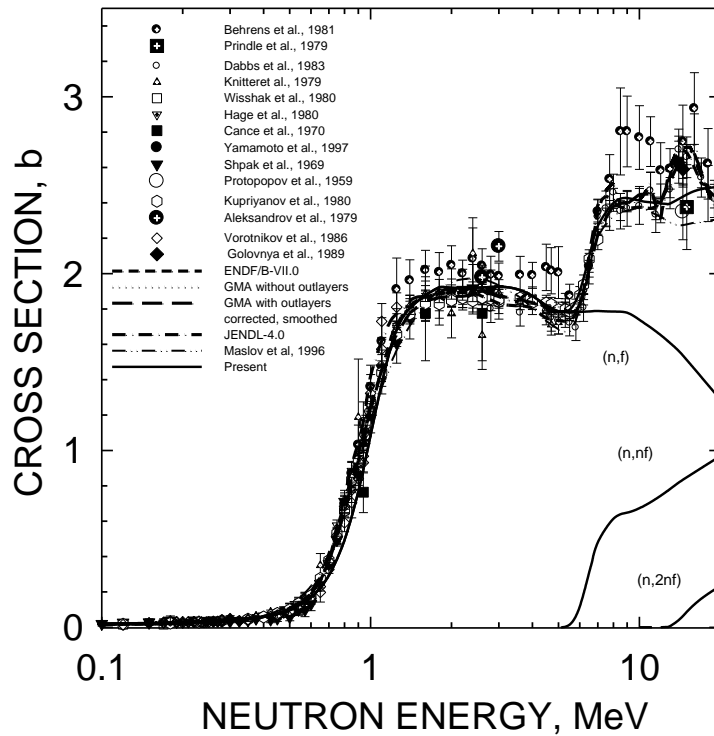


Fig. 8.2 Fission cross section of $^{241}\text{Am}(n, f)$.

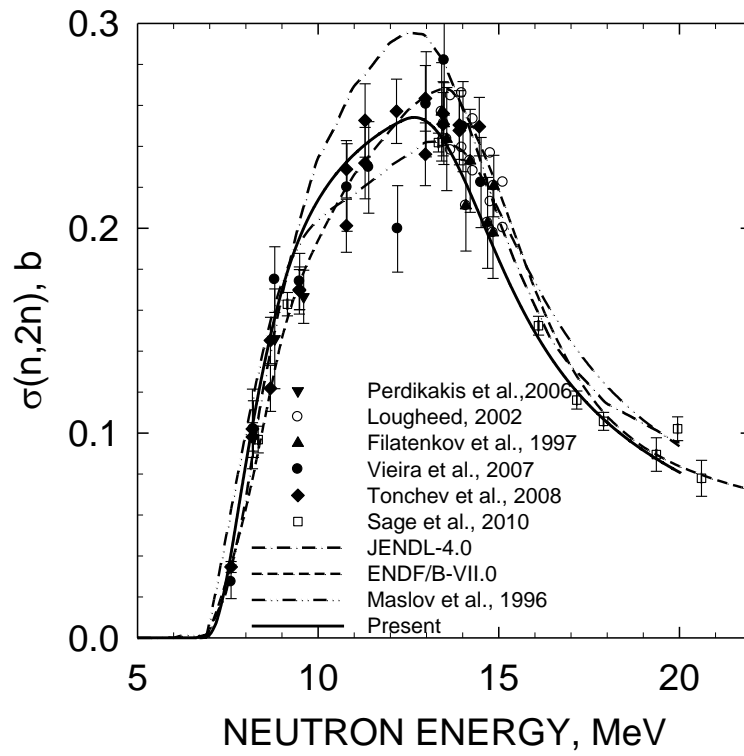


Fig. 9.1 $^{241}\text{Am}(n,2n)^{240}\text{Am}$ reaction cross section

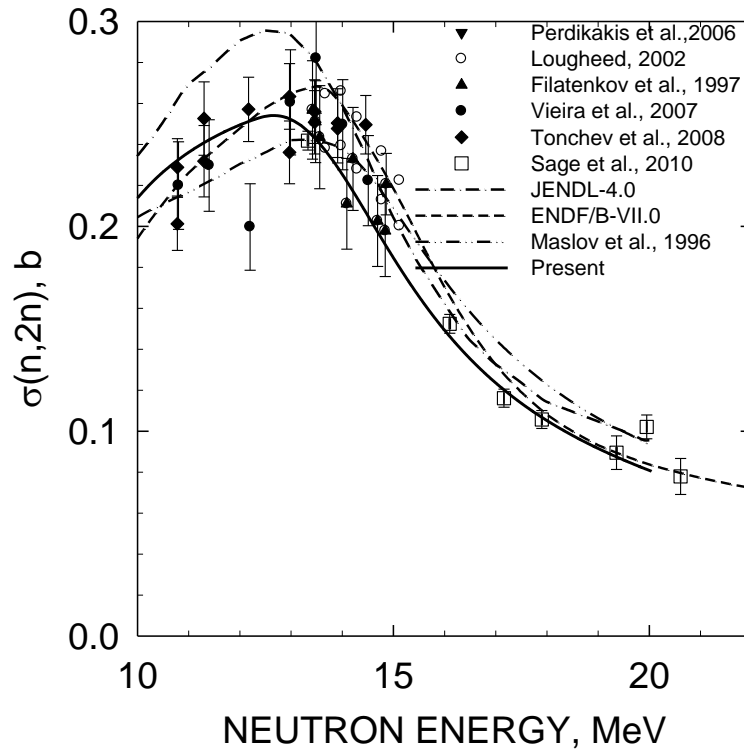


Fig. 9.2 Cross section of $^{241}\text{Am}(n,2n)$ reaction

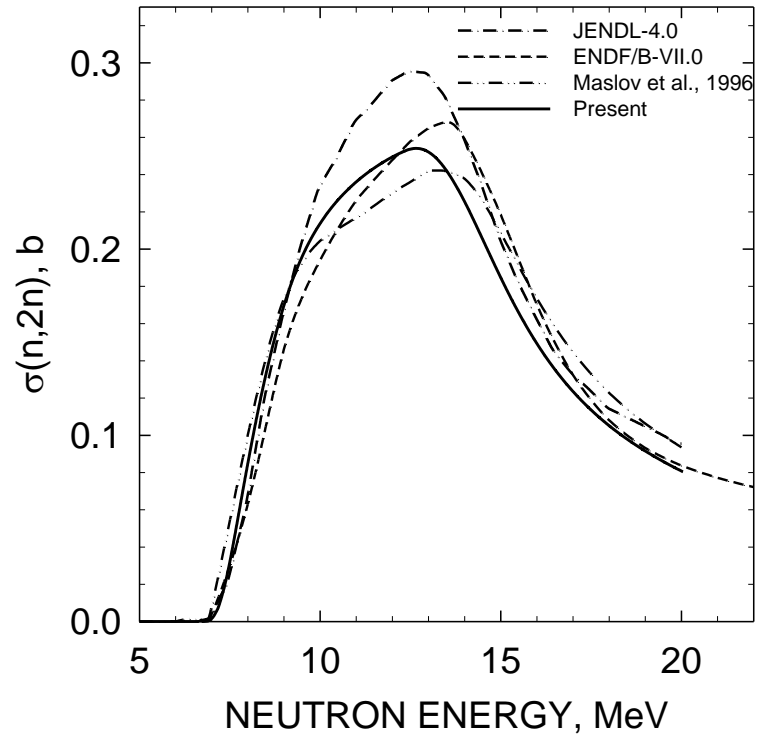


Fig. 9.3 Cross section of ^{241}Am (n, 2n) reaction\

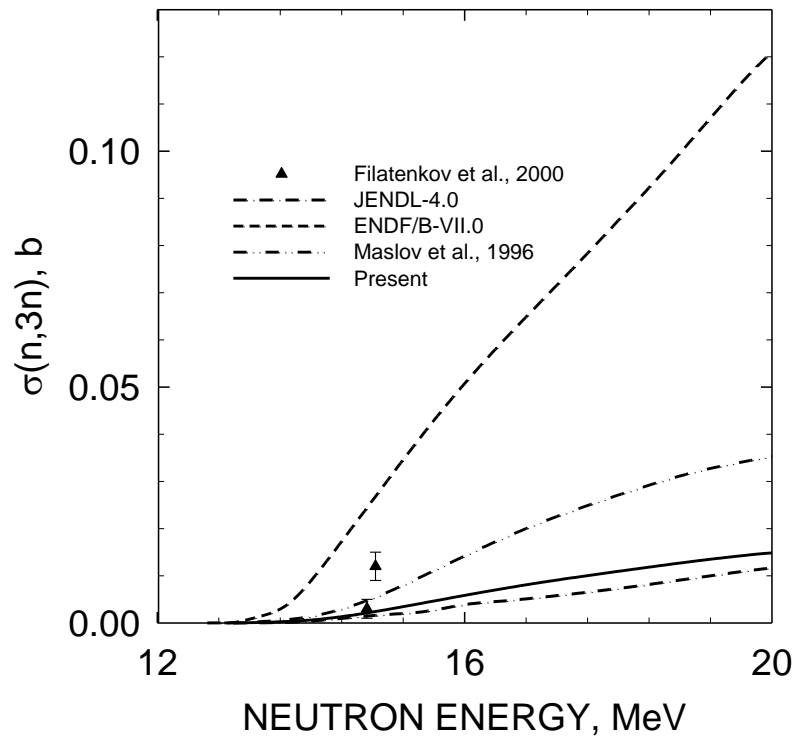


Fig. 9.4 Cross section of ^{241}Am (n, 2n) reaction

Calculated $^{241}\text{Am}(n,2n)$ cross section agrees with measured data better than previous evaluations. The evaluated excitation function for the $^{241}\text{Am}(n,2n)^{240}\text{Am}$ reaction done within polynomial PADE-approximation in the neutron energy range from threshold to 20 MeV is also compatible with calculated data. JENDL-4.0 evaluation [36] in comparison with other evaluations and experimental data gives systematically overestimated cross section values in the energy ranges from threshold to 12.8 MeV and from 9.2 to 14 MeV, respectively. It should be stressed once again, that our evaluation of fission cross section is a simultaneous statistical model description of both $(n,2n)$ and (n, F) reactions for ^{241}Am .

10. Average prompt fission neutron number ν_p for $^{241}\text{Am}(n, F)$ reaction

Average prompt neutron yields in neutron induced fission of ^{241}Am were evaluated in non-model least-squares fit of the experimental data with the use of the GMA code. The experimental data obtained in three groups were used in the evaluation.

A.J. Jaffey and J.L. Lerner [75] measured ν_p for $^{241}\text{Am}(n, F)$ at thermal reactor beam as ratios to ν_p of ^{233}U , ^{235}U , ^{239}Pu and ^{252}Cf . These ratios were converted to absolute yields using standards evaluation [74]. These four data sets were used in the fit as partially correlated data because of the uncertainty of the mass of the ^{241}Am sample. Uncertainties of the data were increased by ~ 2 or ~ 3 times in the final fit to remove discrepancy between these four values. The uncertainty of the data of other measurements was increased introducing additional components of the uncertainty. The final chi-square value per degree of freedom in the fit was close to 1.

V.I. Lebedev and V.I. Kalashnikova measurements [77] also were done at thermal reactor neutron beam, relative to the ν_p for $^{235}\text{U}(n, F)$. Standard value for ν_p of $^{235}\text{U}(n,F)$ [76] was used. Measured data are lower than the ν_p values obtained in [75], but agree with the linear extrapolation to the thermal point energy of the spline curve, which fits data at higher energy. The uncertainty of the data [77] was increased ~ 3 times to make data consistent with [75].

The measurement by Khokhlov et al. [78] was done in the energy range between 0.77 and 11 MeV. The measurement was done relative to ν_p of $^{252}\text{Cf}(sf)$. They have been renormalized to new standard value for $^{252}\text{Cf}(sf)$ [79]. That is a single measurement of the energy dependent ν_p . The experimental data above thermal energy were reduced to the nodes of the evaluated ν_p , covariance matrix of uncertainties was constructed from the components of uncertainties of [75].

The results of non-model GMA evaluation (central values only) were smoothed using the polynomial fits of different orders. Above 11 MeV the present model calculations were used. The best consistency with the statistical model calculations above ~ 11 MeV was obtained for the 3-rd order polynomial fit of GMA non-model evaluation.

Final smoothed evaluation, measured data and ENDF/B-VII.0 evaluation are shown in Figs. 10.1, 10.2, 10.3 in different scales and energy ranges. Figure 10.4 compares different calculations and evaluations. The uncertainty of the evaluation at thermal point is about $\sim 1.2\%$, it is not correlated with uncertainties at higher energies. The uncertainty increased from $0.7 - 0.8\%$ at ~ 1 MeV to $3 - 4\%$ at ~ 11 MeV. The cross-energy correlations between uncertainties at low energies are relatively high ($0.4 - 0.6$) and low at high energies. That is explained by relative contribution of statistical component of the uncertainty. The energy dependence ν_p may increase at energies higher than thermal energy. At energy of a few tens of keV it may reach thermal value and increase in a linear fashion (see e.g. evaluations of ν_p for nuclei with a large number of measured data [78]), we may conclude, that the measurements by A.J. Jaffey and J.L. Lerner [75] overestimate the ν_p by

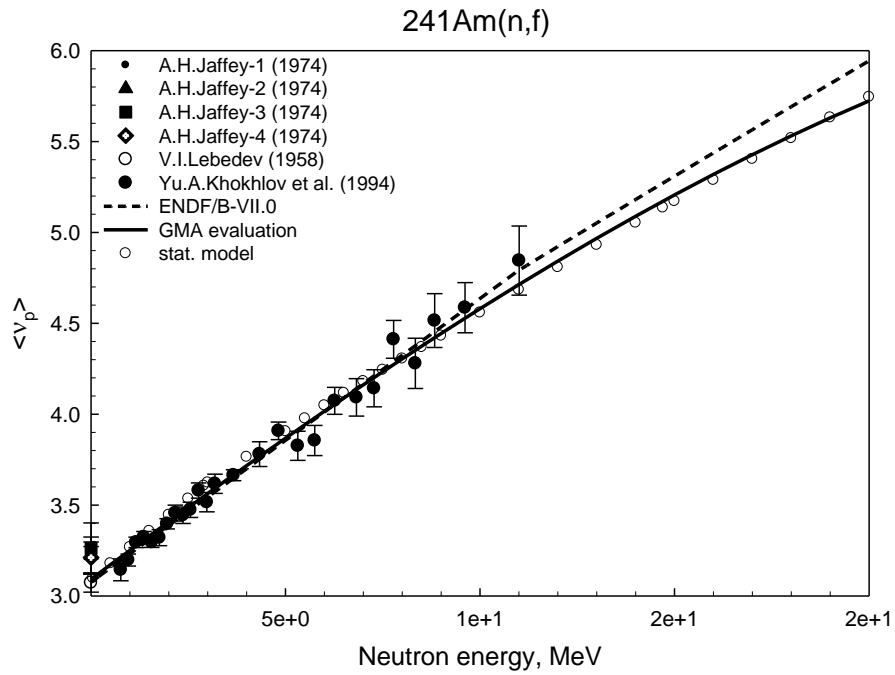


Fig.10.1. Comparison of experimental data with the results of GMA evaluation, results after the smoothing and ENDF/B-VII.0 evaluation.

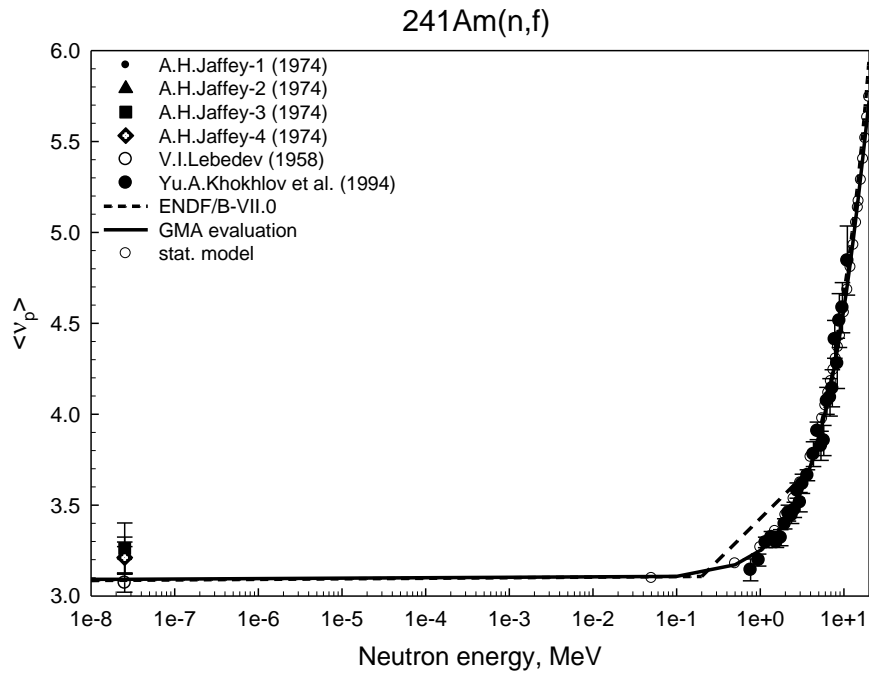


Fig. 10.2. Comparison of experimental data with the results of GMA evaluation, results after the smoothing and ENDF/B-VII.0 evaluation.

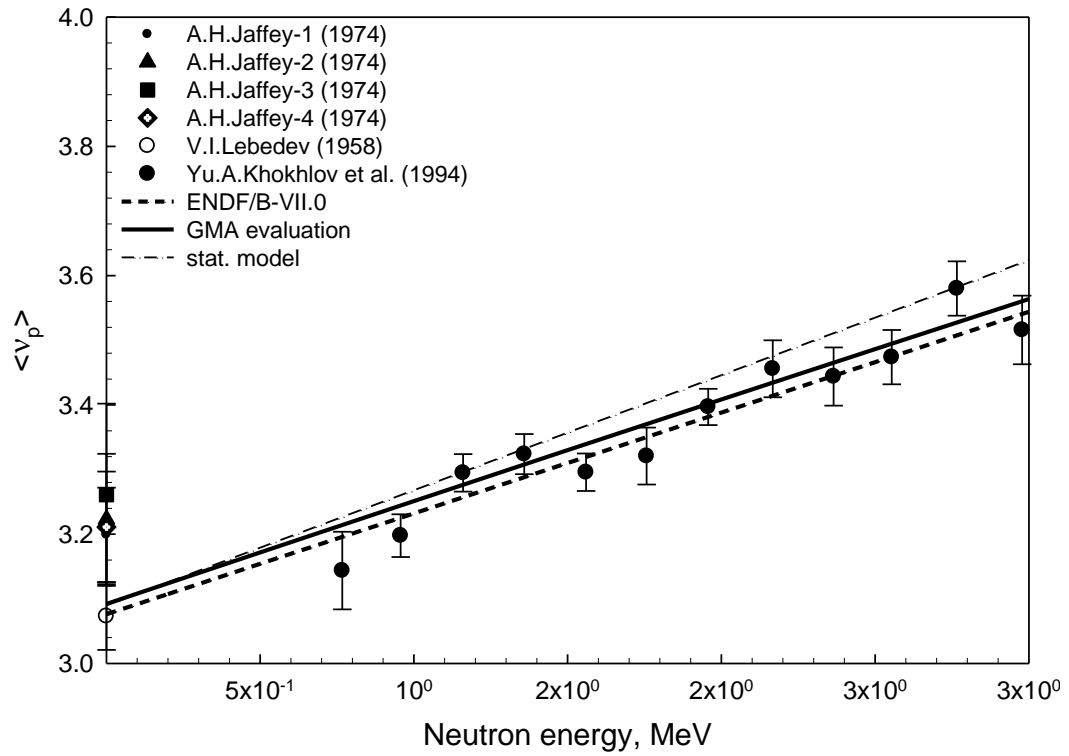


Fig. 10.3. Comparison of experimental data with the results of GMA evaluation, results after the smoothing and ENDF/B-VII.0 evaluation.

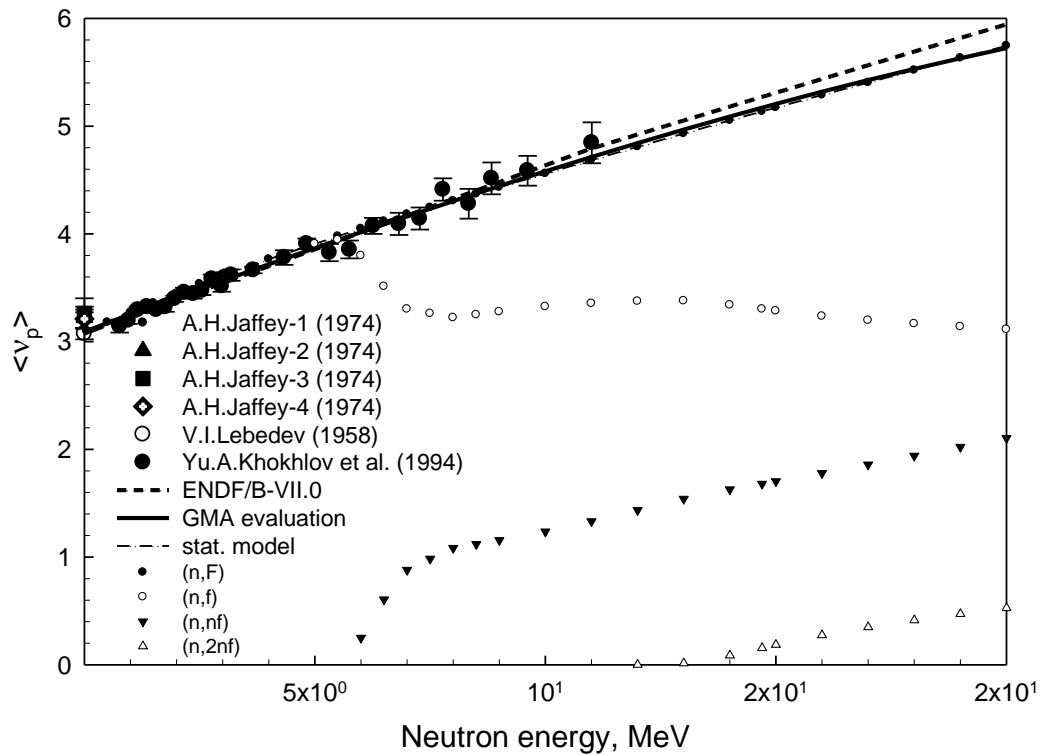


Figure 10.4 Comparison of model calculation and evaluations of ν_p .

several percents. There is a need to repeat the measurements of ν_p for ^{241}Am at thermal point using modern techniques.

At incident neutron energies above emissive fission threshold the number of prompt fission neutron ν_p calculated as

$$\nu_p(E_n) = \sum_{x=1} \nu_{px}(E_{nx}) + \sum_{x=1} (x-1) \cdot \beta_x(E_n), \quad (10.1)$$

here $x = 1, \dots, X$ is the multiplicity for x -th fissioning nucleus $A+1, A, A-1, A-2$ with $\nu_{px}(E_{nx})$ after emission of x pre-fission neutrons, $\beta_x(E_n)$ is the x -chance contribution to the observed fission cross section. The excitation energy E_{nx} of $(A+1-x)$ nuclides, formed after emission of $(n, xn_f)^{1 \dots x}$ pre-fission neutrons, depends on their average energies $\langle E_{n, xn_f}^k \rangle$, calculated for each exclusive pre-fission spectrum $d\sigma_{n, xn_f}^k / d\varepsilon$ ($x=1, 2, 3, 4; k=1, \dots, x$) (see section 12):

$$E_{nx} = E_r - E_{fx}^{pre} + E_n + B_n - \sum_{x=0, 1 \leq k \leq x} \left(\langle E_{n, xn_f}^k \rangle + B_{nx} \right), \quad (10.2)$$

E_r is the fission reaction energy. TKE values of E_F^{pre} , kinetic energy before neutron emission from the fragments, are a superposition of E_{fx}^{pre} , TKE of x nuclide contributing to the observed fission cross section:

$$E_F^{pre}(E_n) = \sum_{x=0} E_{fx}^{pre}(E_{nx}) \cdot \sigma_{n, xn_f} / \sigma_{n, F} \quad (10.3)$$

pre-fission neutron. The incident neutron energy dependence of neutron multiplicity in the energy range $E_n \leq 6$ MeV for all fissioning $^{242}, ^{241}, ^{240}, ^{239}\text{Am}$ nuclei $\nu_{px}(E_{nx})$ was taken from evaluation by Malinovskij [79], to reproduce the measured data on ν_p (see Table 10.1). Energy dependence of ν_p versus incident neutron energy estimated with this equation is compared on Fig. 10.2 with GMA' evaluation and previous evaluations. Relevant partial contributions to ν_p are shown on Fig. 10.1. "Step" in ν_p around (n, nf) reaction threshold is due to the pre-fission neutrons, emitted in $^{241}\text{Am}(n, nf)$ reaction. The similar behavior was evidenced in measured data for $^{232}\text{Th}(n, F)$ and $^{238}\text{U}(n, F)$, it was reproduced with the present model [67].

Table 10.1 Evaluated [79] first chance ν_p –values for $^{241}, ^{240}, ^{239}, ^{238}\text{Am}$ target nuclides.

Target	ν_p^{th}	$\nu_p(E_n \text{ MeV})$	$\nu_p(6 \text{ MeV})$
^{241}Am	3.090*	3.624 (3.0)	4.047
^{240}Am	3.205	3.623 (3.0)	4.034
^{239}Am	3.187	3.599 (3.0)	4.005
^{238}Am	3.180	3.583 (3.0)	3.980

*)tuned to measured data

11. Delayed neutron yield

There are only four direct measurements of the average total delayed neutron yield $\bar{\nu}_d$ for $^{241}\text{Am}(n,f)$. Namely, a) measurements by Saleh et al. [80] and Waldo et al. [81] for thermal neutrons (see Fig. 11.1) and b) measurements by Cesana et al. [82] and Gudkov et al. [83] for fast neutron spectrum with a mean energy about 1.0 - 1.2 MeV, which are also rather consistent. The thermal neutron –induced data are ~20% higher than the fast neutron data.

To prepare the total delayed neutron yields for $^{241}\text{Am}(n,f)$ from thermal energies up to 20 MeV, we investigated several approaches. First, we used the summation technique of cumulative fission yields multiplied by neutron emission probability after the β -decay (P_n) of a given precursor [84]. The influence of different factors on the energy dependence of delayed neutron yields was described in [84] for $^{235}\text{U}(n, F)$ and $^{237}\text{Np}(n, F)$ reactions. It was shown, that the fission chances strongly influence the energy dependence of the delayed neutron yield. Nuclides ^{241}Am and ^{237}Np are odd-even, however, sub-threshold fission cross section in the thermal energy range of ^{241}Am is about 2 orders of magnitude higher than that of ^{237}Np . The energy dependence of cumulative fission product yields was taken from UKFY-4 library [85] developed using latest systematic by A.C. Wahl [86]. P_n values are defined for more than 270 delayed neutron precursors and were taken from compilation [87]. New measurements and calculations of P_n are generally in good agreement with the data of [87]. However, the predicted cumulative yields in the Wahl systematic [86] are known with poorer accuracy than neutron emission probability P_n values, especially for low yields. The calculated, by summation using Wahl systematic [86], $^{241}\text{Am}(n, F)$ total delayed neutron yield of 0.006752 per fission at thermal energy, is ~30% higher than measured data [82, 83]. The values for 8 precursors, obtained by Wahl [86], were corrected using the experimental values obtained at fast neutron spectrum measurements (average energy of the spectrum is ~1.2 MeV). After summation done with corrected values of cumulative yields, the average delayed yield at 1 MeV equals 0.004959 per fission, at thermal energy it equals 0.005111 per fission. This is in good agreement with experimental data at thermal energy.

The same correction coefficients were used at other neutron energies of 8 precursors, predicted by Wahl systematic [86]. The results of summation for neutron energies up to 20 MeV, are shown at Fig. 11.1 by thick solid line (summation, $T_{1/2} > 0.17$ sec). Measurements can be done with a higher time delays for the neutron registration, the results of summation with $T_{1/2} > 0.2$ and $T_{1/2} > 0.39$ sec are also shown. In summation procedure, only 32 main precursors giving 99.0 % contribution to the total delayed neutron yield were used. The results of ENDF/B-VII.0 and JENDL-4.0 evaluations are also shown. The influence of the fission chances (effective fission threshold ~5 MeV for (n, nf)) on the delayed neutron yield is rather small. Note, however, that the Wahl's systematic [89] of cumulative yields does not include the contribution of fission chances explicitly. The uncertainty of the calculated delayed neutron yield shown at Fig. 11.1 was obtained from uncertainty of the cumulative yields, given in Wahl's systematic [86] and uncertainty of evaluated P_n values. It is a crude estimate, ignoring the cross-energy correlation components.

Experimental data on delayed neutron yields from $^{241}\text{Am}(\gamma, F)$ reactions, in principle, can be used to estimate the contribution to the total delayed neutron yield, coming from $^{241}\text{Am}(n, nf)$ fission chance. Although the spin and energy spectra in neutron- and gamma-induced fission reaction are rather different, which may influence the yield of delayed neutron precursors, they are complementary.

The measurement of bremsstrahlung spectrum average delayed neutron production cross sections was done by Ganich et al. [88] in the energy range of gammas of 6 -18 MeV. The measured

data [88] for $^{232}\text{Th}(\gamma, \text{F})$, $^{235}\text{U}(\gamma, \text{F})$, $^{238}\text{U}(\gamma, \text{F})$, $^{237}\text{Np}(\gamma, \text{F})$, $^{239}\text{Pu}(\gamma, \text{F})$ and $^{241}\text{Am}(\gamma, \text{F})$ show some anomaly for the $^{241}\text{Am}(\gamma, \text{F})$ reaction. Maximum delayed neutron production cross section for

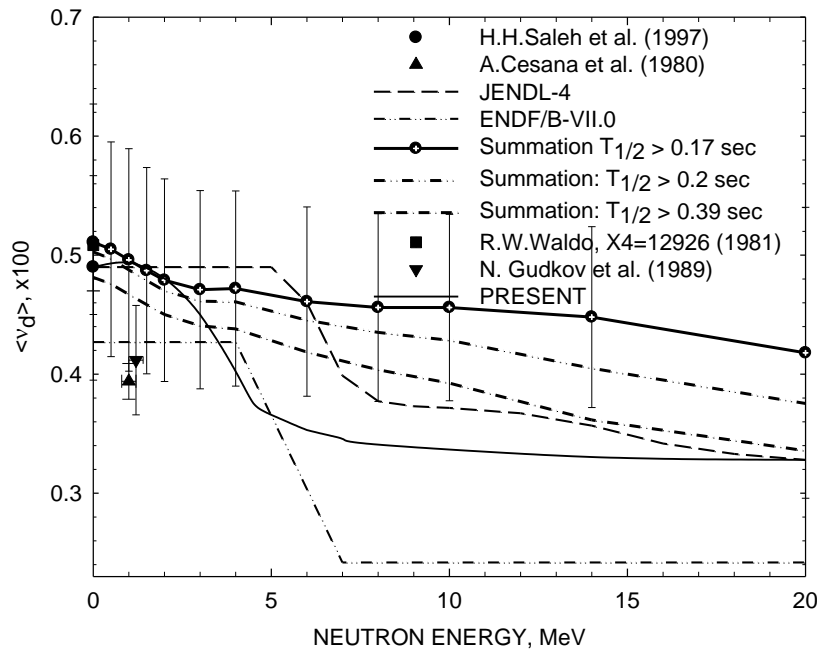


Fig. 11.1. Energy dependence of the average delayed neutron yields for $^{241}\text{Am}(\text{n},\text{f})$. Present evaluation (summation, $T_{1/2} > 0.17 \text{ sec}$) are compared with experimental data and evaluations.

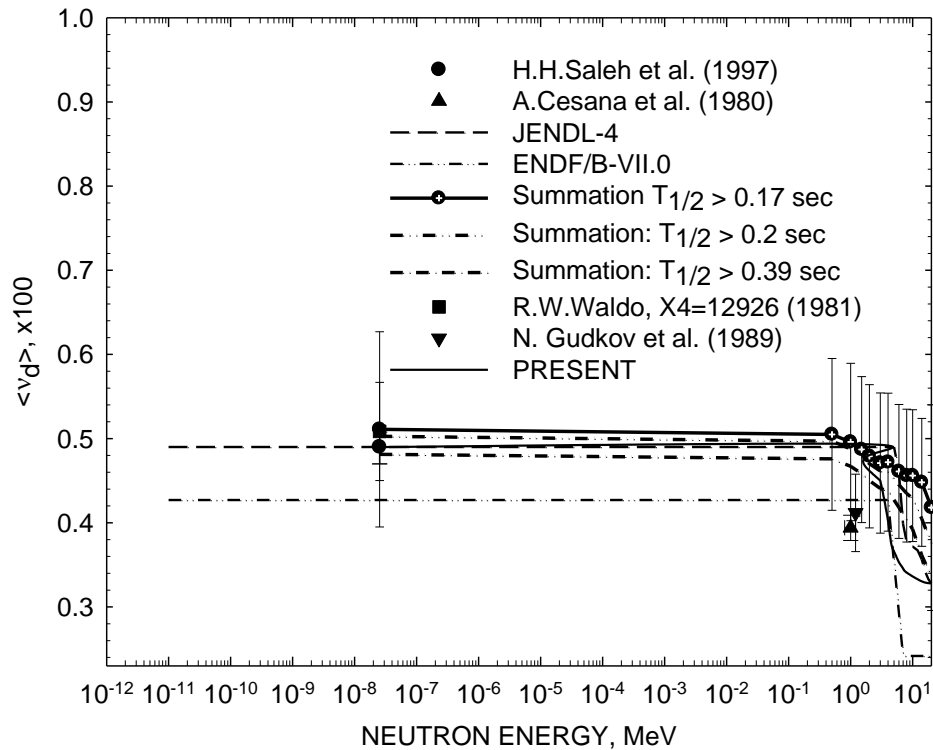


Fig. 11.2. Energy dependence of the average delayed neutron yields for $^{241}\text{Am}(\text{n},\text{f})$. Present evaluation (summation, $T_{1/2} > 0.17 \text{ sec}$) are compared with experimental data and evaluations.

all nuclides, with exclusion of ^{241}Am , is close to the maximum in the (γ, F) cross section. The ratio of delayed neutron production cross section to the bremsstrahlung spectrum averaged (γ, F) cross section determines the delayed neutron yield for (γ, F) and (γ, nf) reactions. It seems the results of measurements for ^{241}Am have some systematic error and can not be used in estimation of contribution to the delayed neutron yields of $^{241}\text{Am}(\text{n}, \text{nf})$ and $^{241}\text{Am}(\text{n}, 2\text{nf})$ fission chances. The delayed neutron yields estimated with these data would be extremely high at energies of gammas of 7- 8 MeV and too low at higher energies of 14-15 MeV.

The shape of the present estimate of delayed neutron average number, shown on Figs. 11.1 and 11.2, was obtained scaling the shape, obtained for the delayed neutron average number of $^{237}\text{Np}(\text{n}, F)$ reaction in [8], fitting the respective measured data. It is made consistent with the summation approach at thermal energies, but in the first chance fission domain it predicts stronger decrease with energy of the delayed neutron average number, as observed for the $^{237}\text{Np}(\text{n}, \text{f})$ reaction. At higher energies it also predicts much lower delayed neutron average number, as observed for the $^{237}\text{Np}(\text{n}, \text{f})$ and we adopted it for the present evaluation. It is assumed implicitly, that the $^{237}\text{Np}(\text{n}, \text{xf})$ and $^{241}\text{Am}(\text{n}, \text{xf})$ partial channel contributions are similar. Adopted estimates seem to be more consistent with the influence of the (n, xf) channel opening, predicted in JENDL-4.0 [37], on the delayed neutron average number.

12. Energy distributions of secondary neutrons

Energy distributions for $(\text{n}, 2\text{n})$, $(\text{n}, 3\text{n})$ and (n, n') reactions were calculated with a Hauser-Feshbach statistical model of cascade neutron emission [47, 67], taking into account exclusive pre-fission (n, xf) and $(\text{n}, \text{xn}\gamma)$ neutron spectra, with the allowance of pre-equilibrium emission of first neutron.

Prompt fission neutron spectra (PFNS) were calculated with a phenomenological model, developed for the first-chance fission by Kornilov et al. [89]. Afterwards, it was extended to the emissive fission domain adding exclusive pre-fission neutron spectra by Maslov et al. [67]. Exclusive pre-neutron spectra of (n, xf) reactions, either equilibrium and pre-equilibrium spectra of pre-fission (n, xf) neutrons are strictly correlated with (n, F) and (n, xn) reaction cross sections. This approach was used previously for the description of the PFNS and neutron emission spectra for $^{238}\text{U}+\text{n}$ [67], $^{235}\text{U}+\text{n}$ [90] and $^{232}\text{Th}+\text{n}$ [67] interactions. A number of experimental signatures were revealed and correlated with the exclusive pre-fission (n, xf) and $(\text{n}, \text{xn}\gamma)$ neutron spectra. This validated approach is used for the $^{241}\text{Am}(\text{n}, F)$, $^{241}\text{Am}(\text{n}, 2\text{n})$ and PFNS description/prediction for $\text{n}+^{241}\text{Am}$ interaction for non-emissive and emissive fission domain. Average energies of PFNS would predict distinct lowering in the vicinity of (n, nf) and $(\text{n}, 2\text{nf})$ reaction thresholds [67] well known in measured PFNS shapes for major actinides.

12.1 $(\text{n}, \text{xn}\gamma)$ and (n, xf) neutron emission spectra

Exclusive $(\text{n}, \text{xn}\gamma)$ and (n, xf) neutron emission spectra for $x = 1, 2, 3$, reactions are calculated with Hauser-Feshbach model taking into account fission and gamma-emission competition to neutron emission, actually neutron spectra are calculated simultaneously with fission and (n, xn) reaction cross sections. The pre-equilibrium emission of first neutron is fixed by the description of high energy tails of $(\text{n}, 2\text{n})$ reaction cross sections and (n, F) reaction cross sections for ^{235}U , ^{238}U and ^{232}Th target nuclides [67].

First neutron spectrum of the $^{241}\text{Am}(\text{n}, \text{nf})$ or $^{241}\text{Am}(\text{n}, \text{n}\gamma)$ reactions is the sum of evaporated and pre-equilibrium emitted neutron contributions. Second and third neutron spectra for $^{241}\text{Am}(\text{n},$

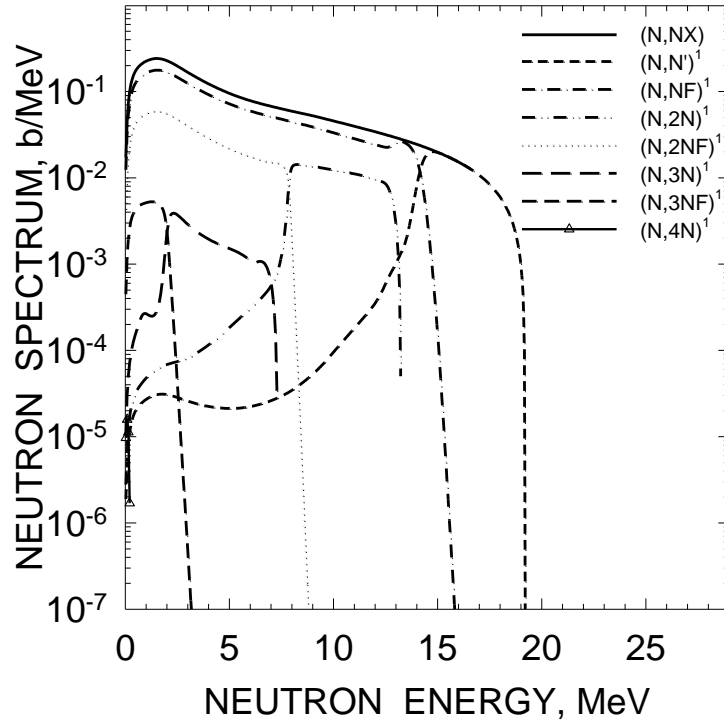


Fig. 12.1 Components of first neutron spectrum of ^{241}Am p+n interaction for incident neutron energy 20 MeV.

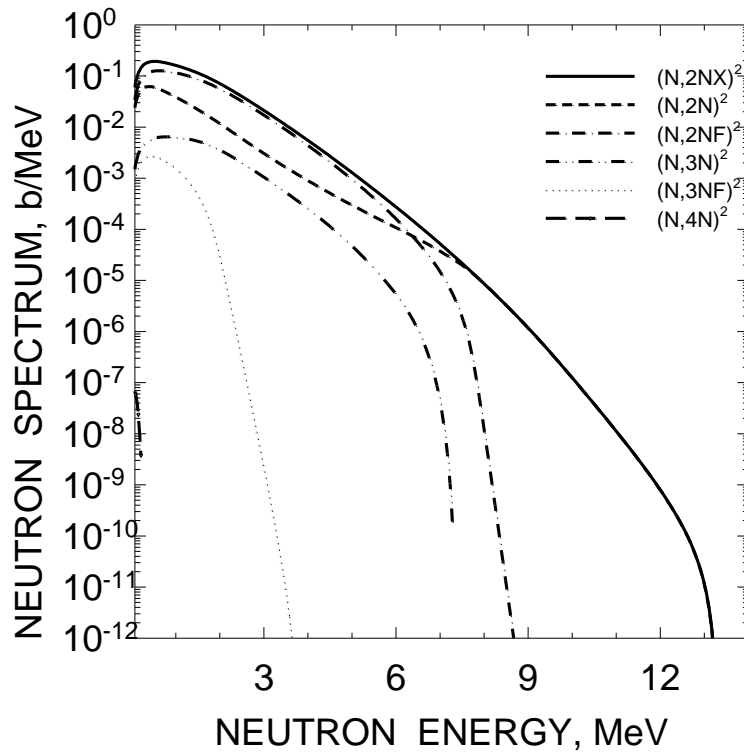


Fig. 12.2 Components of second neutron spectrum of ^{241}Am +n interaction for incident neutron energy 20 MeV.

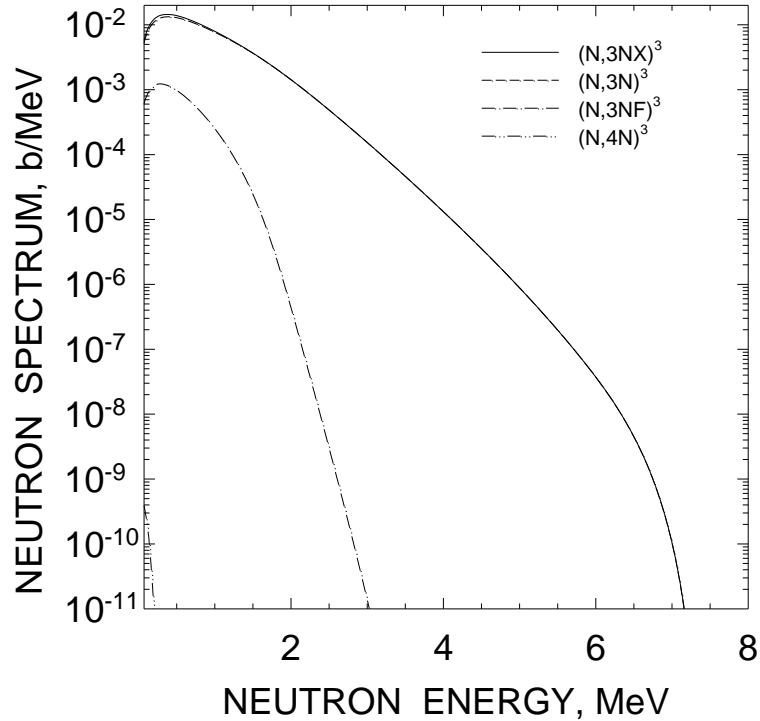


Fig. 12.3 Components of third neutron spectrum of $^{241}\text{Am} + n$ interaction for incident neutron energy 20 MeV.

$xnf(\gamma)$ reactions are assumed to be evaporative. Pre-fission neutron spectrum of $^{241}\text{Am}(n, nf)$ reaction, especially its hard energy tail, is sensitive to the description of fission probability of ^{241}Am nuclide near fission threshold.

Components of first neutron spectra for $E_n = 20$ MeV are shown on Fig. 12.1. Components of second neutron spectra for $E_n = 20$ MeV are shown on Fig. 12.2. Components of third neutron spectra for $E_n = 20$ MeV are shown on Fig. 12.3.

That is an illustration of the strong dependence of the partial contributions of the exclusive first neutron spectra on the fissilities of the composite $(A+1)$ nuclides as well as relative fissilities of A , $A-1$, $A-2$ nuclides. Summarizing, we anticipate that partial (n, xnf) pre-fission neutron spectra for ^{241}Am target nuclide would be pronounced in observed PFNS to a different extent as compared with $n+^{238}\text{U}$ and $n+^{232}\text{Th}$ interactions.

12.2 Prompt Fission Neutron Spectra

PFNS from fission fragments are calculated as a superposition of two Watt distributions for heavy and light fission fragments (FF), the partial contributions being equal, while the temperatures of the fragments are different [89]. Fission fragments' kinetic energy is the superimposed phenomenological parameter, generally lower, than total kinetic energy (TKE) of accelerated fission fragments.

In case of $n+^{237}\text{Np}$ system for normalization purposes the measured PFNS at $E_n \sim 0.52$ MeV [66] was used. For $n+^{241}\text{Am}$ system normalization is impossible. The prompt fission neutron

spectrum $S(\varepsilon, E_n)$ is calculated as a sum of two Watt [91] distributions, modified to take into account the emission of prompt fission neutrons before full acceleration of fission fragments. The neutrons, emitted from heavy and light fission fragments are included with equal weights:

$$S(\varepsilon, E_n) = 0.5 \cdot \sum_{j=l,h} W_j(\varepsilon, E_n, T_j(E_n), \alpha), \quad (12.1)$$

$$W_j(\varepsilon, E_n, T_j(E_n), \alpha) = \frac{2}{\sqrt{\pi} T_j^{3/2}} \sqrt{\varepsilon} \exp\left(-\frac{\varepsilon}{T_j}\right) \exp\left(-\frac{E_{vj}}{T_j}\right) \frac{sh(\sqrt{b_j \varepsilon})}{\sqrt{b_j \varepsilon}}, \quad (12.2)$$

$$b_j = \frac{4E_{vj}^0}{T_j^2}, \quad T_j = k_j \sqrt{E_j^*} = k_j \sqrt{E_r - TKE + E_n + B_n}, \quad (12.3)$$

$$E_{vl}^0 = \frac{A_h}{A_l A} \cdot \alpha \cdot TKE, \quad E_{vh}^0 = \frac{A_l}{A_h A} \cdot \alpha \cdot TKE. \quad (12.4)$$

The coefficient α is the ratio of the kinetic energies of the fragments at the moment of neutron emission to the kinetic energy of fully accelerated fragments and is, in fact, a free parameter. The ratio of the temperatures of the light and heavy fragment $r=T_l/T_h$ is another free parameter, which ensures the model [89] flexibility to reproduce the soft and hard tails of the PFNS. The parameters $\alpha=0.808$ and $r=1.248$ were fixed in [89] by fitting, in fact, the PFNS for $n+^{237}\text{Np}$ system at $E_n=7.8$ MeV. For $n+^{241}\text{Am}$ they are defined by systematics [89].

In case of $^{241}\text{Am}(n, F)$ the partial $^{241}\text{Am}(n, xnf)$ contribution could be calculated consistently with the $^{241}\text{Am}(n, F)$ and $^{241}\text{Am}(n, 2n)$ neutron cross sections, though it is impossible within present model/neutron absorption cross section to reproduce large contribution of $(n, 2nf)$ chance to the observed fission cross section. Exclusive (n, xnf) pre-fission neutron spectra, as described above, are calculated. At E_n higher than the emissive fission threshold $S(\varepsilon, E_n)$ is calculated as a superposition of pre-fission (n, xnf) neutrons $-d\sigma_{n, xnf}^k/d\varepsilon$ ($x=1, 2, 3, 4$; $k=1, \dots, x$) and post-fission spectra $S_{A+2-x}(\varepsilon, E_n)$ of the neutrons from the fission fragments:

$$\begin{aligned} S(\varepsilon, E_n, \theta) = & \tilde{S}_{A+1}(\varepsilon, E_n, \theta) + \tilde{S}_A(\varepsilon, E_n, \theta) + \tilde{S}_{A-1}(\varepsilon, E_n, \theta) + \tilde{S}_{A-2}(\varepsilon, E_n, \theta) = \\ & v_p^{-1}(E_n, \theta) \cdot \{ v_{p1}(E_n) \cdot \beta_1(E_n, \theta) S_{A+1}(\varepsilon, E_n, \theta) + v_{p2}(E_n - \langle E_{n, n, f}(\theta) \rangle) \beta_2(E_n, \theta) S_A(\varepsilon, E_n, \theta) + \\ & \beta_2(E_n, \theta) \frac{d^2 \sigma_{n, n, f}^1(\varepsilon, E_n, \theta)}{d\varepsilon d\varepsilon} + v_{p3}(E_n - B_n^A - \langle E_{n, 2, n, f}^1(\theta) \rangle - \langle E_{n, 2, n, f}^2(\theta) \rangle) \beta_3(E_n, \theta) S_{A-1}(\varepsilon, E_n, \theta) + \beta_3(E_n, \theta) \times \\ & \left[\frac{d^2 \sigma_{n, 2, n, f}^1(\varepsilon, E_n, \theta)}{d\varepsilon d\theta} + \frac{d^2 \sigma_{n, 2, n, f}^2(\varepsilon, E_n, \theta)}{d\varepsilon d\theta} \right] + v_{p4}(E_n - B_n^A - B_n^{A-1} - \langle E_{n, 3, n, f}^1(\theta) \rangle - \langle E_{n, 3, n, f}^2(\theta) \rangle - \langle E_{n, 3, n, f}^3(\theta) \rangle) \times \\ & \beta_4(E_n, \theta) S_{A-2}(\varepsilon, E_n, \theta) + \beta_4(E_n, \theta) \left[\frac{d^2 \sigma_{n, 3, n, f}^1(\varepsilon, E_n, \theta)}{d\varepsilon d\theta} + \frac{d^2 \sigma_{n, 3, n, f}^2(\varepsilon, E_n, \theta)}{d\varepsilon d\theta} + \frac{d^2 \sigma_{n, 3, n, f}^3(\varepsilon, E_n, \theta)}{d\varepsilon d\theta} \right] \} \end{aligned} \quad (12.7)$$

Figures 12.4-12.7 compare present PFNS with those of JENDL-4.0 [7]. Some shape differences for the first- and higher chance fission are noticed, though reasonable consistency of the average energies (Fig. 12.8) of emitted prompt fission neutron spectra both in first-chance and emissive fission domains is observed.

Figure 12.9 shows the partial contributions of $^{241}\text{Am}(n, f)$ and $^{241}\text{Am}(n, xnf)$ reactions to the observed PFNS, shown on previous Fig. 12.7. The contribution of $^{241}\text{Am}(n, nf)$ reaction in the soft

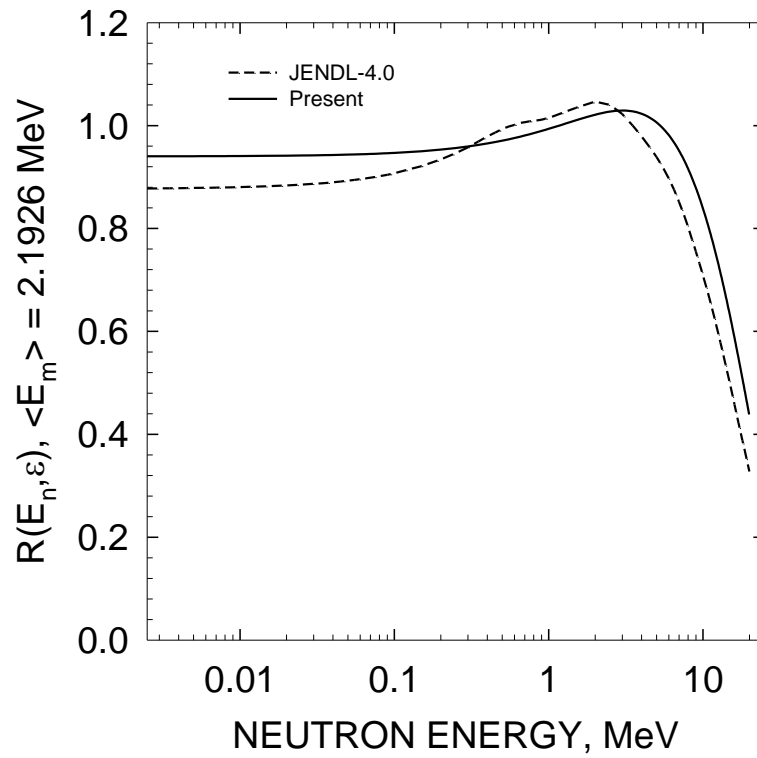


Fig. 12.4 Comparison of the prompt fission neutron spectrum for ^{241}Am (n, F) reaction at incident neutron energy of 10^{-5} MeV.

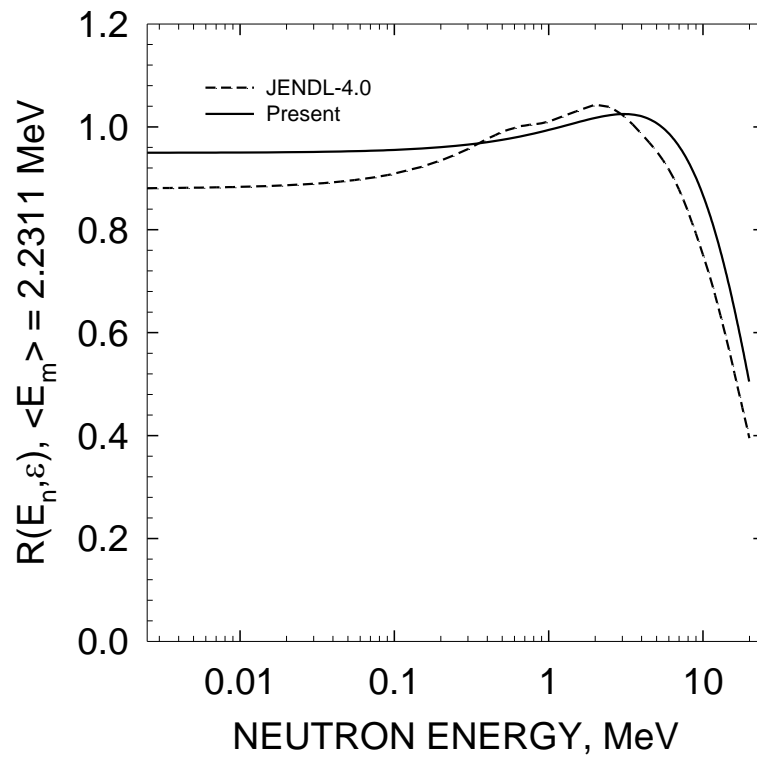


Fig. 12.5 Comparison of the prompt fission neutron spectrum for ^{241}Am (n, F) reaction at incident neutron energy of 2 MeV.

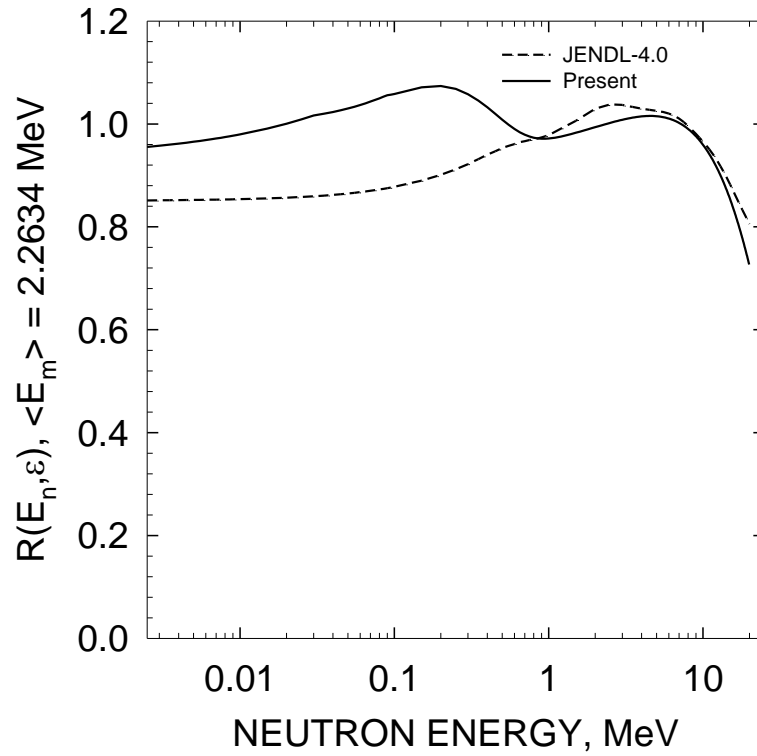


Fig. 12.6 Comparison of the prompt fission neutron spectrum for ^{241}Am (n, F) reaction at incident neutron energy of 6 MeV.

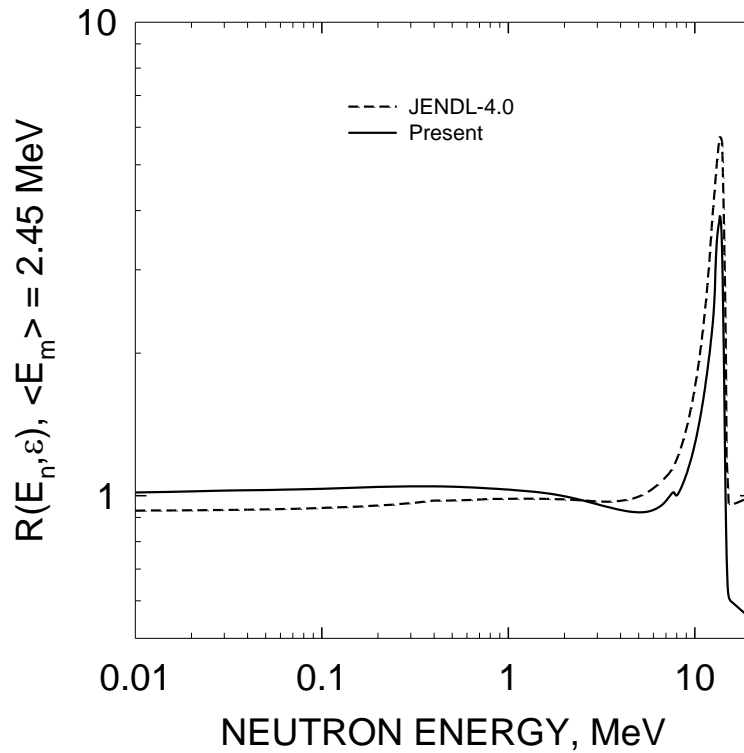


Fig. 12.7 Comparison of the prompt fission neutron spectrum for ^{241}Am (n, F) reaction at incident neutron energy of 20 MeV.

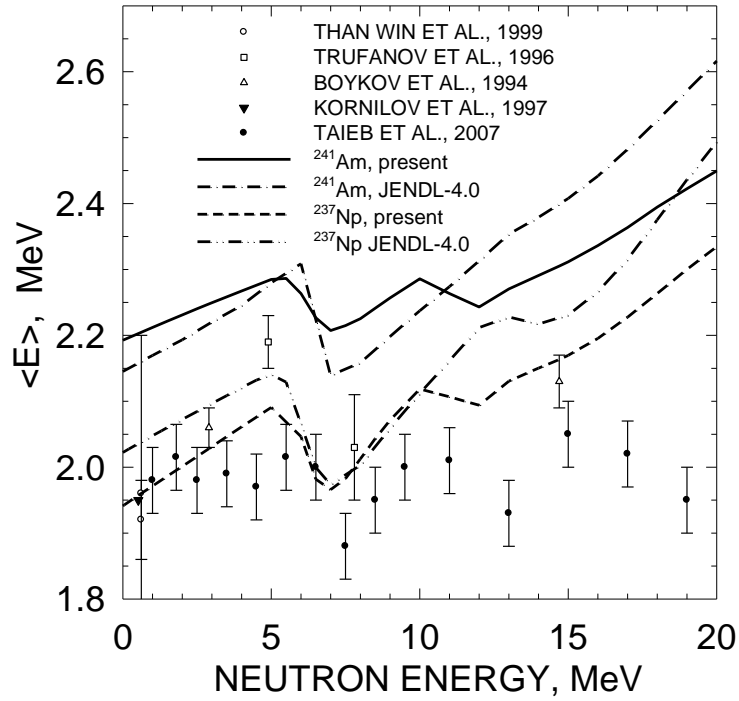


Fig. 12.8 Dependence of average energy of ^{241}Am (n, F) and ^{237}Np (n,F) prompt fission neutron spectra on the incident neutron energy.

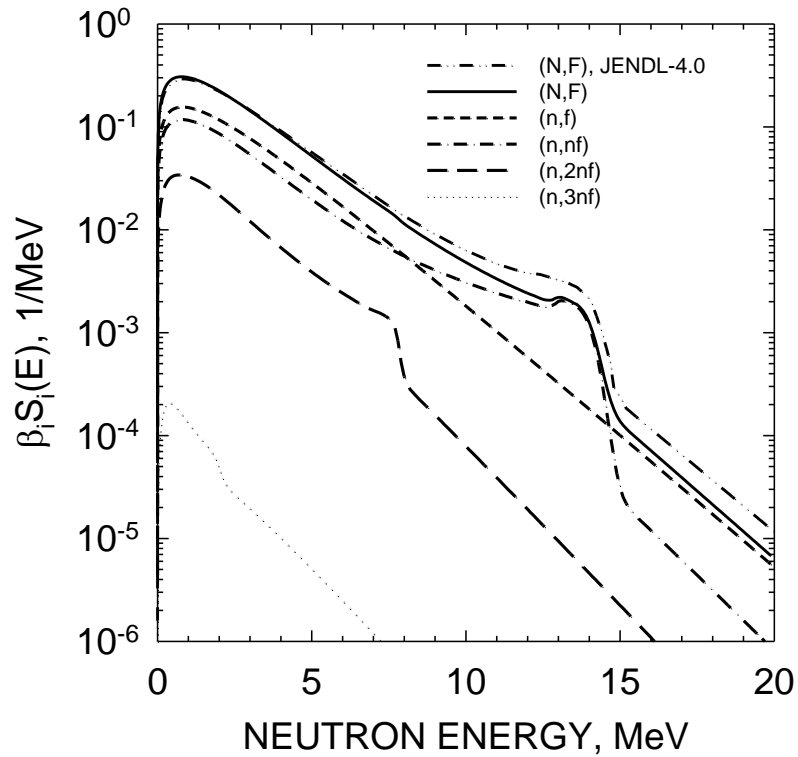


Fig. 12.9 Multiple-chance fission contributions to the prompt fission neutron spectrum for ^{241}Am (n, F) reaction, incident neutron energy 20 MeV.

part of the spectrum is systematically lower than that of $^{241}\text{Am}(n, f)$ reaction. The contribution of (n, nf) reaction is higher in case of JENDL-4.0 [37] for the hard part of the spectrum.

The combined effect of fission chances and exclusive pre-fission neutron spectra leads to the lowering of the average energy of the PFNS of $^{241}\text{Am}(n, F)$ in the vicinity of the $^{241}\text{Am}(n, nf)$ and $^{241}\text{Am}(n, 2nf)$ reaction thresholds. The dips are evidenced in measured PFNS average energy $\langle E \rangle$ of different U nuclei. In JENDL-4.0 [37] the PFNS is calculated with Madland-Nix model [92], the pre-fission neutron spectra are calculated as exclusive ones. However, some discrepancies are noticed with measured data for $^{237}\text{Np}(n, F)$, a second dip due to $(n, 2nf)$ reaction is not reproduced in JENDL-4.0 [37] both for ^{237}Np and ^{241}Am .

12.3 (n,xn) Reactions Neutron Spectra

There is no measured data on neutron emission spectra for $^{241}\text{Am} + n$ interaction. For incident neutron energy higher than emissive fission threshold, emissive neutron spectra are de-convoluted, components of 1st, 2nd and 3d exclusive neutron spectra are provided, where applicable. We have calculated exclusive 1st, 2nd and 3d neutron spectra for the $(n, n\gamma)$, $(n, 2n)$ and $(n, 3n)$ reactions.

According to the ENDF/B-VII format specifications the exclusive secondary neutron spectra for the $(n, n\gamma)$, $(n, 2n)$ and $(n, 3n)$ reactions were provided.

Spectrum of $(n, n\gamma)$ reaction actually is just hard energy tail of ‘pre-equilibrium’ component of first neutron spectrum (see Figs. 12.1, 12.2, 12.3).

Spectrum of the first neutron of $(n, 2n)$ reaction is much softer, although ‘pre-equilibrium’ component still comprise appreciable part of it. Figures 12.10, 12.11 and 12.12 illustrate the variation of the partial contributions of the 1st and 2nd neutrons to the combined spectrum of $^{241}\text{Am}(n, 2n)$ and $(n, 3n)$ reactions.

First neutron spectrum of $(n, 3n)$ reaction is actually of evaporative nature. First neutron spectrum of (n, nf) reaction has rather long pre-equilibrium high-energy tail. First neutron spectrum

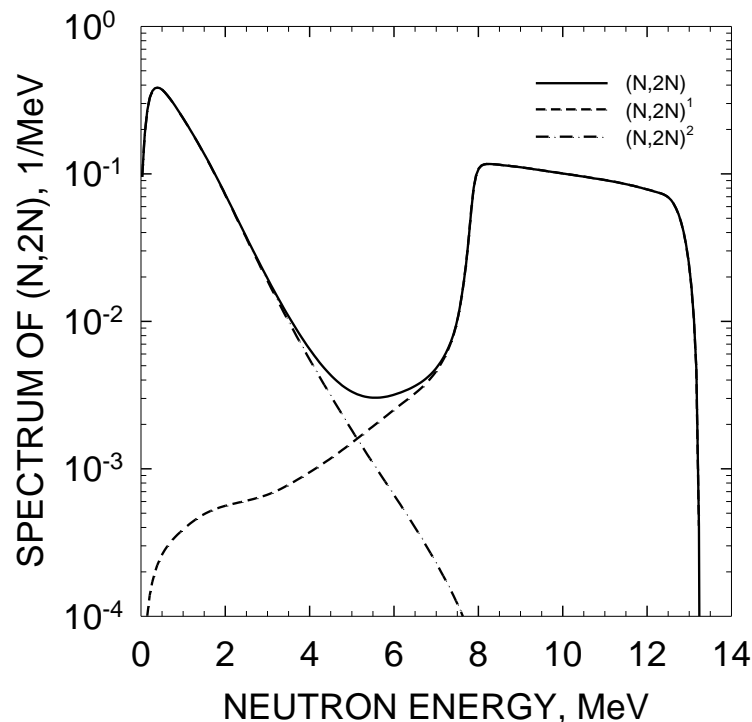


Fig. 12.10 (n, 2n) reaction neutron spectra of $^{241}\text{Am} + n$ for incident neutron energy 20 MeV.

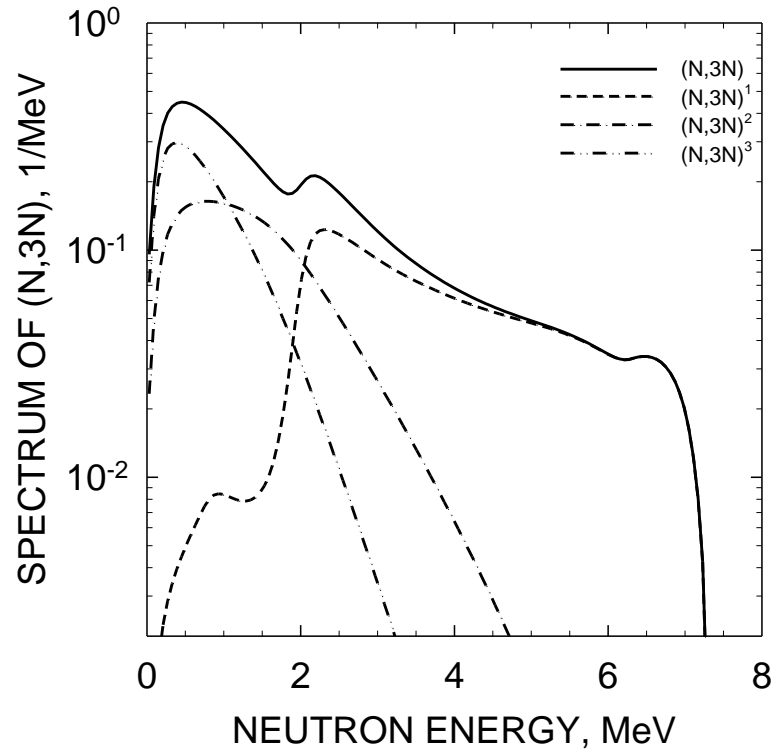


Fig. 12.11 (n, 3n) reaction neutron spectra of $^{241}\text{Am} + n$ for incident neutron energy 20 MeV.

^{241}Am , $E_n = 14 \text{ MeV}$

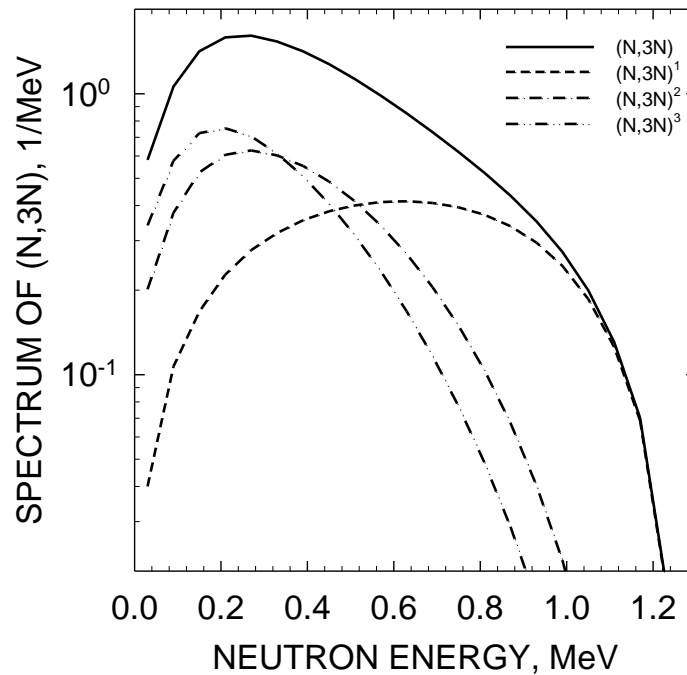


Fig. 12.12 Comparison of (n, 3n) reaction neutron spectra for $^{241}\text{Am} + n$ for incident neutron energy 14 MeV.

of (n, 2nf) reaction, as that of (n, 3n) reaction, is of evaporative nature. Figures 12.11 ($E_n = 20$ MeV) and 12.12 ($E_n = 14$ MeV) illustrate the variation of the partial contributions of the 1st, 2nd and 3d neutrons to the combined spectrum of ^{241}Am (n,3n) reaction, softening of higher multiplicity neutrons is evident.

13. Conclusion

The diverse measured data base of $n+^{241}\text{Am}$ is analyzed using a statistical theory and generalized least squares codes. Important constraints for the measured capture cross section might come from the average radiative, S_0 and S_1 strength functions, however, the observed capture cross section needs anomalously high capture width to produce a consistency with measured data, fitted with GMA code approach in keV-energy range. A change of the inelastic data shape at $E_n \sim 1.5$ MeV is explained by the sharp increase of the level density of the residual odd-even nuclide ^{241}Am due to the onset of three-quasi-particle excitations.

Prompt fission neutron spectra data for the first-chance fission and emissive fission reactions are predicted. The influence of exclusive (n, xn) pre-fission neutrons on prompt fission neutron spectra (PFNS) and (n, xn) spectra is modelled. Contributions of emissive/non-emissive fission and exclusive spectra of (n, xn) reactions are defined by a consistent description of the ^{241}Am (n, F), ^{241}Am (n, 2n) ^{240}Am reactions. There is still a need in fission cross section measurements around 14-15 MeV, two data sets available can not be considered normalized unambiguously. In ^{241}Am neutron capture the branching ratio data of the yields of short-lived (1^-) and long-lived (5^-) ^{242}Am states measured at thermal and around average energy of the fast reactor spectrum is calculated without arbitrary normalizations, though in a simplified manner. Excited levels of ^{242}Am are modelled using predicted Gallher-Moshkowski doublets.

The job is supported by International Science and Technology Center (Moscow) under B-1604 Project Agreement.

References

1. Kessler G. Nucl. Sci. Eng. 159, 56 (2008).
2. Dias M., 7th Intern. Conf. Nucl. Criticality Safety, 2003, Japan.
3. Maslov V.M., Teterova N.A., Pronyaev V.G. et al. Atom. Energ., 108, 352 (2010).
4. Poenitz W.P., Aumeier S.E., The simultaneous evaluation of the standards and other cross sections of importance for technology, Report ANL/NDM-139 (1997).
5. Maslov V.M., Porodzinskij Yu.V., Baba M., Hasegawa A. Nucl. Sci. Eng. 143, 177 (2003).
6. Maslov V. M. In: Proc. of the 13th International Seminar on Interaction of Neutrons with Nuclei, May 25-28, 2005, Dubna, Russia, p. 321.
7. Maslov V.M., Sukhovitskij E.Sh., Porodzinskij Yu.V. et al. INDC(BLR)-005, 1996.
8. Maslov V.M., Pronyaev V.G., Teterova N.A. et al. INDC(BLR)-021, 2010.
9. An International Evaluation of Neutron Cross Section Standards, Report STI/PUB/1291, IAEA, Vienna, Austria (2007).
10. Behrens J.W., Browne J.C., Nucl. Sci. Engng. 77, 444 (1981).
11. Prindle A.L., Sisson D.H., Nethaway D.R., Kantelo M.V., Sigg R.A. Phys. Rev. C20, 1824 (1979).
12. Dabbs J.W.T., Johnson C.H., Bemis Jr. C.E. Nucl. Sci. Engng. 83, 22(1983).
13. Cunningham B.B., Ghiorso A. Phys. Rev. 82, 558 (1951)
14. Knitter H.-H., Budtz-Jorgensen C. Atomkernenergie. Kerntechnik, 3, 205 (1979).
15. Wisshak K., Kappeler F. Nucl. Sci. Eng. 76, 148 (1980).
16. Hage W., Wisshak K., Kappeler F. Nucl. Sci. Eng. 78, 248 (1981)
17. Cance M., Gimat D., Grenier G., Parisot D. CEA-N-1969, 57, 1977
18. Kobayashi K., Yamamoto SH., Miyoshi M., et al. JAERI-M-9757,,81)
19. Yamamoto S., Kobayashi K., Miyoshi M., et al., Nucl. Sci. Eng. 126, 201, 1997.
20. Shpack D.L., Ostapenko Yu.B., Smirenkin G.N. JETP Lett. 10,175 (1969).
21. Zhuravlev K.D. Kroshkin N.I., Chetverikov A.P. At. Energy 39, 2856 (1975).
22. Protopopov A.N., Selitskij Yu.A., Solov'ev S.M. Sov. J. At. Energy 6, 36 (1959).
23. Kuprijanov V.M., Fursov B.I., Ivanov V.I. G.N.Smirenkin., Atomnaya Energiya, 45, 440 (1978).
24. Aleksandrov B.M., Nemilov JU A., Selitskij JU.A., et al., Atom. Energ. 46 (1979) 416.
25. Kazarinova M.I., Zamyatnin Yu.S., Gorbachev V.M. Sov. J. At. Energy 8, 125 (1961)
26. Vorotnikov P.E., Dmitriev S.V., Molchanov Yu.D., Otroshchenko G.A. Yadern. Fyzika, 44 (1986) 1403.
27. Golovnya V.YA, Bozhko V.P., Oleynik S.N., Shpakov V.P., Kalinin V.A. JINR-E3-419, 293, 1999.
28. Weston L.W. and Todd J.H. Nucl. Sci. Eng., 61 (1976) 356.
29. Gayther D.B. and Thomas B.W. Proc. 4th All-Union Conf. Neutron Physics, Kiev, Soviet Union, April 18-22, 1977, III, 3, Atomizdat (1977).
30. Mughabghab S. F. Atlas of neutron resonances.2006, NNDC, BNL, Upton, USA.
31. Jandel M., Bredeweg A., Bond E.M., et al. Phys. Rev., C 78, 034609 (2008).
32. Vanpraet G., Cornelis E., Raman S., Rohr G. Nuclear Data for Basic and Applied Science, Proc. Int. Conf., Santa Fe, 1985, vol. 1, p. 493.
33. Fioni G., Gribier M., Marie F., et al. Nuclear Physics A 693, 546 (2001).
34. Nakamura S., Ohta M., Harada H. et al. J. Nucl. Sci. Techn., 44 (2007) 1500.
35. Maidana N.L., Dias M.S., Koskinas M.F. Rad. Chem. Acta, 89 (2001) 419.

36. Bringer O., AlMahamid I., Chabod S., et al. Proc. of Int. Conf. on Nuclear Data for Science and Technology. Nice, France, Vol. 1, p. 619 (2008).
37. Shibata K., Iwamoto O., Nakagawa T. . Nucl. Sci. Techn., 48 (2011) 1.
38. Ignatjuk A.V., Istekov K.K., Smirenkin G.N. Sov. J. Nucl. Phys. 29, 450 (1979). 1984.
39. Chadwick M.B., P. Oblozinsky, M. Herman e.a. Nucl. Data Sheets, 107, pp. 2931-3060 (2006).
40. Moldauer P.A. In: Proc.Conf. on Neutron Cross Sections and Technology, Washington, D.C., USA, March 22-24, 1966, p. 613-622, AEC (1966).
41. Stavinskij V.S. and Shaker M.O. Nucl. Phys. 62 (1965) 667.
42. ENSDF, 1995.
43. Strutinsky V.M. Nucl. Phys.A95 (1967) 420.
44. Phillips T.W., Howe R.E. Nucl. Sci. Eng. 69, 375 (1979)
45. Sood P.C., Singh R.N. Nucl. Phys. A373, 519 (1982).
46. Strutinsky V.M., Groshev L.V., Akimova M.K., Atomnaya Energiya, 38, 598 (1960).
47. Uhl M., Strohmaier B., A Computer Code for Particle Induced Activation Cross Sections and Related Quantities IRK-76/01, IRK, Vienna (1976).
48. Harbour R.M., NacMurdo K.W., McCrosson F.J., Nucl. Sci. Eng. 50, 364 (1973).
49. Wisshak K., Wickenhauser J., Kaeppler F. Reffo G., Fabbri F. Nucl. Sci. Eng. 81, 396 (1982).
50. Bak M.A., Krivochatskiy A.S., Petrzhak K.A., et al. Atomnaya Energija, 23, 316 (1967).
51. Dovbenko A.G., Ignatyuk A.V. and Tolstikov V.A., Nuclear Constants. 7, 201(1974); INDC(CCP)-43/L.
52. Gavrillov V.D., Goncharov V.A., Ivanenko V.V., Kustov V.N., Smirnov V.P. Atomnaya Energiya, 41, 185 (1976).
53. Shinohara N., Hatsukawa Y., Hata K., Kohno N., Nuclear Science and Technology, Vol. 34, No. 7, pp. 613-621, July 1997.
54. Fomushkin E.F., Gavrillov V.V., Andreev M.F., et al. Proc. of Int. Conf. on Nuclear Data for Science and Technology. Nice, France, Vol. 1, pp. 425-428 (2008).
55. Sagara H., Yamamoto T, Koyama S., et al., Materials Science and Engineering Vol. 9, 012006, IOP Publishing Ltd, (2010).
56. Ivanova N.I., Kobzev A.N., Krylov N.G., et al. Atomnaya Energija (Sov.), 30 (1971) 369.
57. Cullen D. PREPRO2000: 2000 ENDF/B Pre-Processing Codes.
58. NJOY 94.10 Code System for Producing Pointwise and Multigroup Neutron and Photon Cross Sections from ENDF/B Data, RSIC Peripheral Shielding Routine Collection, ORNL, PSR-355, LANL, Los Alamos, New Mexico (1995).
59. Moldauer P.A. Phys. Rev., C11, 426 (1975).
60. Tepel J.W., Hoffman H.M., Weidenmuller H.A. Phys. Lett. 49, 1 (1974).
61. Fu C. Nucl. Sci. Eng. 86 (1984) 344.
62. Maslov V.M. Yadern. Fyzika, 63 (2000) 214.
63. Myers W.O. and Swiatecky W.J. Anomalies in Nuclear masses. Ark. Fyzik. 36 (1967) 243.
64. Bjørnholm S. and Lynn J.E. The double humped fission barrier. Rev. Mod. Phys. 52 (1980) 725.
65. Howard W.M. and Möller P. Atomic Data and Nuclear Data Tables 25 (1980) 219.
66. Kornilov N.V., Kagalenko A.V., Baryba V.Ya. et al. Ann. Nucl. Energy, 27, 1643 (2000).
67. Maslov V.M., Porodzinskij Yu. V., Baba M., et al. Phys. Rev. C, 69, 034607, 2004.
68. Filatenkov A.A., Chuvaev S.V., Aksenov V.N., Yakovlev V.A., Report RI-252, M.: CNIIAtominform, May 1999
69. Lougheed R.W., Webster W., Namboodiri M.N. et al., Radiochim. Acta, 90, 833 (2002).
70. Perdikakis G., Papadopoulos C.T., Vlastou R., et al. Phys. Rev. C 73, 067601 (2006).
71. Vieira et al. Proc. of the Inter. Conf. on Nuclear Data for Science and Technology, p. 551, Nice, France, April 22-27, 2007, EDP Sciences.
72. Tonchev A.P., Angeli C.T., Boswell M. et al. Phys. Rev. C77, 054610 (2008).

73. Sage C., Semkova V., Bouland O., et al., Phys. Rev. C81, 064604 (2010).
74. International Evaluation of Neutron Cross-Section Standards, IAEA, Vienna, Austria, IAEA Publication STI/PUB/1291 (2006).
75. A.J. Jaffey and J.L. Lerner, Nucl. Phys., A145, p. 1 (1970).
76. International Evaluation of Neutron Cross-Section Standards, IAEA, Vienna, Austria, IAEA Publication STI/PUB/1291 (2006).
77. V.I. Lebedev, V.I. Kalashnikova, At. En., 5, p. 176 (1958).
78. Yu.A. Khokhlov, I.A. Ivanin, V.I. In'kov, Yu.I. Vinogradov, L.D. Danilin, B.N. Polynov, in Proc. of Int. Conf on Nucl. Data for Sci. and Technology, Gatlinburg, v. 1 p. 272 (1994).
79. Malinovskij V.V. VANT (ser. Yadernie constanty), 1987, No.2, 25.
80. H.H. Saleh, T.A. Parish, N. Shinohara, Nucl. Sci. and Eng., 125, p.51 (1997).
81. R.W. Waldo, R.A. Karam, R.A. Meyer, Phys. Rev., C23, p. 1113 (1981).
82. A. Cesana, G. Sandrelli, V. Sangiust, M. Terrani, Report INDC(NDS)-113, p. 33, (1980).
83. A.N. Gudkov, S.V. Krivashev, A.B. Koldobskiy, At. Energy, 67, p. 218 (1989).
84. V.G. Pronyaev, V.M. Piksaikin, VANT, issue 1-2, p.32 (1997).
85. R.W. Mills, JEF/DOC-1232, UKNSF, p. 227 (2008)
86. A.C. Wahl, Fission Product Yield Data for the Transmutation of Minor Actinides Nuclear Waste, Report STI/PUB-1286, IAEA (2006).
87. T.R. England et al. In: Proceedings of the Specialist's Meeting on Delayed Neutron Properties, University of Birmingham Report, p. 117 (1987).
88. P.P. Ganich, A.S.Krivokhatskiy, A.I. Lendel et al., Report R, KIYAI-86-36 (1986).
89. Kornilov N.V., Kagalenko A. B, Hamsch F.-J. Phys. At. Nucl. 1999, 62, 209.
90. Maslov V.M., Kornilov N.V., Kagalenko A. B., Tetereva N.A. Prompt fission neutron spectra of ^{235}U up above emissive fission threshold. Nucl. Phys. A760 (2005) 274.
91. Watt B.E. Energy spectrum of neutrons from thermal fission of ^{235}U . Phys. Rev. 87, 1037 (1952).
92. Madland D., Nix J., Nucl. Sci. Engng. 81, 213 (1982).

Nuclear Data Section
International Atomic Energy Agency
Vienna International Centre, P.O. Box 100
A-1400 Vienna, Austria

E-mail: nds.contact-point@iaea.org
Fax: (43-1) 26007
Telephone: (43-1) 2600 21725
Web: <https://nds.iaea.org>
